OPTIMAL CONTROL OF LOWER EXTREMITY MUSCULOSKELETAL MOTION

BY

MUSA lATANGRANG AUDU

Submitted in Partial Fulfillment of the Requirements

for the Degree of Doctor of Philosophy

Department of Mechanical Engineering

case western reserve university

January, 1985



Copyright © 1985 by
Musa Latangrang Audu

OPTIMAL CONTROL MODELING OF LOWER EXTREMITY MUSCULOSKELETAL MOTION

Abstract by

MUSA L. AUDU

The application of optimal control theory in the study of musculoskeletal motion was investigated. The research includes a comparative study of muscle models of varying complexity. Four such models ranging in complexity from simple input-output models to very sophisticated phenomenological models were examined. A model was developed which was able to strike a compromise between model complexity and practicability in musculoskeletal motion applications.

In the solution process several optimal control algorithms were compared to determine their ability to handle the large scale nonlinear constrained optimization problems typically encountered in these studies. These algorithms were used to solve four different problems of varying complexity.

The selected muscle model and optimal control algorithm were used to solve the muscle-force sharing

problem of gait analysis. The objective function used is the metabolic energy consumption. This quantity was described empirically by deriving appropriate expressions for its components in terms of the state and control variables of the muscle model. The results using this dynamic optimization algorithm are compared with similar results obtained using a static optimization approach.

DEDICATION

To the Memory of

ALHAJI AUDU DODO KALTUNGO

ACKNOWLEDGEMENTS

I would like to express my sincere gratitude to my advisor Professor Dwight T. Davy for his guidance and support throughout the years that were spent on this research project. His inspiration and unfailing support has been timely through several trying times for me. He has always been available to give me a helping hand at the many times that I ran out of steam. He has helped to make life worth living and I have enjoyed every minute I spent with him throughout my stay in this country. I deeply appreciate his fatherly kindness and support.

I am also grateful to Professors Joseph M. Mansour and Eugene E. Bahniuk for their useful suggestions and continuous help throughout the project. To my teacher Professor Kenneth A. Loparo I express my deepest respects for introducing me to many facets of Systems engineering, Control Theory and Optimization. He has opened my eyes to an interesting and satisfying scientific pursuit.

Mr James Berilla of the Orthopaedic Computing Laboratories has devoted several hours helping to ensure the smooth running of many of the algorithms and plotting routines in this dissertation. His enthusiasm and patience has helped to make this project both enjoyable and productive.

Darleen Midkiff has helped me set up the word

processor for typing this dissertation; and she also helped with typing some of the Tables. I am grateful to her for her help.

I am also grateful to the Bauchi State Government of Nigeria and the Ahmadu Bello University, Zaria-Nigeria for supporting me financially for the years I spent here.

Last but by no means the least of all, I would like to express my sincere gratitude to my dear wife Raby M. Audu for her love, friendship and kindness. She has been an excellent and dedicated companion - in times of storm and in times of calm. I am sincerely thankful to her for her constant encouragement. To my son Abdullah, I am also thankful for being such a nice friend. To both these two I am most grateful for the frustrations they have endured with much fortitude.

Computer funds granted by the Office of the Dean of Case Institute of Technology has made the development of a portion of the computational aspect of this project possible. Computer time donated by the Center for Automation and Intelligent Systems Research is also gratefully acknowledged.

TABLE OF CONTENTS

		Page
Title page		i
Abstract		ii
Dedication		iv
Acknowledgements		v
Table of Contents		vii
List of Figures		xi
List of Tables		xiii

Chapter I

Introduction

1.1	Introduction and Motivation	1
1.2	Statement of the Problem	6
1.3	Review of the Literature on Muscle Modeling	11
1.4	Review of the Literature on Gait Analysis by Optimization Techniques	12
1.5	Review of the Literature on Optimal Control in Gait Analysis	22

Chapter II

The Influence of Muscle Model Complexity

in Musculoskeletal Motion Modeling

2.1 Introduction 26

2.2 Problem Statement 29

2.3 Muscle Models 31

2.4 Modeling Passive Joint Structures 55

2.5 Optimal Control Problem 58

2.6 Results 59

2.7 Discussion 71

Chapter III

A Comparison of Optimal Control Algorithms

for Musculoskeletal Motion Modeling

3.1 Introduction 83

3.2 The General Optimal Control Problem 85

3.3 Statements of the Problems 88

3.4 Solution Algorithms 92

3.5 Handling the Constraints..... 98

3.6 Search for the One-dimensional stepsize.... 104

3.7 Computer Implementation 109

3.8 Results and Discussion 110

3.9 Summary and Conclusion 121

References Cited

References 205

Appendix 1

Equations of Motion for Two-degree-of-freedom System of Rigid Bodies 210

Appendix 2

Equations of Motion for Three-degree-of-freedom System of Rigid Bodies 212

Appendix 3

Expressions for p_1 to p_6 in Muscle Model 4 216

Chapter IV

A Dynamic Optimization Technique for Predicting Muscle Forces in the Swing Phase of Gait

4.1 Introduction 123

4.2 The Dynamic Optimization Problem..... 124

4.2.1 Statement of the Problem 124

4.2.2 The Rate of Energy Consumption 126

4.2.3 Calculating Muscle Lengths and Moment Arms . 134

4.2.4 Modeling the Penniform Muscles 142

4.2.5 The Weighting Matrices 144

4.2.6 Handling the constraints on the controls .. 145

4.2.7 The Complete set of State Equations 147

4.3 The Static Optimization Problem 157

4.3.1 Statement of the Problem 157

4.3.2 Calculating the Joint Resultant Moments ... 158

4.3.3 Mathematical Statement of the Problem 164

4.4 Results 166

4.5 Discussion 193

Chapter V

Summary, Conclusion and Recommendations

5.1 Summary 198

5.2 Conclusions 200

5.3 Recommendations 202

LIST OF FIGURES

Figure		Page
1.1	Model of Anthropormorphic Figure	3
1.2	Three-degree-of-freedom lower Limb Model	7
1.3	Feedback loop of muscle control system	18
2.1	Two-degree-of-freedom lower Limb Model	30
2.2	Muscle Model 1	33
2.3	Typical Responses of Model 1	38
2.4	Muscle Models 2, 3 and 4	40
2.5	Typical Responses of Muscle Model 2	45
2.6	Modified Hill Force-velocity Relationship	47
2.7	Rising Exponential Curves	49
2.8	Typical Responses of Muscle Model 3	51
2.9	Typical Joint Torque Curve	56
2.10	Solution for Muscle Model 1	62
2.11	Solution for Muscle Model 2	63
2.12	Solution for Muscle Model 3	64
2.13	Solution for Muscle Model 4	65
2.14	Solution for Torque Actuator Model	66
2.15	Hip and Knee joint Torques	69
2.16	Force Histories for Muscle Group 1	72
2.17	Quick release and stretch simulations	79
2.18	Hip Trajectories for Muscle Model 4	82
3.1	Flow Chart for the 'regula-falsi' technique ..	106
3.2	History of the Objective Function for Problem 1	111

3.3 History of the Objective Function for Problem 2 112
3.4 History of the Objective Function for Problem 3 113
3.5 History of the Objective Function for Problem 4 114
4.1 Three-degree-of-freedom lower limb 125
4.2 Activation Heat Rate Curve 129
4.3 Limb Positions for Muscle Length Calculations 136
4.4 Model of the Penniform Muscles 143
4.5 Typical Finite-difference Derivatives 161
4.6 Frequency Response of Digital Filter 163
4.7 Kinematic Data for Swing Phase of Gait 168
4.8 Kinematic Data for Swing Phase of Gait 171
4.9 Kinematic data for Swing Phase of Gait 175
4.10 Hip, knee and Ankle Joint Torques 176
4.11 Control Histories of Muscle Groups 1 - 9 178
4.12 Predicted Muscle Forces by Dynamic Optimization 181
4.13 Hip, Knee and Ankle Joint Torques 186
4.14 Predicted Muscle Forces by Static Optimization 187
4.15 Predicted Muscle Forces by Static Optimization 190

LIST OF TABLES

Table		Page
2.1	Parameters for Muscle Model 1	36
2.2	Parameters for Muscle Model 2	44
2.3	Parameters for Muscle Model 3	53
2.4	Parameters in Model for Passive Structures ...	57
2.5	Minimum Times Obtained Using Models 1 - 5	70
3.1	Computer Running Times for Problems 1 - 4	116
4.1	Parameters in Muscle Model for Dynamic Optimization	153
4.2	Parameters in Model for Passive Elements	156

CHAPTER I

INTRODUCTION

1.1 INTRODUCTION AND MOTIVATION

The subject of this dissertation is the determination of forces in the musculoskeletal structure, specifically the muscles and the joints. The research which has been carried out focuses on the use of theoretical models to predict muscle force histories and methods of solving these theoretical models.

The mechanics of muscle is a problem of fundamental interest in physiology and biomechanics, and has great practical importance as well. Being able to understand or predict muscle forces would allow the medical community to better deal with a number of serious problems. One is the problem of muscle dysfunction and how it affects motion ability. An allied area which is new and very promising is the use of electrical stimulation of muscles to generate musculoskeletal motion in paralytics. Another problem relates to the loads that must be borne by articulating joints, and the design of prosthetic joints that can withstand these loads. Since the forces in the muscles largely determine the joint forces, predicting the joint forces requires predicting the muscle forces.

In this research the work has concentrated on the

lower limb. Two aspects of the problem of muscle force determination have been studied, the effects of muscle model complexity, and methods of solving the dynamic optimization problem. These areas have been examined in the context of two kinds of problems involving the swing phase of the lower limb motion : 1) an optimal time kicking problem and 2) the swing phase of gait.

To study these kinds of motion, the musculoskeletal system is typically modelled as a series of connected rigid links actuated by internal force generators.
An appropriate model for the skeletal subsystem is depicted in Figure 1.1. The head, neck, arms and trunk are lumped together to constitute a single rigid body (HAT). The other portions of the subsystem are the right and left thighs, shanks and feet. If each foot is assumed to be a single rigid body, then the system can be described by the seven rigid bodies shown. In general the hip joint can be adequately modeled by a ball and socket joint. The general motion at the knee includes a combination of rotation and sliding motions. To a first approximation it suffices to consider the knee as a hinge joint. The ankle joint can be treated likewise.

The lower extremity skeletal subsystem described above is actuated by over 47 force generating members (muscles) on each side [14]. On the whole 31 of these muscles cross the hip joint, 13 cross the knee joint and

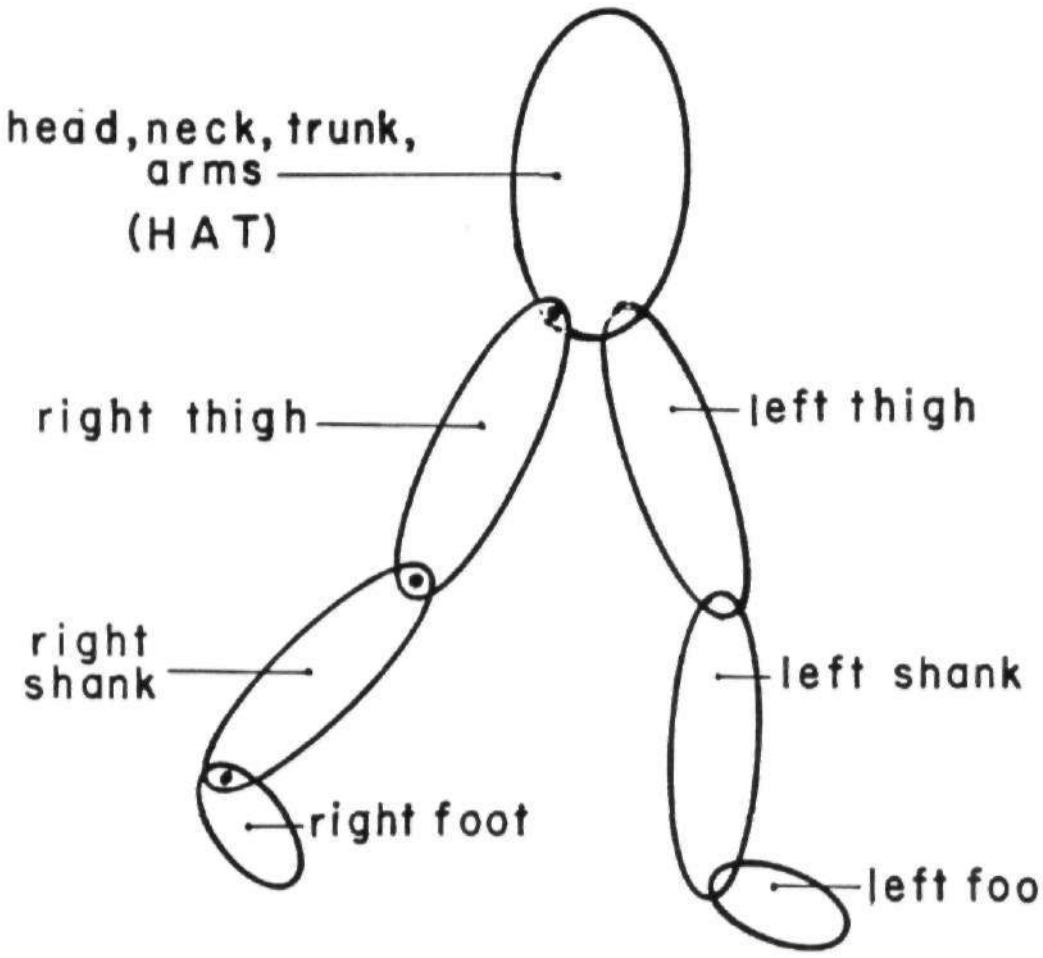


Fig. 1.1 Model of an Anthropomorphic figure showing the left and right shank, thigh and foot. The head, neck, arms and trunk are lumped into a single rigid body -- HAT.

12 cross the ankle joint. A single limb of the subsystem described above will have five degrees-of-freedom and hence can be modeled by at most five independent equations of motion. Consequently, it is impossible using laws of mechanics alone to obtain values of the individual muscle forces during a motion activity. This is the indeterminate problem of muscle force sharing. In addition, noninvasive techniques of measuring muscle force such as electromyography (EMG) do not provide the quantitative accuracy required; nor do they permit access to all the muscles of interest.

Two basic approaches have been used to solve the indeterminate problem of predicting the forces in the muscles. The first of these approaches is to reduce, by anatomic and functional simplification, the indeterminate problem to a determinate problem or to a number of determinate problems [49]. The second commonly utilized approach is to estimate the muscle forces by optimizing (minimizing or maximizing) some kinetic criterion . These optimization techniques also often necessitate some anatomic simplification but not to the same extent as in the first approach.

Part of this research work is related to the second approach to solving the indeterminate problem.

The gait cycle is generally divided into two distinct phases - the stance phase which takes up about

64 percent of the cycle and the swing phase which takes up the remaining 36 percent. During the stance phase one foot is continuously on the ground. During a part of this time the opposite limb is freely swinging in space. As the swinging limb is brought into contact with the ground, there is a short period when both feet are on the ground. This is called the period of double support. Shortly after, the supporting limb goes into swing while the other supports the body. Repetition of this process results in forward progression.

Chow and Jacobson [10] have shown that the optimal control problem of gait analysis can be separated into three sub-problems corresponding to the stance, swing and deploy phases of gait. The resultant cost function for the whole gait cycle is taken as the sum of the costs incurred in the three phases. Since the main purpose of this research is to compare the predictive ability of models of the muscular subsystem and to examine the computational aspects of gait analysis using these models, the swing phase of gait alone will be considered.

In this research it is assumed that the kinematics of the pelvis are specified. Hence along with the assumption that only the swing phase is of interest, it suffices to consider only a single limb of the subsystem. In general there is some amount of movement in every plane. However for this and many studies, it is assumed

that the main movement is that in the saggital plane. Such an assumption considerably decreases the size of the problem. It will shortly be demonstrated that if the problem is now cast as an optimal control problem the storage requirement of the computational problem becomes large. A further simplifying assumption that was found useful is that of lumping the muscles according to their functional groups. Such a grouping was carried out in this research work and resulted in a nine member subsystem acting as actuators for the resultant three-degree-of-freedom skeletal subsystem. The nine muscle groups are : the iliopsoas group made up of the psoas and the iliacus, the hamstring group made up of the semitendinosus, the semimembranosus, and the long head of biceps femoris, the vasti group made up of vastus intermedius, vastus lateralis and vastus medialis, the rectus femoris group, the gastrocnemious group, the soleus group, the tibialis anterior group, the short head of biceps femoris group and the gluteus maximus group. The final form of the model along with the nine muscle groups is depicted in Figure 1.2.

1.2 STATEMENT OF THE PROBLEM

The purpose of the research was to investigate the potential for developing a practical model of the

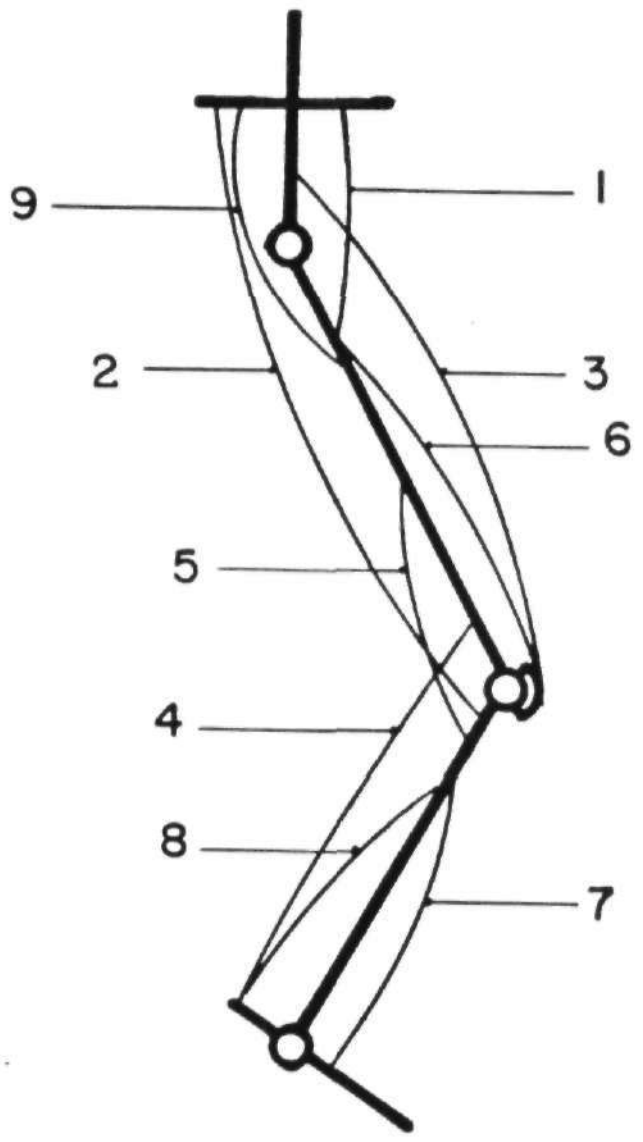


Fig. 1.2 Three-degree-of-freedom Lower limb model. Muscle groups 1 through 9 are described in text.

musculoskeletal system in application to the problem of deducing the forces in the elements of the system (muscle and ligament forces, joint contact forces) in the normal motion of human subjects. A specific product of the work was to be a computational model which would permit the determination of the forces in the elements acting across the hip, knee and ankle during gait.

The model was to incorporate macroscopic aspects of muscle mechanics and muscle control inputs that reflect a realistic synthesis of accepted microscopic muscle models. The model was to allow as well for the incorporation of optimal control models which would have the potential of accounting for more realistic optimality criteria, such as the physiologic energy expenditure.

The final product of the research, the computational procedure in the form of a computer program, was to be used in some preliminary analyses of gait for normal subjects. The evaluation of the model was to be accomplished by comparison with present models, and where possible by comparison with the measured electromygraphic signal information from gait analysis subjects.

The specific problem to be addressed is the problem which includes the following factors. Assume that the following information is known for a given history of musculoskeletal motion:

1. Kinematic history of all moving segments.
2. Inertial and morphological data for all segments.
3. Time histories for all applied external forces, such as forces of contact with surrounding structures.
4. The force-elongation characteristics for the passive internal load carrying structures such as the ligaments.
5. The nature and degrees-of-freedom associated with all joints between adjacent segments.
6. It will be presumed that from the above data the values for the muscle lengths, muscle contracting/lengthening speeds, and the forces in the ligamentous structures can be calculated at any point in time. Therefore their histories over the musculoskeletal motion history of interest are completely known.

In addition to the above, assume that the model for the muscle forces in terms of physical muscle parameters and muscle control models in terms of one or more control parameters (e.g. stimulation rate and stimulation amplitude) are given. Finally, it is assumed that a measure of optimal performance such as an energy consumption measure is described in terms of analytical functions of the state and control variables for the musculoskeletal system.

The problem to be solved from the above data was then the histories of the control parameters and the muscle forces which satisfy the constraint equations of the system and minimize the optimal criterion. The unknown joint contact forces can also be determined.

Specific Aims

1. To review the current state of the art for research in i) the models for individual muscle mechanics, both microscopic and macroscopic; ii) the models for neural control of muscle activation; iii) the models for rigid body dynamics of gross musculoskeletal motion; iv) the methods of solution for the indeterminate problem of inverse dynamics using optimization or optimal control algorithms.

2. To examine the current models generally corresponding to the ones proposed by Chow and Jacobson [10], and the later models by Hatze [21], to evaluate the magnitude of the resulting computational model for major musculoskeletal subsystems, such as the body undergoing gross motion in gait. As part of this aim an attempt should be made to determine the number of unknowns which would necessarily be solved in the solution procedure. Another aspect of this work would be to evaluate the nature of the currently used solution algorithms relating to the solution of the optimal control problem, and to investigate possibilities for

other solution techniques.

3. To propose a specific format for the contractile element model in the muscle model, and for the measure of energy consumption for the motion of musculoskeletal systems.

4. To solve the muscle force sharing problem using the derived muscle model and the rate of energy consumption as the objective function. To compare the results with a typical gait data for normal subjects.

1.3 REVIEW OF THE LITERATURE ON MUSCLE MODELING

The literature on muscle mechanics is so vast that a detailed survey would be an undertaking far beyond a reasonable scope for this dissertation. This section will review some of the major developments that lead to present day models.

One of the early attempts at the quantitative description of muscle mechanics was made by Hill [24]. While analysing his experiments on frog muscles, he made two observations. First, he observed that the velocity of shortening of active muscle is a function of the force it generates. Secondly, that after a single stimulus the muscle becomes fully active for a more or less fixed period of time. Based on these observations he proposed a model of the mechanical activities of muscle consisting

of two components -- one active component which he called the contractile element and one passive elastic component in series with the active component. This latter component is called the series elastic element. While analyzing some of his experiments on muscle thermodynamics Hill [25] deduced a relationship between the heat produced by an isometrically contracting muscle and its velocity of contraction. This relationship leads to the now famous Hill force-velocity relationship. This relationship forms the building block on which many present models are built. The relationship is used mainly to characterize the dynamic behavior of the contractile element. The necessity for a series elastic element was inferred from data such as the Levin and Wyman experiment [39], which showed that there was an instantaneous length change in the muscle for sudden changes in the applied load.

The active state in Hill's force-velocity relationship was assumed to be a constant function of time, and is identified with the maximum isometric force of the muscle. This quantity was obtained by fully stimulating the muscle while it is at its optimum length (which is close to the rest length). Thus at a different level of stimulation and at a different length, the muscle is expected to be at a different active state. This idea was realized by Ritchie and Wilkie [53] who

extended Hill's model by modulating the active state with a function of the length of the muscle and a function of time. They did not derive any mathematical relationships to describe these quantities. However the force-length relationship was obtained experimentally for the contraction phase of activity and depicted graphically. Also the authors did not attempt to use their model to study a gross musculoskeletal motion activity but used it to study some of the intrinsic characteristics of muscle.

A modeling procedure that was based on mammalian rather than amphibian muscle was that of Bahler [2]. He proposed a model of the contractile element in which the output of the element is a function of the length, velocity of contraction and duration of stimulation. He based his model on Hill's two element model. In addition, he modeled the series elastic element by a cubic function of the force and the length-tension relationship by a quadratic function of the length of the contractile element. A step function of time and stimulus frequency was used to model the stimulation-time relationship. Bahler's model came close to describing the excitation dynamics of the muscle in addition to the contraction dynamics as defined by the force-velocity and the force-length relationships. However, his excitation dynamics (as defined by the stimulation-time function) had no physiological basis.

Besides the absence of a physiologically based excitation dynamics for all the models discussed thus far, one other drawback is that the force-velocity relationships were only useful for the shortening phase of contraction. For the lengthening phase the models break down. This is because the hyperbola used to describe Hill's force-velocity relationship increases continuously for positive (lengthening) contractions; whereas experimental evidence has shown that muscle exhibits yielding for such velocities [56]. By muscle yielding it is meant that at positive contraction velocities the length of the muscle increases for no change in the force produced.

The question of excitation dynamics requires an understanding of the underlying mechanism of the excitation-contraction coupling. The works of Ebashi and Endo [17] and other biochemists strongly point to the fact that the presence of calcium in muscle tissue is intimately connected with the excitation-contraction coupling. Taylor [57], was one of the first people to take advantage of this fact in modeling the excitation dynamics of muscle. He proposed that the maximum force (active state) in Hill's model is a measure of the active state and that the magnitude of the active state is proportional to the concentration of the complex of calcium with the muscle machinery. He went further to

account for relaxation in his model by postulating the presence of a carrier pump mechanism for removing calcium from the sarcoplasm of the muscle fiber. Based on the chemical kinetics of the bound calcium and that of the carrier pump, he derived a set of three differential equations ; and along with Hill's force-velocity relationship, he defined the complete dynamics of the contractile element using four first order differential equations. These equations were programmed on an analog computer and the ability of the model to predict some of the intrinsic characteristics of muscle (quick release, re-development of tension etc.) were studied. The model was found to predict muscle behavior with a good degree of precision; however no attempt was made to validate the predictive ability of the model on gross musculoskeletal motions.

Hatze [21] in his study of kicking motions proposed a model whose excitation dynamics closely follows that of Taylor. He also defined the active state in his model as the amount of calcium bound to troponin (a muscle molecule which is associated with the phenomenon of contraction and force production). In addition, the model was that of a muscle fiber; and that the recruitment of fibers in a given muscle constitutes part of the excitation dynamics of the muscle. In his model, he also modified Hill's force-velocity relationship to include

the effect of muscle yielding during lengthening (eccentric contractions). This was done by using the hyperbolic tangent function rather than the hyperbola of Hill's equation. Hatze's muscle model was made up of three first order differential equations that define the excitation and contraction dynamics. Contrary to the other workers who validated their models on the intrinsic properties alone, he validated his model on a gross musculoskeletal motion. The problem he solved was a minimum time kicking problem. The various advantages and disadvantages of this model will be discussed further in Chapter 2.

The earlier model was subsequently modified by Hatze [23] to include the phenomenon of recruitment in further detail. This resulted in a muscle model defined by five first order differential equations.

A simpler model of the contractile element is proposed in this research which while preserving many of the good features of Hatze's models avoids some of their disadvantages.

In summary it is appreciated from this review that the major aspects in modeling the muscular subsystem involve properly identifying the main characteristics of the subsystem. The two obvious ones are the excitation dynamics and the contraction dynamics. It could have been possible to use pre-existing models for gait analysis;

however, our experience with some of them shows that doing this would lead to enormous computational costs.

1.3.1 Feedbacks in the Neuromuscular Subsystem

It should be mentioned that in general the human neuromuscular system is characterized by a number of feedback loops. These feedback loops include displacement, velocity, tension, visual feedbacks among others. The signals from these loops are decoded at the central nervous system (CNS), and integrated and used to regulate the activities of the whole system with respect to its environment. A simplified diagram for the feedback loop of a single muscle is shown in Figure 1.3. The presence of the feedback loops implies that in general the control inputs to the muscles are functions of the state variables (feedback controls). In this research work, these feedback loops are not included in the modeling procedure. The generated control inputs to the muscles are therefore taken to be the lumped effects of the actual inputs to the system and the effects from the feedback loops. The dotted box in Figure 3.1 shows the portion of the system which is being investigated.

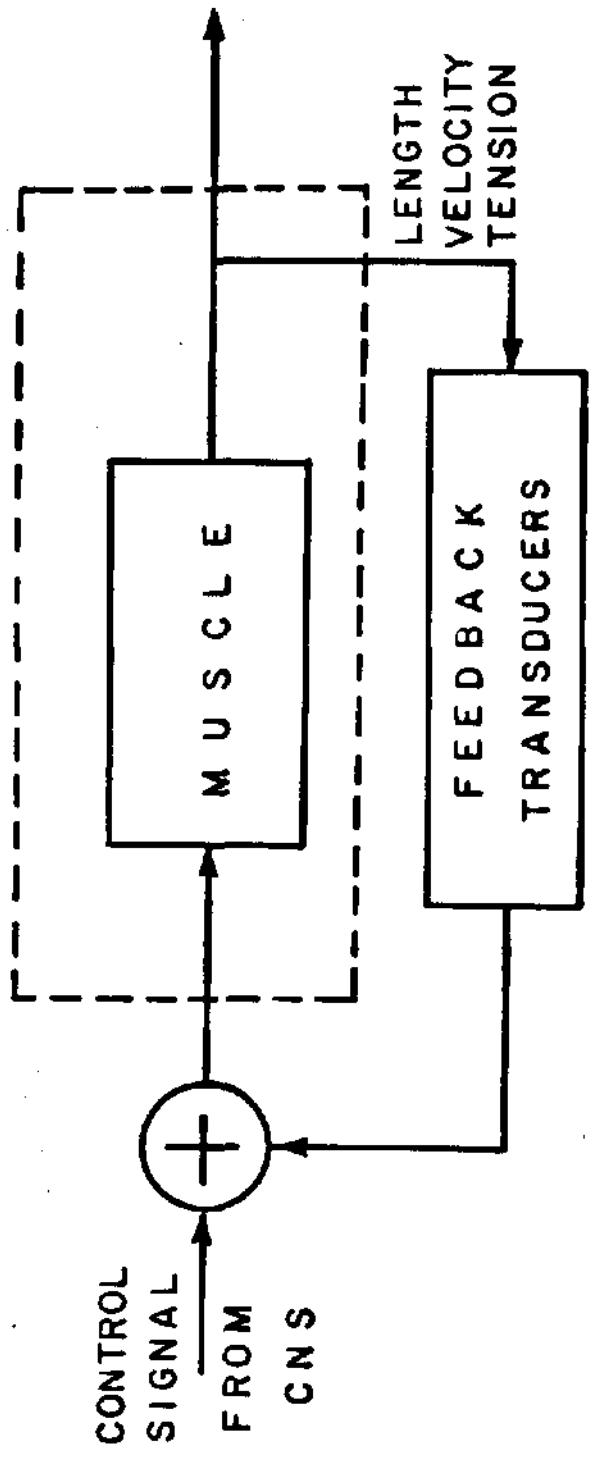


Fig. 1.3 Feedback loop of muscle control system.

1.4 REVIEW OF THE LITERATURE ON GAIT ANALYSIS BY OPTIMIZATION TECHNIQUES

One of the first attempts to apply some principle of optimality to the solution of muscle force sharing was made by Seireg and Arvikar [54]. These authors attempted to find the muscle forces necessary to maintain the body in equilibrium in standing, leaning and stooping postures. To this effect, they modeled the lower limb by four rigid bodies -- the torso, the thigh, the shank and the foot. The muscular subsystem in their study was modeled by 29 members which were modeled by straight line force generators. The resulting problem in their study was defined by 21 static equilibrium equations in over 50 unknowns. They examined four different types of objective functions which are all linear in their arguments. This allowed them to solve the resulting problem using the familiar techniques of linear programming.

Another muscle force sharing problem was proposed by Penrod et al [52]. This time the authors attempted to solve the muscle force sharing problem at the wrist. Their model consisted of a four tendon biaxial system. (They also considered a seven tendon model). The objective function in their case was also linear in the muscle forces again allowing them to use the linear programming algorithm for solving the problem.

At this time, Seireg and Arvikar [55] have resumed their studies on the use of optimization in gait analysis. This time they considered a larger model of the lower extremity which consisted of seven rigid bodies actuated by 31 muscles. The resultant problem was defined by 42 equilibrium equations in 146 unknowns.

Crowninshield et al [14] attempted to solve the muscle force sharing problem by considering a model of the lower extremity and paying special attention to the hip joint. Their model which consisted of 4 rigid bodies was actuated by 30 muscles - 27 crossing the hip, 8 crossing the knee and 2 crossing the ankle. The resultant model had 8 scalar equations of motion in 33 unknowns. An objective function which is linear in the muscle forces was used. This time however, the sum of muscle stresses (muscle force per unit cross-sectional area) was used as the objective function. An upper bound was placed on the muscle stresses in addition to the lower bound of zero.

Pedotti et al [50], in their study of the muscle force sharing problem included a substantial amount of muscle physiology. For instance, they calculated the instantaneous maximum force in the muscle taking into account the contraction velocity. They obtained values for these later quantities by using a modified Hill force-velocity relationship and force-length relationship. Their model of the skeletal subsystem also

takes into account all the inertia and other dynamic forces, although these quantities were calculated and used at instantaneous points in time. The authors studied four different types of objective criteria - the sum of muscle forces, the sum of squares of muscle forces, the sum of normalized muscle forces and the sum of squares of normalized muscle forces.

Many of the subsequent attempts at solving the muscle force sharing problem using static optimization were more or less modifications of the works of Crowninshield et al [14] and of Pedotti et al [50]. One such modification was due to Hardt [20]. In his study Hardt considered the lower limb as a system of three rigid bodies -- the thigh, the shank and the foot. The hip and ankle were modeled as ball and socket joints while the knee was modeled as a hinge joint. The model was actuated by 31 muscles. One of the major merits of Hardt's model is the choice of objective function. He derived an equation which was a measure of the metabolic energy consumption. This function turned out to be a sixth degree polynomial in the contraction velocity of the muscle. To take advantage of the linear programming algorithm, however, he had to use a linearized version of this function.

The work of Hardt had set the pace for abandoning the usual ad-hoc fashion of choosing an objective

function. People now began to seek for an objective function that has more physiological meaning. One of such works is that of Crowninshield and Brand [15]. These authors derived an objective function which is a measure of the muscle endurance. This measure turned out to be the sum of cubes of the muscle stresses. One of the major advantages of this function is that it has a tendency to allow for predicting muscle activity in numerous muscles and selecting preferably those with large cross-sectional areas.

Another work which evolved from the work of Hardt was that of Patriarco et al [48]. In this study, the authors removed the linearity assumption used by Hardt and proceeded to use the sixth order polynomial mentioned earlier. One of the interesting findings of this study is that the precision in calculating the joint moments is a more dominant factor in the solution process than the choice of the objective function.

1.5 REVIEW OF THE LITERATURE ON OPTIMAL CONTROL IN GAIT ANALYSIS

The first major step in the analysis of gait using dynamic optimization techniques was made by Chow and Jacobson [10]. These authors gave a detailed analysis of applying the principles of optimal control theory in

analysing human locomotion. They considered a model of the skeletal system made up of 3 linkages -- the torso, the thigh and the combined shank and foot. Simplification in the solution process was obtained in a number of ways. First, the assumption that the trajectory of the pelvis is specified and the pelvis moves forward with a constant velocity led to the complete decoupling of the two limbs that constituted the lower limb subsystem. Secondly, the whole gait cycle was divided into three phases and the optimality criterion applied to each phase separately. Thirdly, the muscle model proposed was linearized about some nominal muscle characteristics. Finally, the assumption that the ankle was locked throughout the cycle led to further reduction in the dimensionality of the problem.

Another attempt to handle the gait problem using optimal control was made by Chao and Rim [8]. These authors considered a three limb model of the lower limb. Their major pre-occupation however was restricted to solving the inverse dynamics problem of gait; which was to calculate the joint moments required to produce a given kinematic history of the system. To solve this problem the authors cast it as an optimal control problem in which the unknown joint moments were the control variables. The objective function which was to be minimized was the sum of squares of the errors between

the specified and the generated trajectories of the limbs.

In his attempt to validate his muscle model Hatze [21], proposed the minimum-time kicking problem. In this work the author modeled the lower limb as a system of three rigid bodies -- the pelvis (which was fixed), the thigh and the combined shank and weighted foot. The system was actuated by five muscle groups. The objective was to minimize the time required to hit a target from an initial free hanging position of the limb.

Part of the objective of this research is to consider the possibility of incorporating some of these concepts into the muscle force sharing problem of gait analysis.

In the following three chapters are presented the results of the three major aspects of the present research. Chapter 2 is concerned with the problem of muscle model complexity. To examine this problem we chose to use the kicking problem proposed by Hatze [21]. This is because this problem has been fully documented in terms of the general details of the problem and the experimental aspects as well. In Chapter 3 a comparative study of some optimal control algorithms is carried out in order to examine their suitability for solving gait analysis problems. Chapter 4 is concerned with solving the muscle force-sharing problem for the swing phase of

gait using dynamic optimization techniques. Chapter 5 gives a brief summary of what has been accomplished in this study. Some recommendations for future research are also given.

CHAPTER II

THE INFLUENCE OF MUSCLE MODEL COMPLEXITY IN MUSCULOSKELETAL MOTION MODELING

2.1 INTRODUCTION

One of the major problems in modeling large scale problems of musculoskeletal motion is that of describing the actuators, i.e. the muscles, with appropriate models. Numerous muscle models have been proposed in the literature. These models can be divided roughly into two classes. On the one hand are the molecular models which range in complexity from the simple molecular model of Huxley [28] to the considerably more complex models such as that of Hill [26]. On the other hand are the so-called phenomenological models which also range in complexity from simple models such as the linear viscoelastic models [12] to the extremely complex models such as that of Hatze [23]. Theoretically, gross muscle models simply built up directly from the molecular models should represent the best choice because of their explanatory nature. However, attempting to develop gross muscle models by building up in a straightforward way from these molecular models results in overwhelming complexities for practical applications [62]. Consequently, recourse must be made to the more tractable

phenomenological models in gross musculoskeletal motion.

The problem which has been of concern is the problem of describing the dynamic muscle force sharing during musculoskeletal motion. In particular it is of interest to examine the influence of muscle model complexity on the predicted histories of limb kinematics, muscle force histories and joint contact forces during musculoskeletal motion.

It was recognized in the early studies of musculoskeletal dynamics that actual prediction of the muscle force histories could not be done in a straightforward way because of the redundancy of the load-sharing system. In order to overcome this problem a number of researchers have resorted to passive optimization schemes to distribute the resultant forces among muscles across a joint on the basis of optimizing an objective function stated in terms of the muscle forces or stresses [52,54]. The advantage of such an approach is that it is relatively straightforward, and the problem size does not become overwhelming even when several dozens of muscles are included in the model.

The use of optimal control techniques has been much more limited in attempts to determine the problem of muscle force sharing. Chao and Rim [8] used joint torques as actuators in an early model. Subsequently Chow and Jacobson reported using joint torques on a more

complex model [10]. Although these models avoid some of the shortcomings of the passive optimization models in that they reflect optimization over the full history of motion, there is reason to believe that they have not been adequate because the dynamics of the muscle subsystems with their characteristic time lags are ignored.

In the recent work by Hatze [21] an attempt has been made to incorporate highly sophisticated muscle models and optimal control techniques into the solution of muscle force sharing problems. Although the elegant muscle models proposed by Hatze [23] hold promise for much more accurately describing many of the recognized characteristics of muscles, their use in even moderately sized problems appear to lead to enormous computational costs. As a consequence, these models probably preclude their use on moderately sized computing machinery which might be available to most of the biomechanics research community.

The above considerations have provided the motivation for the study which is reported here. The purpose of this chapter is to examine the significance of tradeoffs in muscle complexity, computational results, and computational costs using musculoskeletal actuator models of varying complexity. For purposes of comparison, the minimum time kicking problem described by

Hatze [21] has been used. Details of the statement of this problem and a solution can be found in Hatze [21]. The one major difference is that a true optimal control algorithm has been used in the present study. By this is meant that a fully automated solution algorithm is implemented rather than the interactive procedure used by Hatze [21]. Results are presented for four different actuator models. The advantages and disadvantages which were experienced using the various models are discussed, as well as the implications for parameter estimations in the modeling problem.

2.2 PROBLEM STATEMENT

The minimum time kicking problem has been posed by Hatze [21]. In this problem the dynamic musculoskeletal subsystem consists of a single lower limb which can move in the saggital plane by motion about the hip and knee. The resulting two-degree-of-freedom system is activated by five muscle groups (Figure 2.1). Group 1 consists of the iliacus and psoas (iliopsoas) muscles. Group 2 consists of the vasti (vastus lateralis, medialis and intermedius). Group 3 consists of the rectus femoris. Group 4 consists of the hamstrings (semitendinosus, semimembranosus and the long head of biceps femoris). Group 5 consists of the gastrocnemius, the short head of

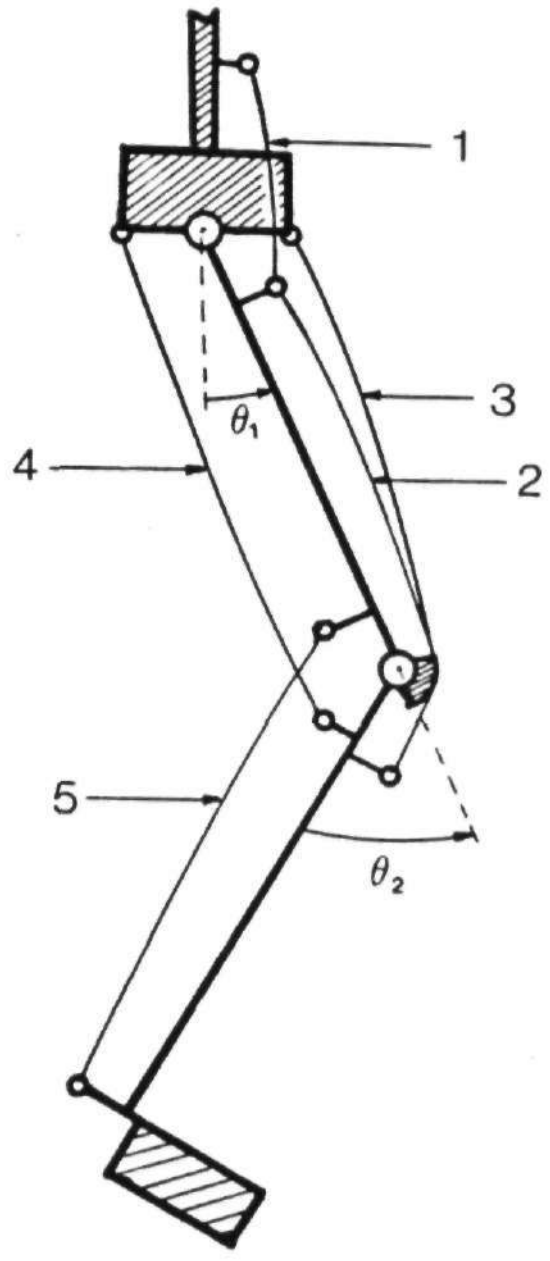


Fig.2.1. Lower limb link model. (After Hatze [21]). Two-degrees-of freedom are defined by angle θ_1, between fixed trunk and thigh segment and angle θ_2 between thigh segment and shank/foot segment. Muscle groups 1 through 5 are described in text.

biceps femoris and the popliteus.

The minimum time problem consists of starting from an initial free-hanging limb position and moving the limb forward to a final fixed position as quickly as possible. At the final point, both hip angle θ_1, and knee angle θ_2 (Figure 2.1) are specified and knee velocity $\dot{\theta}_2$ is zero. The solution for the problem defines control histories for the muscle actuators such that the kicking time is minimal and the final conditions are satisfied within some tolerance. The control inputs vary according to the model complexity, but typically represent normalized stimulation rates. The corresponding mathematical statement of this optimal control problem follows in a subsequent section of this paper. The equations of motion for the two-degree-of-freedom linkage are readily derived using d'Alembert's Principle. The results are summarized in Appendix 1.

2.3 MUSCLE MODELS

In the context of this problem four muscle models of varying complexity have been considered. Models 1 to 3 are described in detail below, and model 4 is Hatze's model [21] and is only briefly treated. In each case, there is a single control input to each actuator which is considered to be stimulation frequency. Hatze's original

model included two control parameters, frequency and recruitment rate. However, their histories were identical in the solution so they may be regarded as a single input.

In addition to the models of muscle actuator groups, a fifth model was examined in which the actuators and controls were the two joint torques.

All of the link and many of the muscle parameters used in the original study by Hatze [21] were specific to the experimental subject. Because of that as many of these parameters as are deemed necessary to permit model comparisons are retained in this study. The remaining parameters were chosen so that they matched as closely as possible features which were common among models, for example, parameters were chosen so that isometric force capabilities were matched, and others chosen to match stimulation response times of the muscles.

Model 1

This model assumes that the whole muscle is a simple force generator in parallel with a spring and a dashpot. The two latter elements represent the passive properties of the muscle. Figure (2.2) shows a diagramatic representation of the model.

The force output of the generator is modeled as

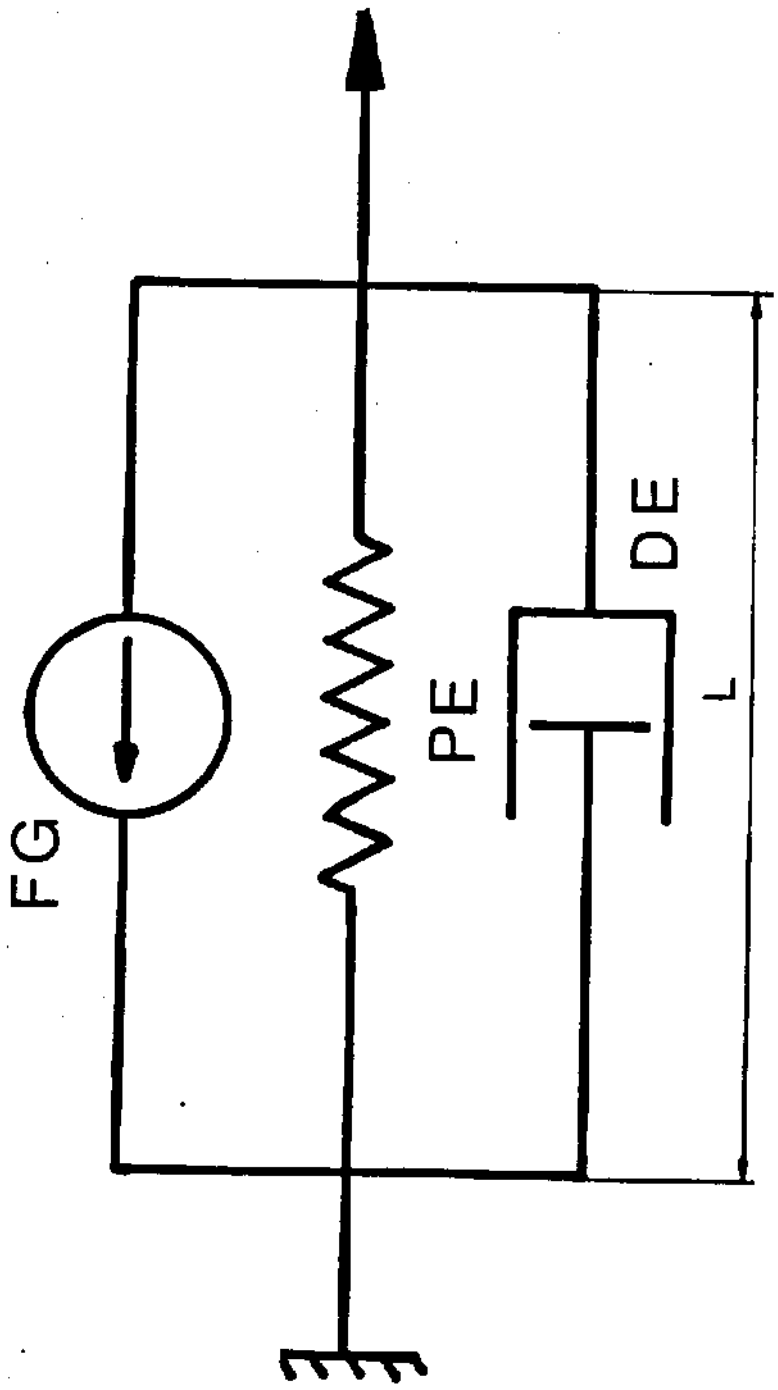


Fig. 2.2 Muscle model 1. Model consists of force generator FG, elastic element PE and damping element DE in parallel. L is the total muscle length.

$$F^G(g,L) = F^G_{max} f(g(s),L) \qquad (2.1)$$

The excitation dynamics of the muscle is defined through the function g(s). In this case, there are no well defined contraction dynamics. The contraction of the muscle is therefore directly proportional to the excitation. Using similar concepts as those defined by Hatze [21] we define the function g(s) as the normalized calcium ion concentration which is controlled by the normalized stimulus rate s. L is the total length of the muscle from origin to insertion, and F^G_{max} is the maximum force capability of the muscle. It is required that at full stimulation and at optimum length of the muscle the force generator produces maximum force, i.e.

$$F^G_{max} = F^G(1,\bar{L}) = b_5 \qquad (2.2)$$

where $\bar{L}$ is that length at which a fully stimulated isometrically contracting muscle reaches its maximum force capability. This quantity is usually calculated by using the relation $\bar{L} \approx 1.2\ L_0$ [11] where L_0 is the rest length of the muscle.

The measure of muscle activity f(g,.) can be associated with the chemistry of contraction; for instance as the amount of calcium ions bound to the contraction molecular structures. This idea of

associating the 'active state' of the muscle with the calcium bound to contraction molecules was proposed by Taylor [57] and later modified by Hatze [21]. The influence of muscle length and active state on the force generator output have typically been experimentally examined separately by fixing either one and varying the other [53]. Correspondingly, we follow the approach used by others [22] and represent their combined influence in the model as a separable function:

$$f(g,L) = f_1(g) f_2(L) \tag{2.3}$$

Appropriate expressions for $f_1(g)$ and $f_2(L)$ have been derived by Hatze [23] and are of the form

$$f_1(g) = 1-a_o(m_1\exp(m_2 b_1 g)-m_2\exp(m_1 b_1 g))/(m_1-m_2) \tag{2.4}$$

$$f_2(L) = \exp(-(L/\bar{L}-1)^2/b_2) \tag{2.5}$$

where a_o, m_1, m_2 are constants given below, and b_1 and b_2 are muscle specific parameters given in Table 2.1. The function $g(s)$ is chosen so that it satisfies the first order differential equation

$$\dot{g}(s) = b_3(b_4 s-g) \tag{2.6}$$

TABLE 2.1

Parameters for Muscle Model 1 (SI Units)

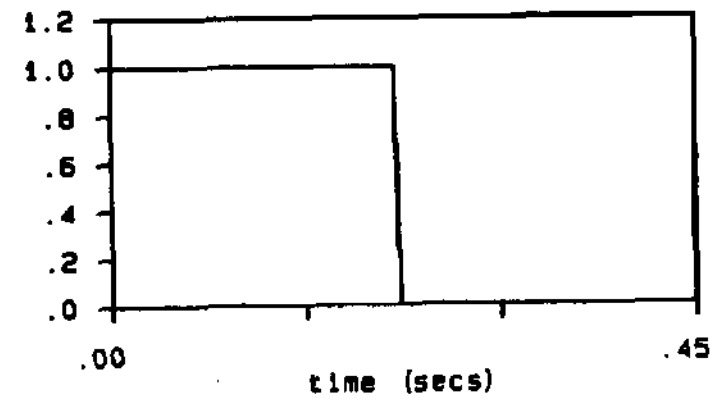
MUSCLE GROUP	1	2	3	4	5
b_1	8.5	4.1	5.2	4.3	2.2
b_2	.3	.3	5.	5.	.3
b_3	32.2	21.3	11.2	11.2	11.2
b_4	.83	.8	.8	1.	1.
b_5	4681.4	4572.7	1507.7	1076.0	519.
k_1	0.	0.	5.393	64.7	0.
k_2	0.	0.	90.4	23.95	0.
k_3	0.	0.	.58	.48	0.
k_4	0.	0.	0.	.0068	0.
k_5	0.	0.	0.	239.8	0.
k_6	0.	0.	0.	.53	0.
c	0.	0.	257.1	378.	0.

where b_3 and b_4 are muscle specific parameters given in Table 2.1. Figures 2.3a-c show typical responses of the model to an on-off excitation. Part a of the figure shows the on-off control s, part b shows the history of the corresponding normalized calcium ion concentration g(s), and part c shows the active state function $f_1(g)$. The maximum isometric force for this muscle is directly proportional to $f_1(g)$.

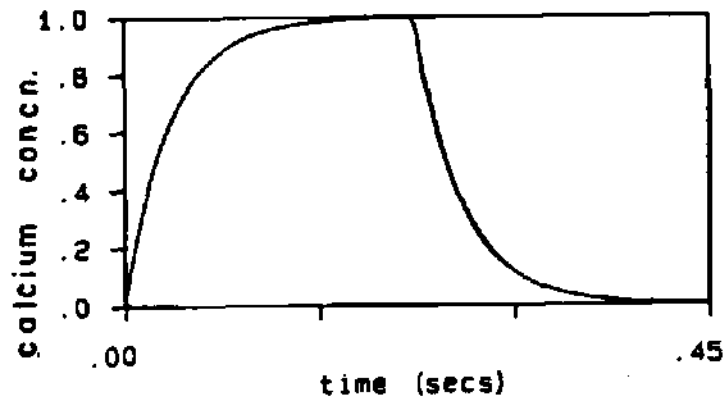
The parameters b_1, b_3, and b_4 were chosen using an interactive approach to fit the functions $f_1(g)$ and g(s) to the forms described in [23]. The parameter b_2 in equation (5) was chosen in a similar way to match the corresponding function, equation (2.28), in Hatze's muscle model (model 4 in this Chapter). The parameter b_5 is the maximum isometric force of the muscle obtained by multiplying the average cross-sectional area of the muscle with an average stress of 60 N/cm^2 [13]. It is suggested by Hatze [23] that the constants m_1, m_2 and a_0 be assigned the values -.73, -1.37 and .995 respectively.

The parallel elements were modeled in the same fashion as was done by Hatze [21] i.e.

(a)



(b)



(c)

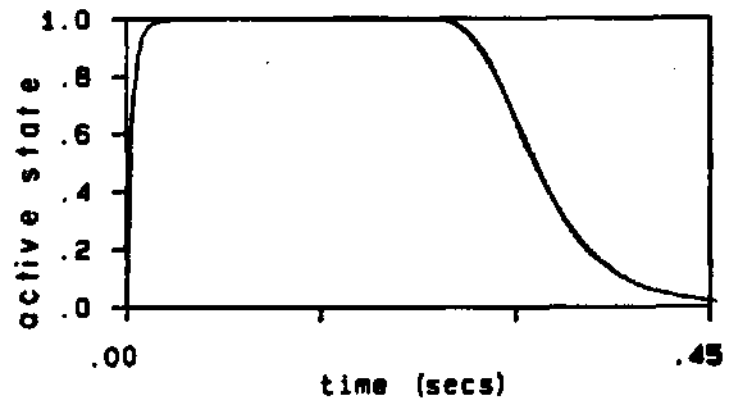


Fig. 2.3 Typical responses of muscle model 1. (a) applied on-off control, (b) resultant normalized calcium ion concentration and (c) active state function.

$$F^{PE} = k_1(\exp(k_2(L-k_3))-1)+k_4(\exp(k_5(L-k_6))-1) \quad (2.7)$$

$$F^{DE} = c\dot{L} \quad (2.8)$$

where k_1 through k_6, and c are subject specific parameters given in [21] and listed in Table 2.1.

These last two equations apply only to the two joint muscle groups since those for the one joint variety are incorporated into the passive joint torques. In these equations the parameters are subject specific.

The resultant force output of the muscle is then given by the expression

$$F^{M} = F^{G}(g,L)+F^{PE}+F^{DE} \quad (2.9)$$

Model 2

This is a four element lumped model of the muscle shown in Figure (2.4). The elements CE, SE, PE and DE are respectively the contractile element, the series elastic element, the parallel elastic element and the damping element. The equations and parameters for PE and DE are the same as those for model 1.

The SE element is modeled as a linear spring; and the CE is assumed to have a linear force-velocity relationship. Despite the fact that none of these

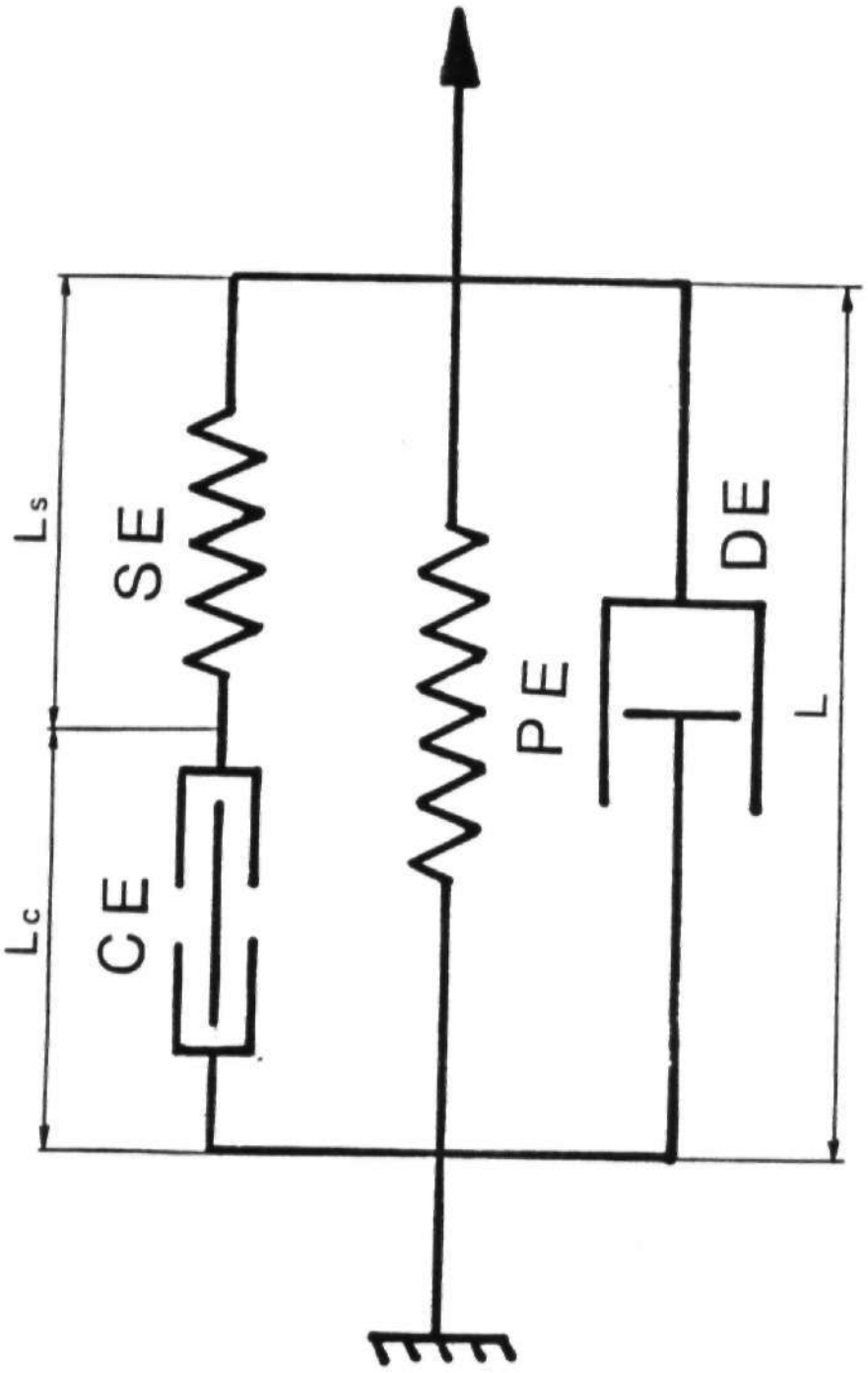


Fig. 2.4 Muscle models 2, 3 and 4. Model consists of a contractile element CE, a series elastic element SE in parallel with an elastic element PE and a damping element DE.

assumptions of linearity agrees particularly well with physiological reality, this model is treated here because there is a tendency to use linear (or linearized) models by researchers in this field [9], [47]. Along with equations (2.3) and (2.6), the equations for the model are given below.

Let the normalized length of the CE be given by

$$Q_c = L_c/\bar{L}_c \tag{2.10}$$

An appropriate expression for the linear force-velocity relationship of the contractile element will then take the form

$$v = aF^{CE} + b \tag{2.11}$$

where v is the contraction velocity, F^{CE} is the force generated by the contractile element and a and b are constants. The boundary conditions are that when $v = 0$, $F^{CE} = \bar{F}$; and when $F^{CE} = 0$, $v = v_{max}$. This leads to $b = v_{max}$ and $a = -b/\bar{F}$. The normalized form of this relationship takes the form

$$\dot{Q}_c = - b_6(1. - F^{SE}/\bar{F}) \tag{2.12}$$

where $b_6 = -v_{max}/L_c$ (shortening velocities are considered

negative).

In these equations L_c, $\bar{L}_c$, F^{SE}, $\bar{F}$ are the instantaneous length of the CE, the isometric length of the CE, the force in the SE and a modulated maximum isometric force respectively.

To incorporate the excitation dynamics of the muscle into the model, the maximum isometric force is modulated according to the length of the contractile element, the active state of the muscle and the geometrical orientation of the fibers of the muscle. An appropriate expression takes the form

$$\bar{F} = b_{10} f_1(g) f_2(L_c) f_3(Q_c) \qquad (2.13)$$

$f_3(Q_c)$ is a function of the type of muscle (fusiform or bipennate) and is given by [21]

$$f_3(Q_c) = [1-b_7/(b_8 Q_c - b_8 + b_9)^2]^{1/2} \qquad (2.14)$$

$f_2(L_c)$ is the same as equation (2.5) with L_c replacing L

The function $f_1(g)$ is the same as that defined in equation (2.4)

The force in the SE is given by

$$F^{SE} = b_{10}\,\delta \tag{2.15}$$

where

$$\delta = (L_s - L_{so})/(\bar{L}_s - L_{so}) \tag{2.16}$$

Hatze [21] has shown that this expression for δ can be written as

$$\delta = b_{13}[L-(Q_c b_8 - b_8 + b_9)^2 - b_{11})^{1/2} - b_{12}] \tag{2.17}$$

where $\bar{L}_s$, L_{so}, L_s are the optimum length, rest length and instantaneous length of the SE element respectively.

The parameters b_6 - b_{13} are given in Table 2.2. The parameter b_6 is the normalized maximum speed of contraction and is chosen to lie within the range 2. - 10. [23]. On some occasions, however, it was found that such a choice leads to numerical stability problems with the model. In such cases, slightly lower values are used. The other parameters in the model are the same as those used in Hatze [21].

Figures 2.5a-c show typical responses of this model to an on-off control input in an isometric simulation of the model. It is noted that even though the active state function is saturated, the isometric force does not reach the maximum possible value of 4400 N set for that muscle.

TABLE 2.2

Parameters for Muscle Model 2* (SI Units)

MUSCLE GROUP	1	2	3	4	5
b_5	3381.4	3172.7	717.7	1076.4	519.
b_6	1.9	2.1	3.	2.	1.4
b_7	0.	.07	.024	0.	0.
b_8	.08	.0408	.0583	.302	.038
b_9	0.	.14	.07	0.	0.
b_{10}	12250.	13683.	2780.7	3900.	1880.
b_{11}	0.	.0049	.0005731	0.	0.
b_{12}	.275	.19	.429	.487	.087
b_{13}	111.1	34.8	18.1	20.8	163.3

* The parameters b_1 to b_4 for all 5 muscle groups are the same as for model 1.

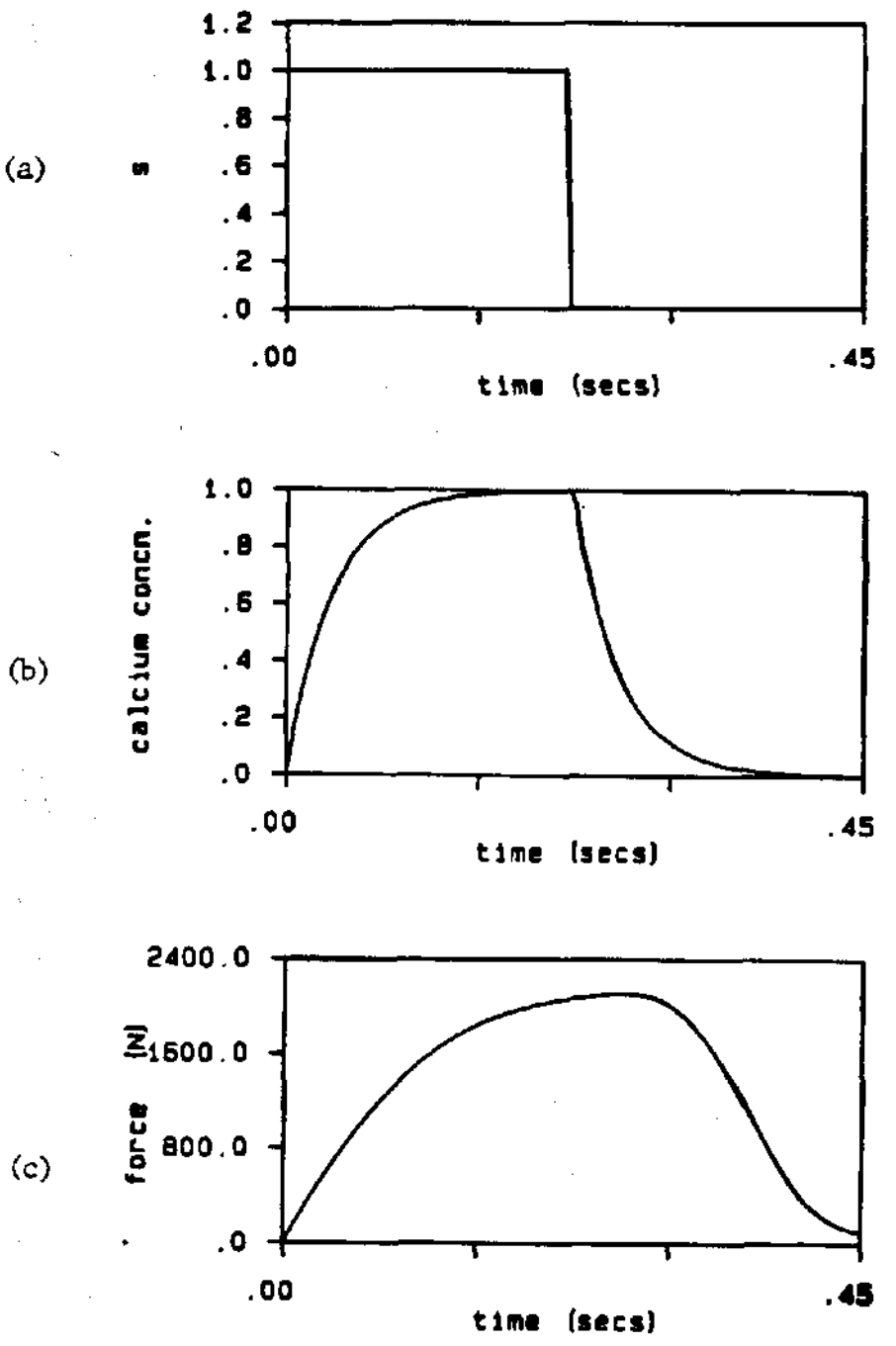


Fig. 2.5 Typical responses of muscle model 2. (a) applied on-off control, (b) normalized calcium ion concentration and (c) resultant isometric force.

Model 3

This is the same as model 2 except that the CE is assumed to have a hyperbolic force-velocity relationship (Hill's Force-Velocity relation) [24]. The SE is modeled as a nonlinear spring. The equations incorporating these features into the model are:

$$\dot{Q}_c = \begin{cases} -b_{14}(\bar{F} - F^{SE})/(F^{SE} + b_{15}\bar{F}) & \text{for } F^{SE} \leq \bar{F} \\ -b_{16}(\bar{F} - F^{SE})/(1.33\bar{F} - F^{SE}) & \text{for } F^{SE} > \bar{F} \end{cases} \quad (2.18)$$

where $\bar{F}$ is given by equation (2.13). The first portion of equation (2.18) matches the original Hill equation. The second portion models muscle behavior during eccentric (lengthening) contractions. The combined function closely matches the hyperbolic trigonometric function of model 4 (equation (2.24)), but was found to avoid some of the numerical stability problems encountered with the latter formulation.

A plot of the normalized form of this equation is shown in Figure 2.6.

The basis for the extension to the original Hill equation is from the equation

$$R = \alpha Q/(\beta + Q) \quad (2.19)$$

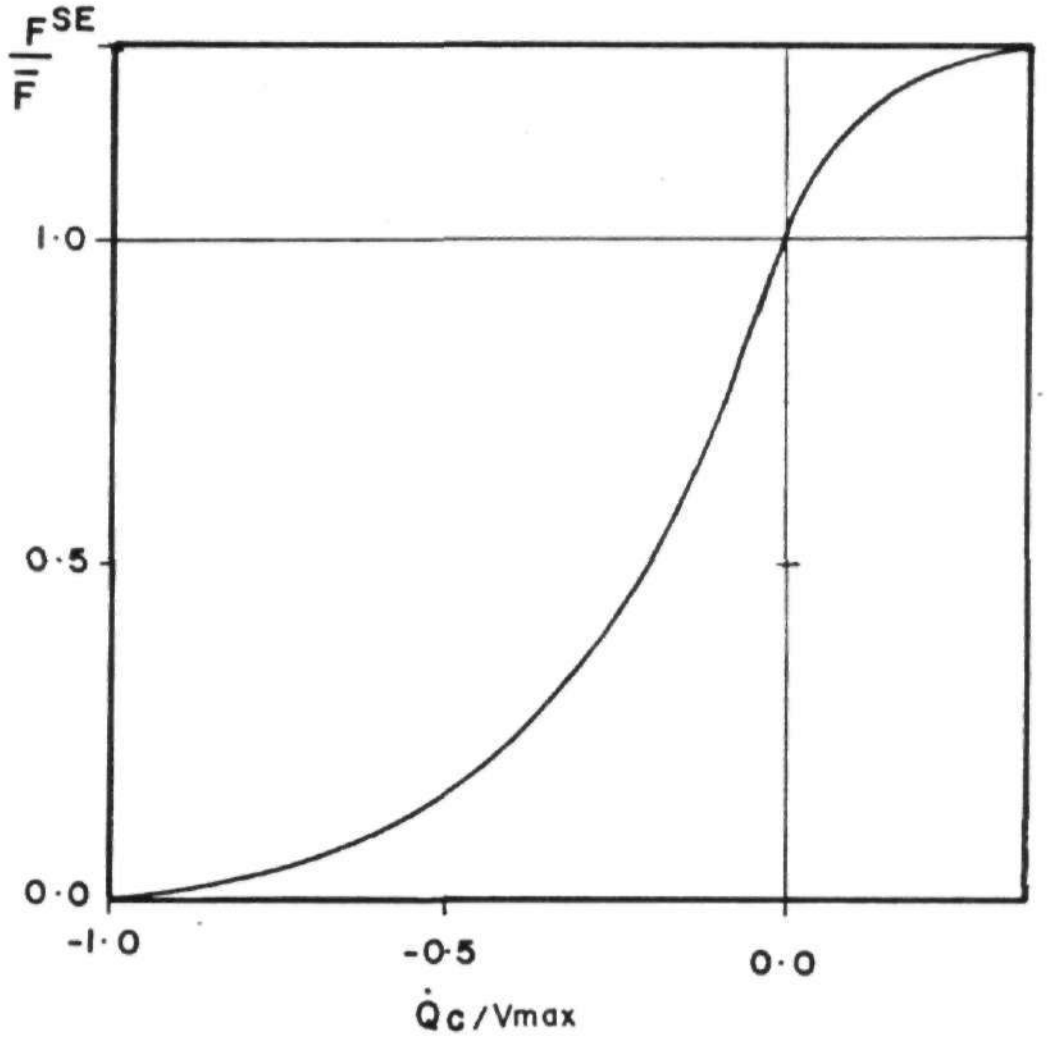


Fig. 2.6 Modified Hill force-velocity relationship. Relationship is normalized with respect to maximum isometric force F and maximum contraction velocity.

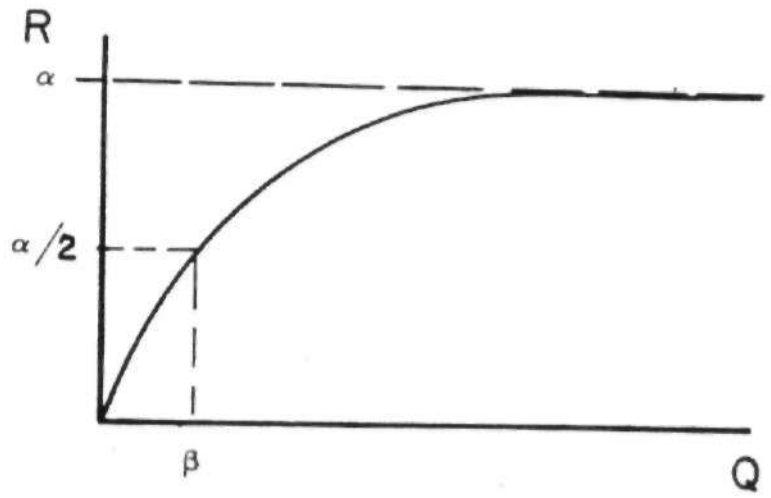
This relationship is plotted in Figure 2.7a. The parameter β is the value of Q at which R is equal half its maximum value and α is the corresponding asymptote. Another relationship that could have been equally used is the rising exponential. However, the use of the exponential leads to a logarithmic function when the contraction velocity is expressed in terms of the force. Such an expression could lead to the same numerical stability problems as the ones encountered with model 4 in this Chapter.

From equation (2.19) it is apparent that β determines the rate of rise of the function. To apply this equation to the force velocity relationship, consider Figure 2.7b. From this figure it is appreciated that for positive velocities R in equation (2.19) can be identified with $F - \bar{F}$ i.e.

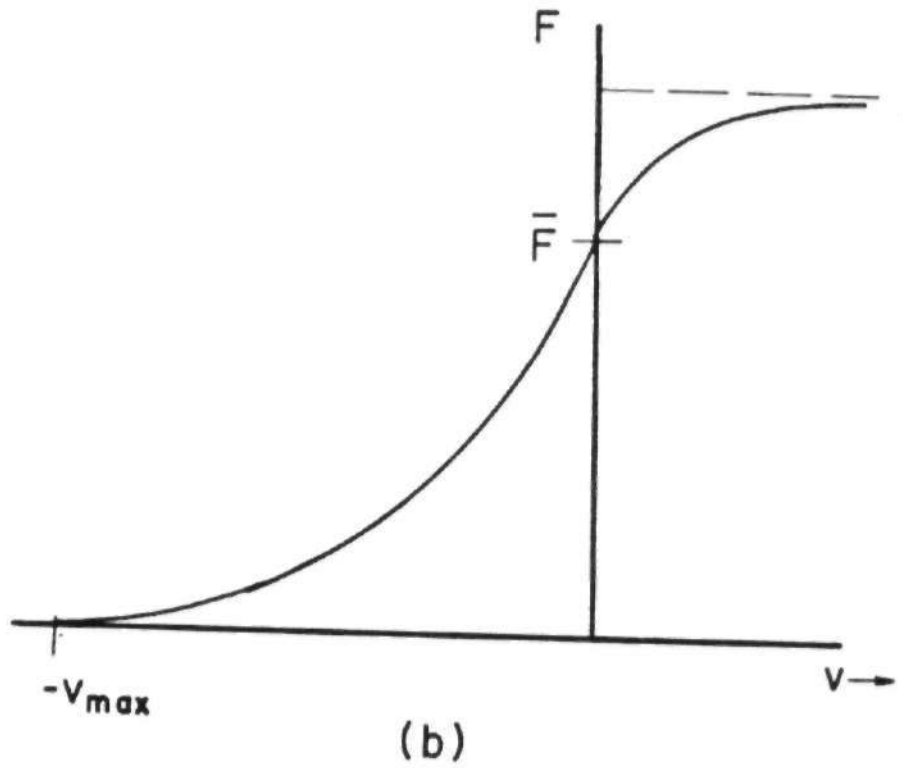
$$F - \bar{F} = \alpha\, v/(\beta + v) \qquad (2.20)$$

A typical value for the asymptote is $1.33\bar{F}$ [23]. This leads to the condition $F - \bar{F} = .33\bar{F} = \alpha$.

The value of β is obtained by matching the slope of this equation and that of the Hill force-velocity relationship. To this effect, write the two equations as



(a)



(b)

Fig. 2.7 (a) Function defined by equation (2.19). (b) Modified Hill force-velocity relationship depicting muscle yielding at positive (lengthening) velocities.

$$v_1 = b(\bar{F} - F)/(F + a)$$

$$v_2 = \beta\ (F - \bar{F})/(1.33\bar{F} - F) \qquad (2.21)$$

By differentiating these expressions, evaluating the derivatives at the point $F = \bar{F}$, it is easily deduced that

$$\beta = .33b/(1.+ a/\bar{F}) \qquad (2.22)$$

Experimental data abounds to show that the force-extension characteristics of the tendons which generally constitute the series elastic element is a nonlinear relationship. An appropriate fit for this relationship is the exponential relationship of the form given below [22].

$$F^{SE} = b_5[\exp(1.531\ \delta\ )-1] \qquad (2.23)$$

with δ given by equation (2.17).

The responses of this model to an isometric simulation are depicted in Figures 2.8a-c. Part a of the figure shows an on-off control, part b shows the corresponding active state function $f_1(g)$ while part c shows the history of the isometric force, the maximum value of which was set at 4400 N.

The parameters b_{14}, b_{15} and b_{16} are given in

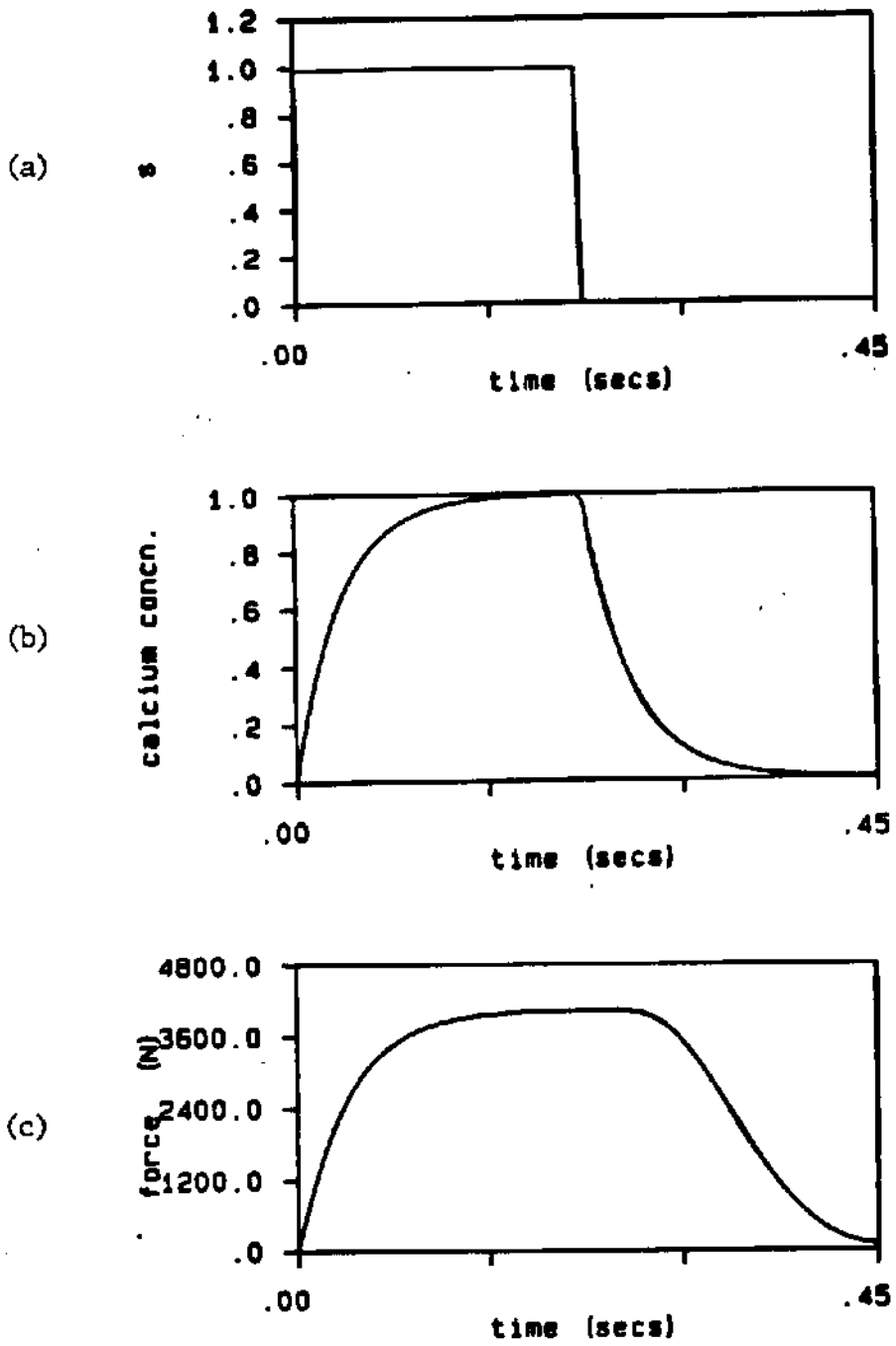


Fig. 2.8 Typical responses of muscle model 3. (a) applied on-off control (b) normalized calcium ion concentration and (c) maximum isometric force.

Table 2.3. The parameter b_{15} is the constant $a/\bar{F}$ in Hill's force-velocity relationship and is selected to lie within the range .18 - .25 normally used in that equation [24]. b_{14} is the same as b_6 of model 2 multiplied by b_{15}.

Model 4

This is the model described in Hatze [21]. The primary differences between this model and model 3 concern the force-velocity relationship (equation 2.18) and the activation-stimulation frequency relationship (equation 2.4). Because Hatze's model description comprises the major part of a paper, only the primary equations are repeated here. The reader is referred to [21] for additional details.

The differential equations describing the model are as follows.

The contractile element velocity $\dot{L}_c$ is given by

$$\dot{L}_c = \tanh^{-1}[(F^{SE}/b_1 kap_6 - 1)\tanh p_3]/C \qquad (2.24)$$

A measure of activity a, is defined by :

$$\dot{a} = m[r(U-.005)+.005-a] \qquad (2.25)$$

The active state q is defined by

TABLE 2.3

Parameters for Muscle Model 3* (SI Units)

MUSCLE GROUP	1	2	3	4	5
b_{14}	.38	.42	.6	.4	.28
b_{15}	.2	.2	.2	.2	.2
b_{16}	.1045	.1155	.165	.11	.077

* The parameters b_1 to b_{13} in this model are the same as those used in model 2.

$$\dot{q} = m(U-q) \tag{2.26}$$

where

$$U = .5025 + .4975 \tanh[p_4(s-p_5)] \tag{2.27}$$

$$k = b_{12} + p_1 p_2 \tag{2.28}$$

The quantities p_1-p_6 are given in full in Appendix 3.

Model 5

Since a number of researchers [8], [10], have used joint torques as controls in other studies, we have examined them also for the minimum time kicking problem. For this model then, the only state equations are the link dynamic equations, and the joint torques, actuators and controls are equivalent. To avoid widely varying control values and therefore enhance solution convergence the hip and knee torques were normalized so that the resulting control variable u was bounded between 0 and 1. To obtain the actual torques, the controls are substituted into the equation

$$M = u(M_{max}-M_{min})+M_{min} \tag{2.29}$$

where M_{max} and M_{min} are 240. and 0. N-m for the hip and 160. and -80. N-m respectively for the knee. Because no explicit data were available on the actual ranges of

torques; these values were chosen to match the range of torques generated using muscle model 3.

2.4 MODELING THE PASSIVE JOINT STRUCTURES

For all the models in this study severe numerical problems were encountered when the equations for passive joint torques given in [21] were used. A careful observation of experimental joint torque curves [27], [40], [61], show that they all follow a similar trend as shown in Figure (2.9); i.e. for most values of the joint angle within a certain range I shown in the figure, the passive joint structures exert a small torque. However, as the joint limits are approached the torques rise sharply. Hof and Van den Berg [40] proposed a single exponential to model this behavior while Yoon and Mansour [61] used a double exponential. It is easy to see that another form of the double exponential easily models this behavior. This is given as:

$$M_p = k_1 \exp(-k_2(\theta - \theta_2)) - k_3 \exp(-k_4(\theta_1 - \theta)) \quad (2.30)$$

Thus from this relation we see that for $\theta_2 \leq \theta \leq \theta_1$ M_p is small, while for $\theta > \theta_1$ or $\theta < \theta_2$ M_p rises sharply. The parameters of this model are given in Table 2.4. The parameters $k_1 - k_4$ and θ_1, θ_2 are obtained

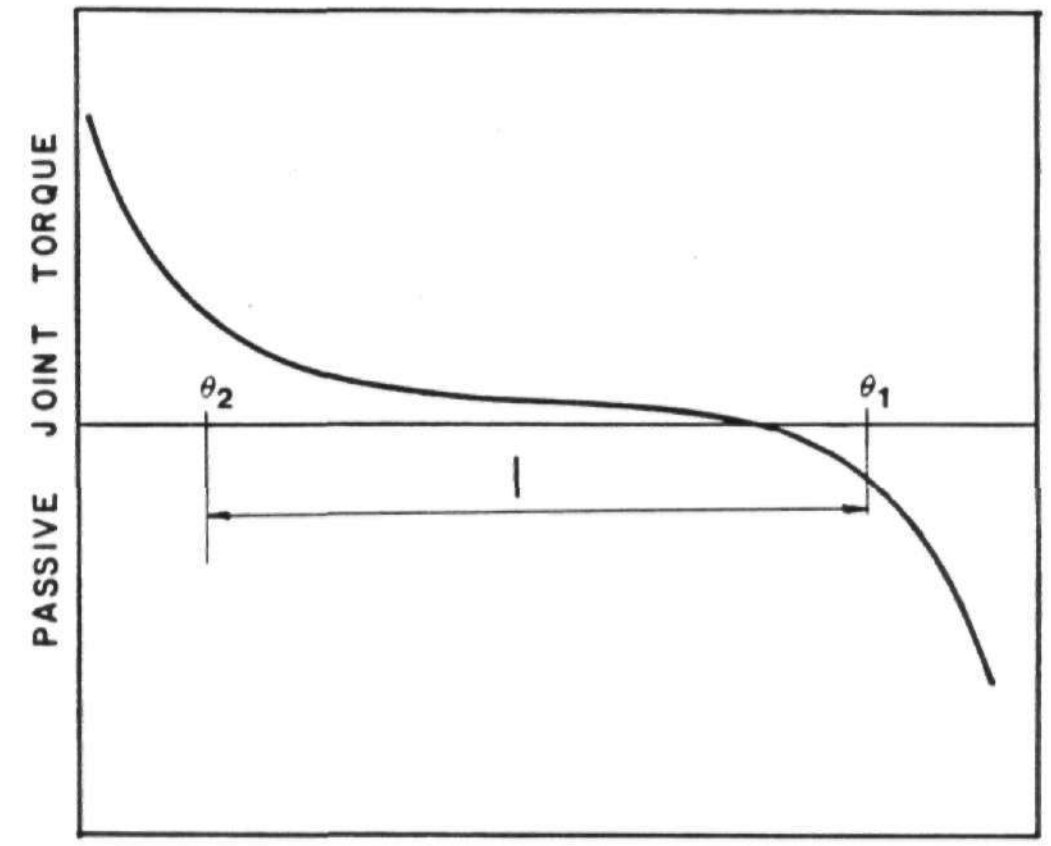


Fig. 2.9 Typical joint torque curve. The angles θ_1 and θ_2 define the region I over which the joint structures are essentially inactive.

TABLE 2.4

Parameters in Equation. (2.30)

	Hip Joint	Knee Joint
k_1	2.6	3.1
k_2	5.8	5.9
θ_2	.1744	-1.218
k_3	8.7	10.5
k_4	1.3	11.8
θ_1	.95	-.09

by fitting equation (2.30) to the curves obtained by plotting the corresponding relations in [21].

2.5 OPTIMAL CONTROL PROBLEM

The general form of the optimal control problem is discussed in detail in Chapter 3.

For the minimum time kicking problem under study, the form of the problem to be solved is as follows:

$$\text{Minimize} \quad I = t_f \tag{2.31}$$

subject to the differential constraints

$$\begin{aligned} \dot{x}_1 &= f_1 = x_3 \\ \dot{x}_2 &= f_2 = x_4 \\ \dot{x}_3 &= f_3(x) \\ \dot{x}_4 &= f_4(x) \\ \dot{x}_{4+k} &= f_{4+k}(x,s) \quad , \; k = 1,\ldots,5 \\ \dot{x}_{9+k} &= f_{9+k}(x,s) \quad , \; k = 1,\ldots,5 \end{aligned} \tag{2.32}$$

the control and state variable constraints

$$\begin{aligned} &0 \leq s_k \leq 1 \; , \quad k = 1,\ldots,5 \\ &x_2 \leq .05 \end{aligned} \tag{2.33}$$

and the end conditions

$$\begin{aligned} x_1(0) &= .1 \\ x_2(0) &= -.15 \\ x_3(0) &= 0 \end{aligned}$$

$$x_4(0) = 0$$

$$\dot{x}_{4+k}(0) = 0 \ , \quad k = 1,\ldots, 5$$

$$x_{10}(0) = 1.0871$$

$$x_{11}(0) = .8637$$

$$x_{12}(0) = 1.1127 \qquad (2.34)$$

$$x_{13}(0) = 1.0732$$

$$x_{14}(0) = 1.4263$$

$$x_1(t_f) = .8$$

$$x_2(t_f) = .05$$

$$x_4(t_f) = 0$$

2.6 RESULTS

The state equations (2.32) are represented by the link dynamic equations (the exact forms of the functions f_3 and f_4 representing the link angular accelerations are given in Appendix 1); and the equations describing the dynamics of the muscles (i.e. muscle model equations). The state variables are then the link angles and angular velocities, the normalized calcium concentration defined by equation (2.6) and the normalized length of the contractile element defined by equation (2.10). The control variable is the normalized stimulus rate s for each muscle group. The constraint equation (2.33b) specifies that the knee cannot go into extension beyond a certain angle.

For the minimum time problem t_f is unknown and hence it is necessary to develop a scheme for carrying out the integration mentioned above. In solving the minimum time problem using model 4 Hatze [21] used a trial and error scheme. This scheme involves picking an arbitrary t_f, and solving the optimal control problem using the error in the end conditions as the objective function. This procedure is repeated for several values of t_f, and the value of t_f that gives the lowest value of the objective function is assumed to be the minimum time. In this study, however, this ad hoc scheme is avoided by the following technique [44]. The independent variable t of the problem is normalized with respect to t_f resulting in the new independent variable τ defined by

$$\tau = (t-t_0)/(t_f-t_0) \tag{2.35}$$

By this transformation, all integrations are now done in the interval $0 \leq \tau \leq 1$. The unknown quantity t_f is added to the parameter vector p; and thus the final (minimum) time is selected by an optimization procedure.

Using this technique, the time optimal problem was solved using a combination of the ordinary gradient method [6] and a modification of Davidon's variance algorithm [16]. These algorithms were selected because they were found to lead to rapid convergence for such

large scale optimization problems (Chapter 3). In order to minimize the number of function evaluations the state and adjoint equations (3.2) and (3.11) were integrated using the Hamming Predictor-Corrector Method with the fourth order Runge-Kutta algorithm used for a starter. All the quadratures of the problem were evaluated using the Simpson's Formula. The integration step size was set at .01 throughout. All the constraints in the problem were handled using an exterior penalty function technique. For details of these and other algorithms used to solve this problem see Chapter 3.

The results for the solutions obtained using each of the four muscle models are shown in Figures 2.10 through 2.13. In Figure 2.14 are shown a set of results using the joint torques as controls. The results for all models except Hatze's model (Figure 2.13) are results of optimization runs. In this exception, only a simulation run using his controls was made to verify our interpretation of model parameters, etc. in [21].

In Figures 2.10a, 2.11a, 2.12a, 2.13a and 2.14a are shown the hip and knee trajectories which were obtained. The crosses on the hip and knee trajectories indicate the end condition constraints. It can be seen from Figures. 2.10a and 2.11a that there is a substantial amount of dwell before the hip trajectory starts to rise for models 1 and 2. The same follows for the knee trajectory. In

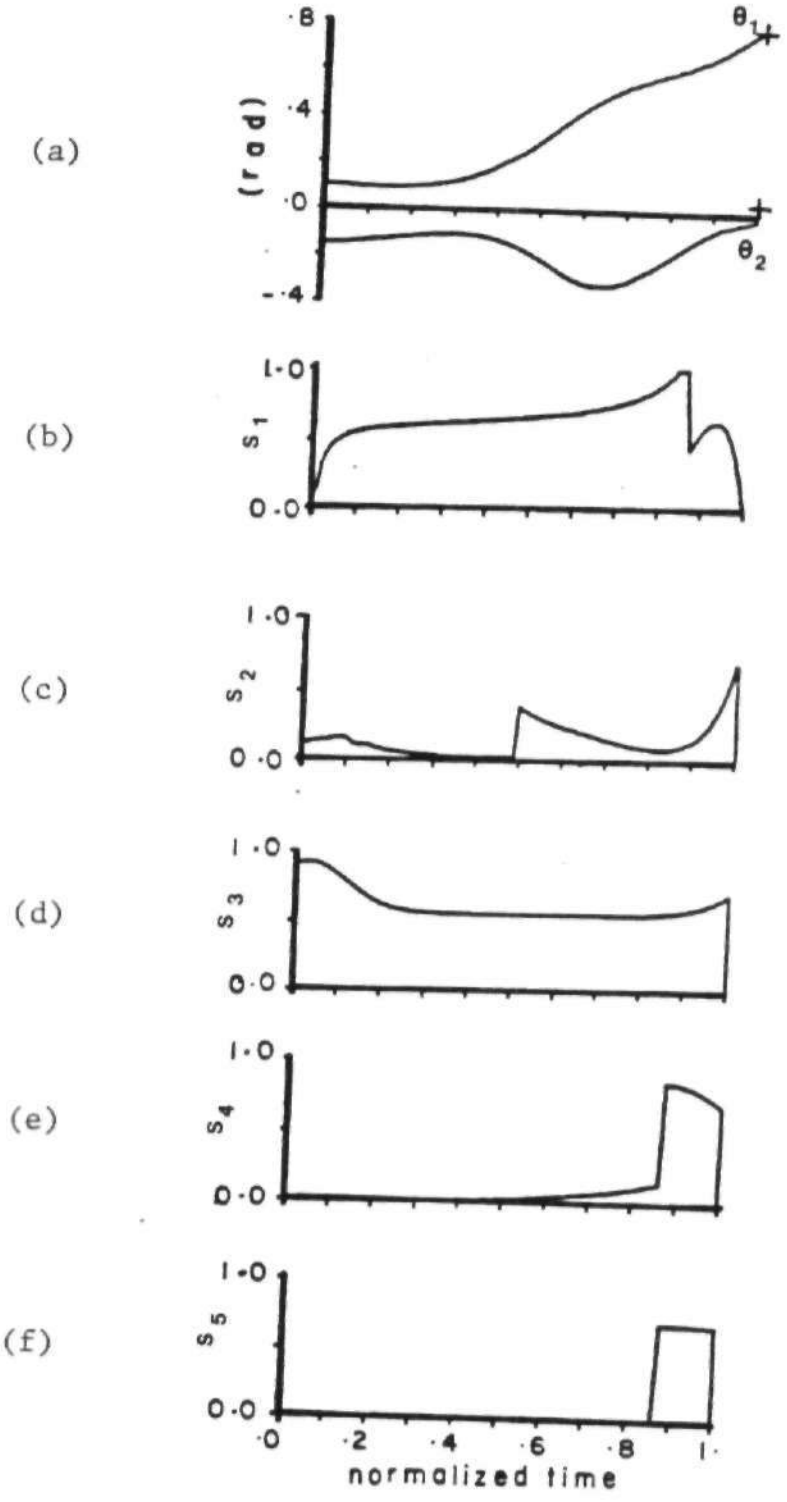


Fig. 2.10 Solution for muscle model 1. (a) Hip (upper) trajectory, knee (lower) trajectory. (b) - (f) control histories for muscle groups 1 through 5.

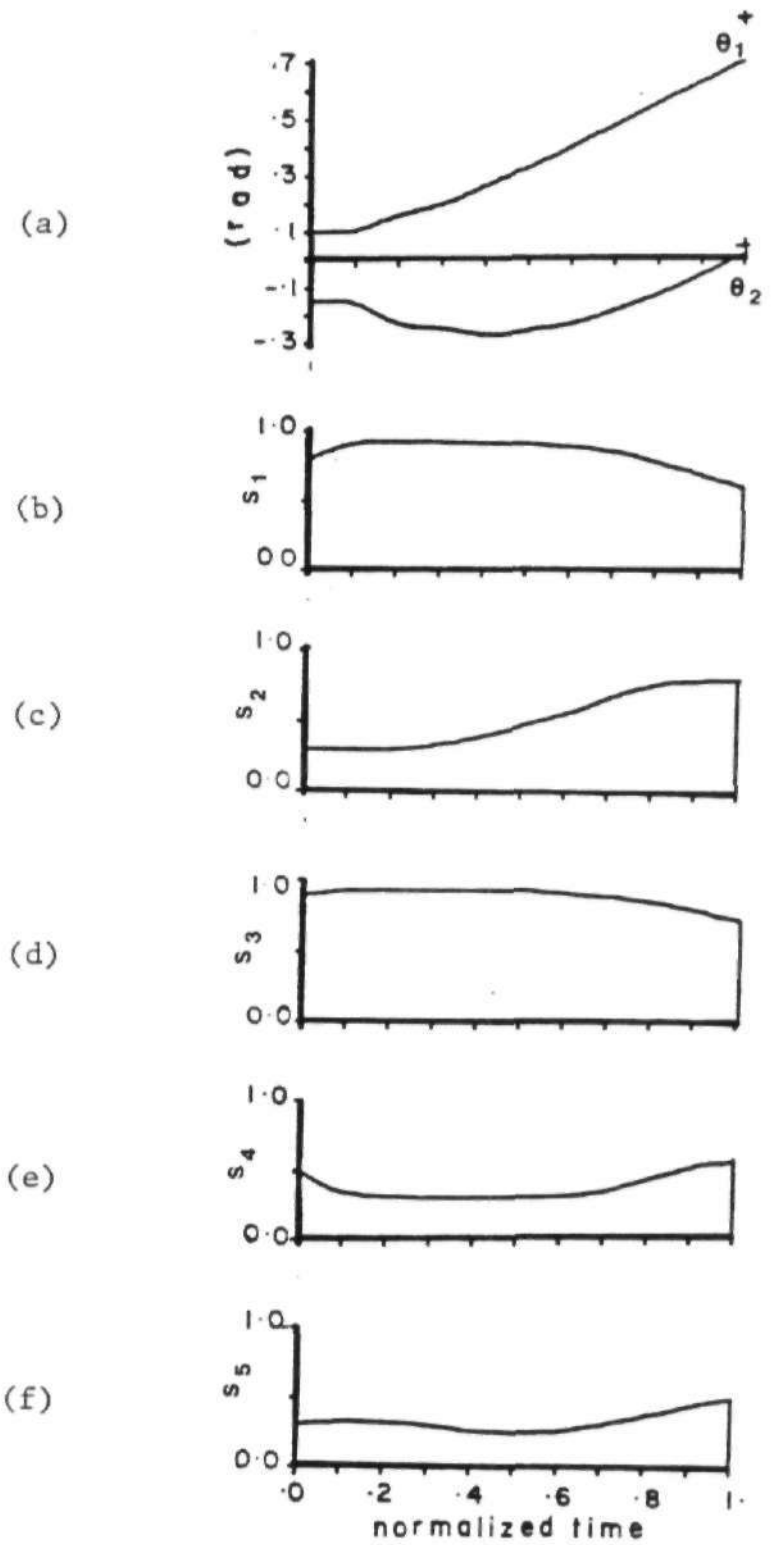


Fig. 2.11 Solution for muscle model 2. (a) Hip (upper) trajectory, knee (lower) trajectory. (b) - (f) control histories for muscle groups 1 through 5.

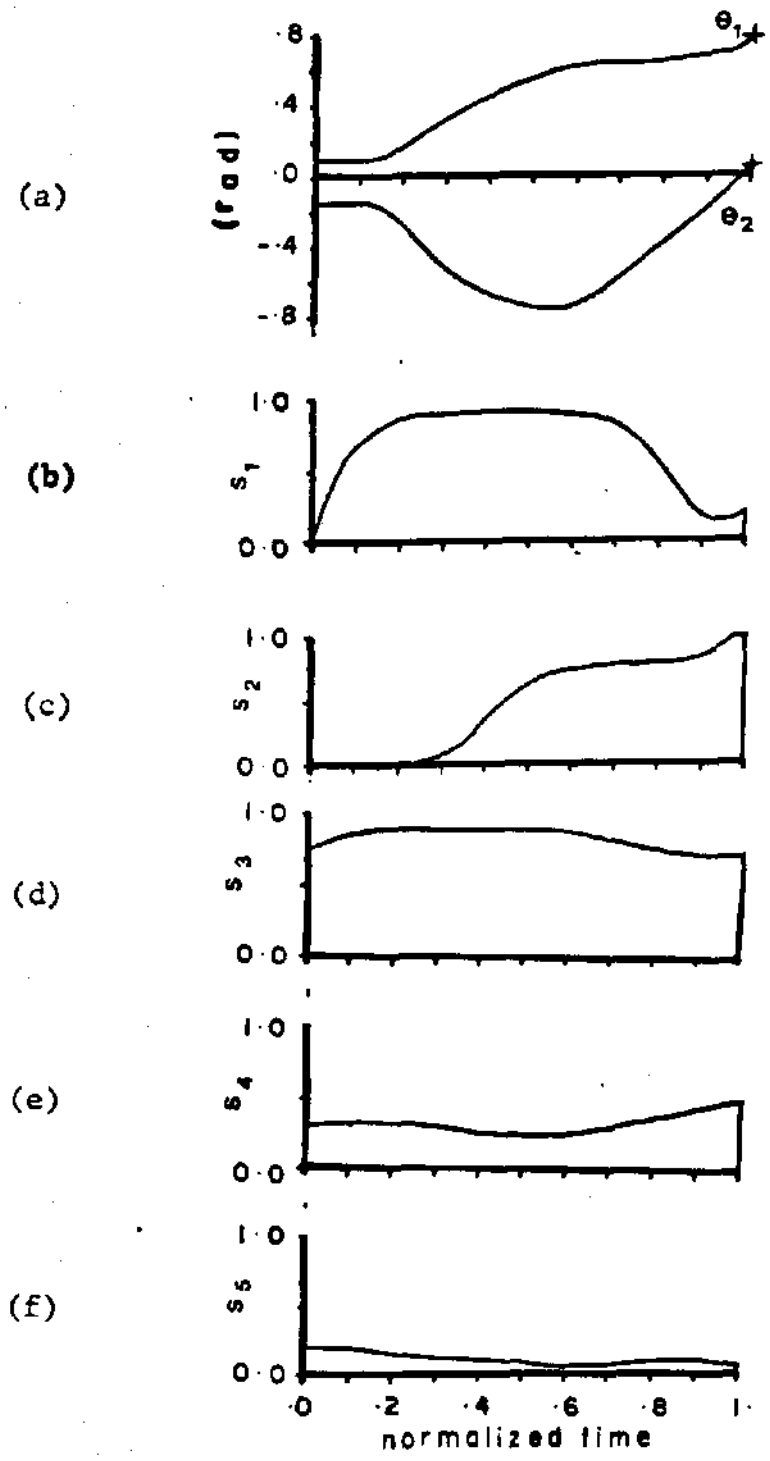


Fig. 2.12 Solution for muscle model 3. (a) Hip (upper) trajectory, knee (lower) trajectory. (b) - (f) control histories for muscle groups 1 through 5.

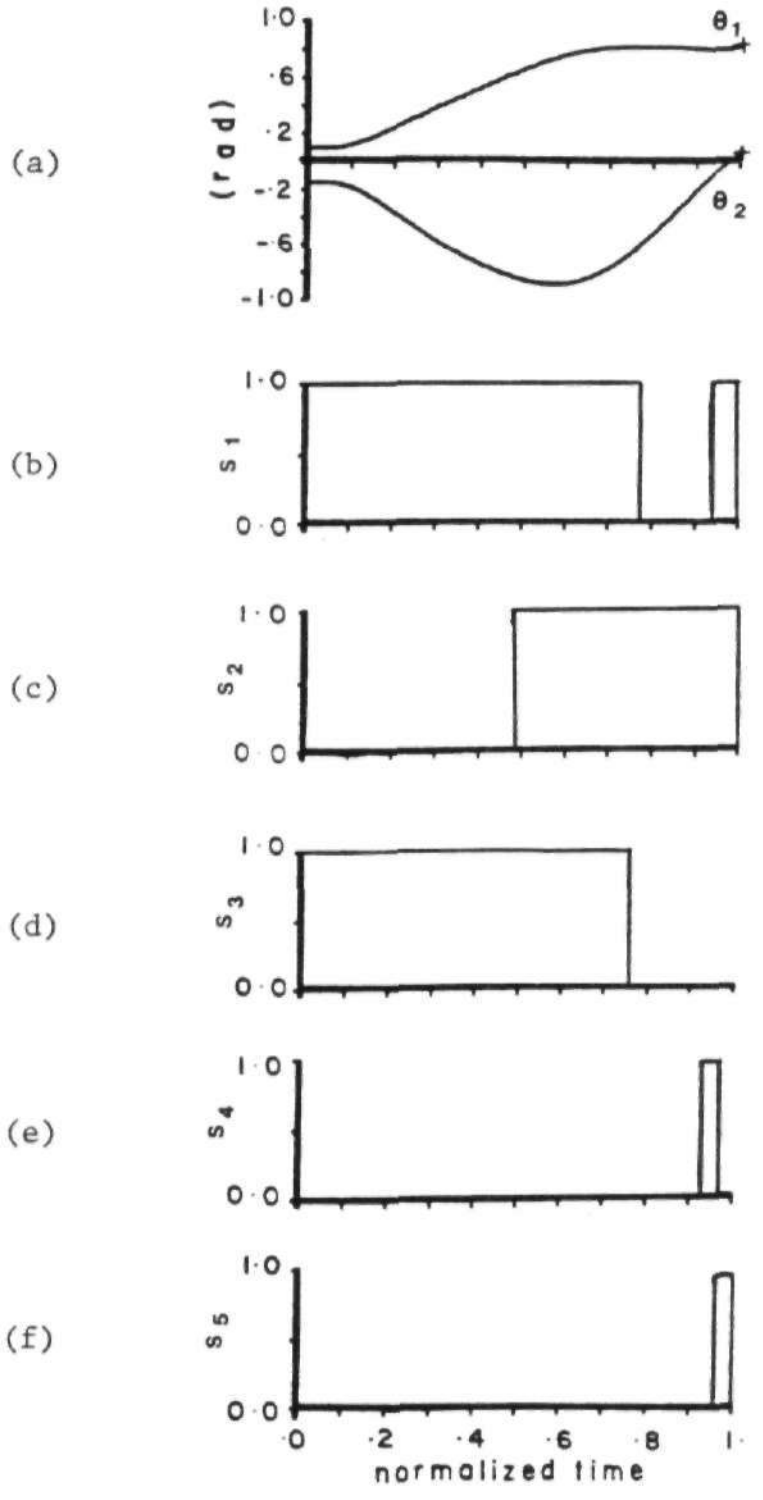


Fig. 2.13 Solution for muscle model 4. (a) Hip (upper) trajectory, knee (lower) trajectory. (b) - (f) control histories for muscle groups 1 through 5.

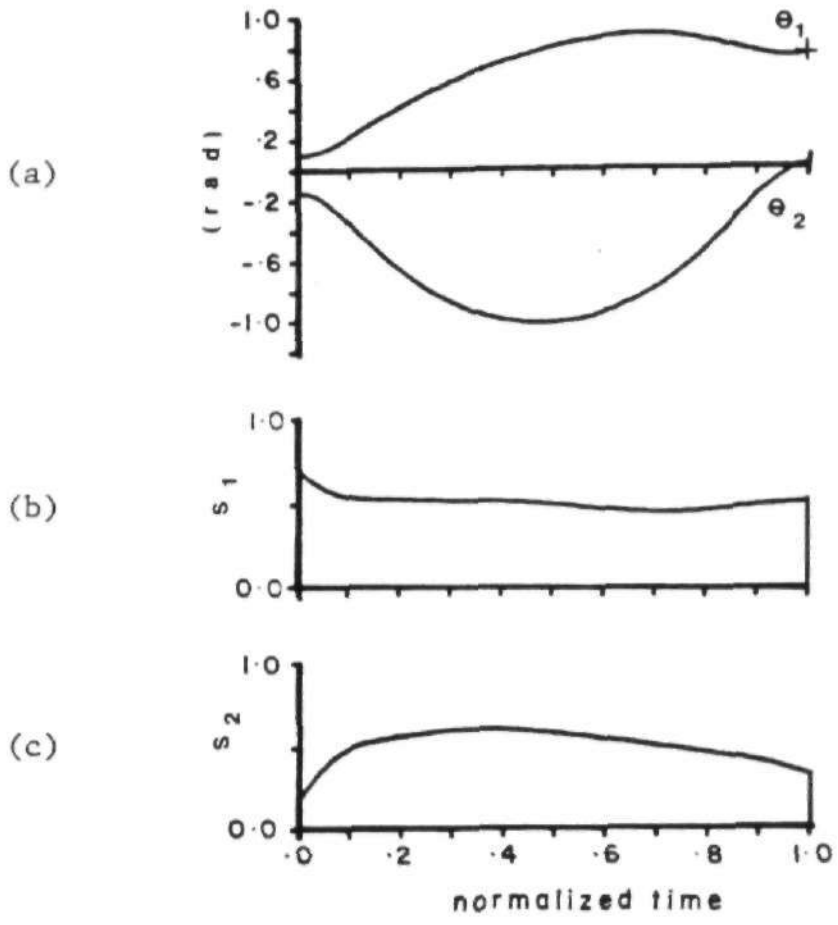


Fig. 2.14 Solution for torque actuator model. (a) Hip (upper) trajectory, knee (lower) trajectory. (b), (c) control histories for hip and knee respectively are normalized joint torques. The actual values for joint torques are obtained by using equation (20).

contrast, the amount of dwell is much shorter for the trajectories predicted by models 3 and 4 (Figures. 2.12a and 2.13a). Also, the knee trajectory, in models 1 and 2 (Figures. 2.10a and 2.11a) do not exhibit the large dips that are obtained using models 3 and 4. Interestingly, the end conditions for the hip trajectory were met to a sufficient precision using all the models. However, the knee end conditions were violated by models 1 and 2. It can be seen from Figure 2.10a that the knee trajectory for model 1 starts to change its curvature too early toward the end of the integration interval. This is in contrast to the trajectories predicted by models 3 and 4 whose curvatures change close to the end. Parts b-f of Figures 2.10-2.13 show the corresponding control histories which were obtained for the five muscle groups. Figures 2.14b and c show the normalized joint torque histories when they were treated as controls.

From Figure 2.10b, it is noted that for model 1, muscle 1 is almost fully active throughout the integration interval. However, muscle 2 is mainly active at the middle and toward the end of the interval. In contrast, the control histories predicted by models 3 and 4 show that muscle 1 (Figure 2.12b and 2.13b) is essentially inactive for the last 15-20% of the interval, while muscle 2 (Figures. 2.12c and 2.13c) is fully active for the last 50%. The predictions by model 1 for the

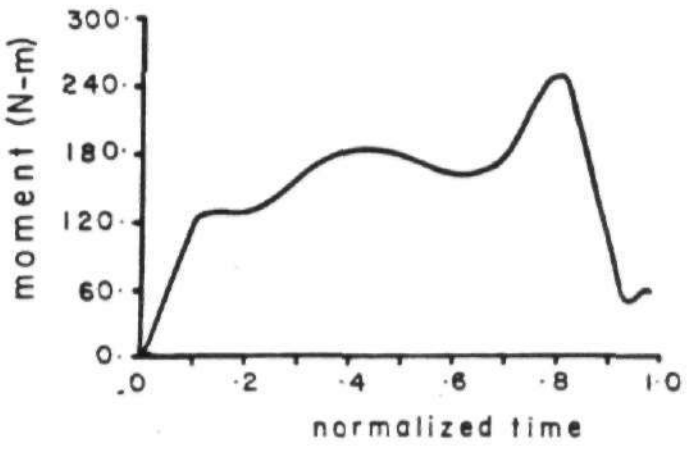
controls of muscles 3, 4 and 5 (Figures. 2.10d, e and f) closely follow those for model 4 (Figures. 2.13d, e and f). Concerning muscles 4 and 5, it is noted that there is a substantial difference between the predictions of model 3 (Figures 2.12e and f) and those of model 4. The significance of these differences will be discussed subsequently.

Finally, when the moments were used as controls, the hip and knee trajectories (Figure 2.14a) compare favorably with those of models 3 and 4. However, the envelope of the moments, which directly correspond to the control histories, do not follow the same time history as the moments generated by models 3 and 4 (Figures 2.15a and b).

Table 2.5 gives the values of the minimum times obtained using the individual models. The minimum time for model 4 was obtained by Hatze [21]. The times for model 1, 2, 3 and 5 were obtained using the optimal control algorithm described earlier.

The control histories for model 2 are not the optimal controls in the sense of reaching a true local minimum. This is because after a certain number of iterations severe oscillations were noted in the solution process making it very difficult to make progress without drastically decreasing the gradient step. This led to excessively long computation times; hence the algorithm

(a)



(b)

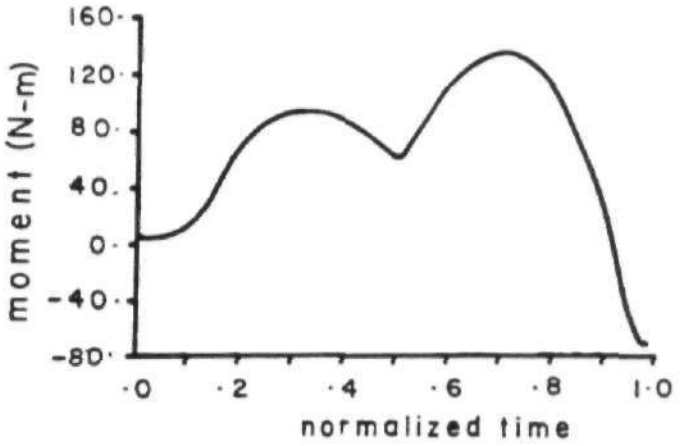


Fig. 2.15 (a) Total hip and (b) total knee torques for muscle model 3.

TABLE 2.5

Minimum Times Obtained using each model (secs)

Model 1	.4693
Model 2	.5248
Model 3	.4615
Model 4	.46*
Model 5	.4751

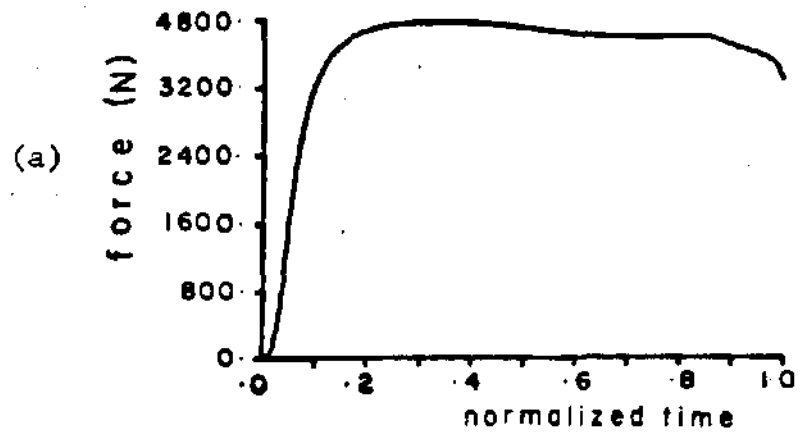
* From Hatze [21]

was halted before convergence was fully achieved.

2.7 DISCUSSION

a. Hip and Knee Trajectories

In comparing results for the various solutions, model 4 from Hatze [21] is used as the basis. In [21] these results were found to compare very favorably with experimental results. From Figures 2.12a and 2.13a it can be appreciated that the trajectories for models 3 and 4 are fairly close. However, the trajectories for models 1 and 2 are markedly different. The primary source for these differences in behavior became evident by studying the descriptions of the various models. Models 1 and 2 are nearly simple input-output models, with essentially a direct proportionality between the input to the muscle (stimulation) and the output (force). For model 1 full activity of the muscle results in a proportional full force activity with the force-length relationship acting as a proportionality factor (equation (2.1)). This fact can be appreciated by studying Figure 2.16a and Figure 2.10b which show the force output and the control input respectively for muscle 1 as produced by model 1. The almost direct proportionality between input and output is obvious. These figures should be compared with Figure 2.16b and Figure 2.12b which show comparable curves as



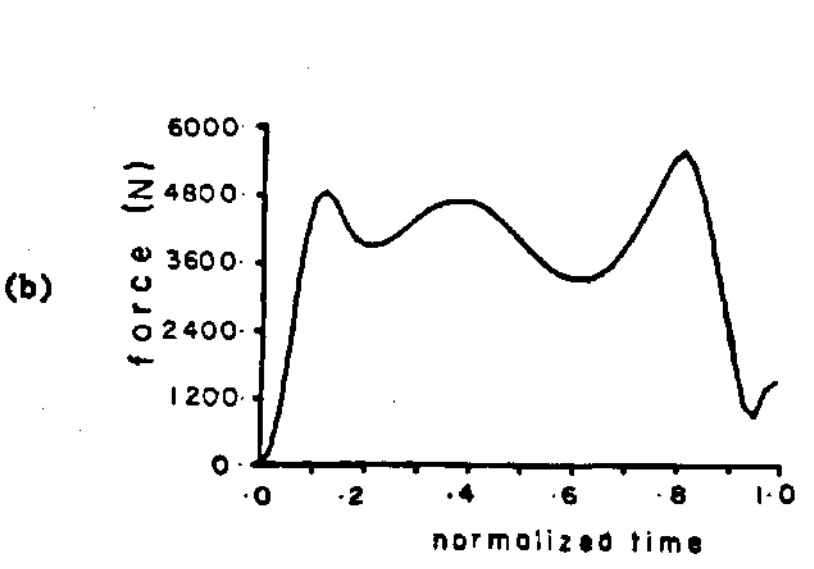


Fig. 2.16 Force histories for muscle group 1. (a) muscle model 1. (b) muscle model 3.

produced by model 3. From these latter figures it is apparent that for the more complex models full muscle activity is not necessarily commensurate with a proportional peak force activity.

The source of this basic difference in results between simpler and more complex models is imbedded in the structural forms of the models. Models 2, 3 and 4 have an elastic element in series with the contractile element. The force output of this element (equation (2.16)) is dependent not only on the changes in the contractile element length but also in the changes in the overall muscle length (which is a function in turn of the positions of the limbs). This relationship between force output and length provides the coupling between the muscle and link dynamics and is a far more sensitive relationship than that between the same variables for model 1. For example, the dips in the force history during high stimulation for muscle 1 (Figure 2.16b) are found to be caused by the decrease in the length of muscle group 1 as a consequence of the increase in hip angle.

The trajectories obtained using torques as controls differ even more widely from those of models 3 and 4 than those of model 1. As for muscle model 1, the absence of the internal muscle dynamics is the reason for the difference between these trajectories and those of models

3 and 4.

b. Control Histories

The control histories for muscle groups 1, 2 and 3 for models 3 and 4 are fairly close, but the controls of muscles 4 and 5 differ appreciably. It has been suggested by Hatze [21] that these muscles serve the function of supplying a braking force at the end of the swing of the limb. To ascertain this function of the two muscle groups, a simulation of model 4 was carried out in which the controls of the two were set equal to zero. It was found that there was no appreciable change in the trajectories of the hip and knee. This indicates that the use of these muscle groups for braking the movement is not crucial especially as the latter function is well served by the passive joint structures.

Another difference in the controls is the fact that the controls of models 1, 2 and 3 are not exactly on-off (bang-bang) as they are for model 4 in [21]. This is in part a consequence of using different optimal control algorithms. For solving the problem using model 4, Hatze [21] used repeated applications of an algorithm called Differential Dynamic Programming; and selected the controls based on the minimum principle. This principle in general predicts that if the Hamiltonian (equation 3.8) is linear in the controls then the optimal controls

will be bang-bang. In the present study use is made of algorithms of the gradient type. These algorithms select the controls by using local information about the gradient of the function being optimized. In general, it takes a large number of iterations before these algorithms achieve instantaneous switching even for problems whose solution is known to be bang-bang. An interesting point connected with this issue is that linearity of the Hamiltonian in the controls is not necessarily a guarantee that the controls must be bang-bang [36].

As noted earlier, the optimization run for model 2 was terminated prior to fully achieving an optimal solution due to numerical difficulties. One source of these difficulties appears to be the choice of the constants in the model. Most of them correspond to those used in the nonlinear models. Thus there is the possibility that for certain values of decision and state variables these parameters were not appropriate for the linear model.

An interesting feature of the control histories obtained when the joint torques are used as controls is that the controls are essentially constant over most of the integration interval. The actual torques are obtained by using equation (2.29). Shown in Figures 2.15a and 2.15b are the corresponding torques obtained

using model 3. The remarkable difference due to the difference between the muscle models is readily apparent.

c. Model Complexity, Numerical Stability and Integration Times

As the model complexity increases the number of first order ordinary differential equations (ODE's) required to define the models typically increases also. For instance model 1 is described by 10 ODE's (both link and muscle equations). Models 2 and 3 are both described by 15 ODE's and model 4 by 19. When the torques are used as controls only 5 ODE's are required. Along with these state equations there are an equal number of adjoint equations. Thus twice the above number of ODE's must be integrated each time the decision variables (controls and parameters) are altered. In general, the integration of this combination of linear and nonlinear ODE's consumes a substantial amount of computation time. For example integrating the whole set of 30 equations describing model 3 requires approximately 64 cpu seconds on an Eclipse S-250 computer using the Hamming Predictor-Corrector integration routine. Thus on the average a single iteration of the optimal control algorithm (using the method of steepest descent) requires from 10-15 minutes. Since there are tens of iterations to be done before convergence is achieved the overall

computation takes several hours.

Associated with the problem of integration is that of numerical stability of the model equations. This is a problem that bedevils mainly models 2, 3 and 4. This problem arises primarily from the fact that these models exhibit extreme sensitivity to the choices of the various parameters within them. Typically these models are described using a number of exponentials. Consequently each time the decision parameters are updated, there is a possibility that the updates may cause some of the arguments of the exponentials to become unacceptably large. This problem was prominent in this study and usually calls for taking very small steps while updating the decision parameters -- a process that has been found to slow down considerably the progress of the algorithms. This increases further the already long computing time required to make one iteration step. This problem in another form was found to occur for model 4 where Hatze found it necessary to decrease the integration step size from .005 to .0005 [21]. Model 3 of the present study takes about 2 times less the integration time of model 4 and gives quite comparable results.

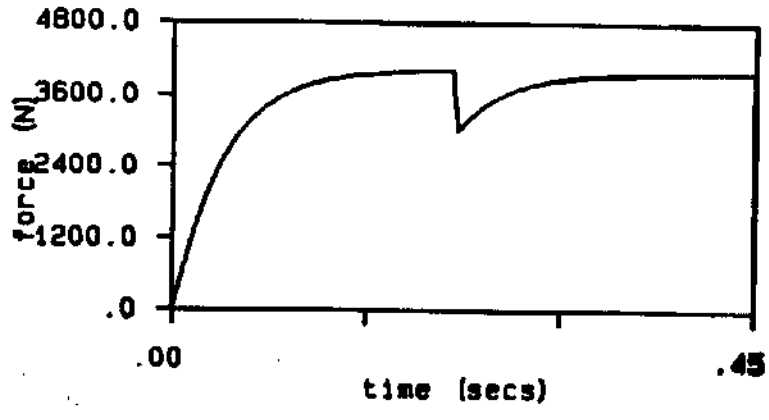
Other numerical stability problems with the more complex models were prominent when these models were subjected to step changes in length (quick release and quick stretch experiments). Typical results of these

simulations using models 3 and 4 are depicted in Figure 2.17. In Figure 2.17a are shown the results of subjecting muscle model 3 to a step decrease in length of one percent after it has developed full isometric force. Figure 2.17b shows the results of the same experiment carried out with muscle model 4. Figure 2.17c shows the results of subjecting muscle model 3 to a step decrease in length of one percent and then to a step increase in length of one percent after it has redeveloped full isometric force. It was found during these simulations that muscle model 3 could withstand a ten percent step increase in length without numerical difficulties. However, a step increase of one and a half percent or over was not accommodated by muscle model 4. This is because the argument of the inverse hyperbolic tangent function in equation (2.24) becomes unacceptable at the instant of stretching the muscle if that stretch is on the order of 1.5 percent.

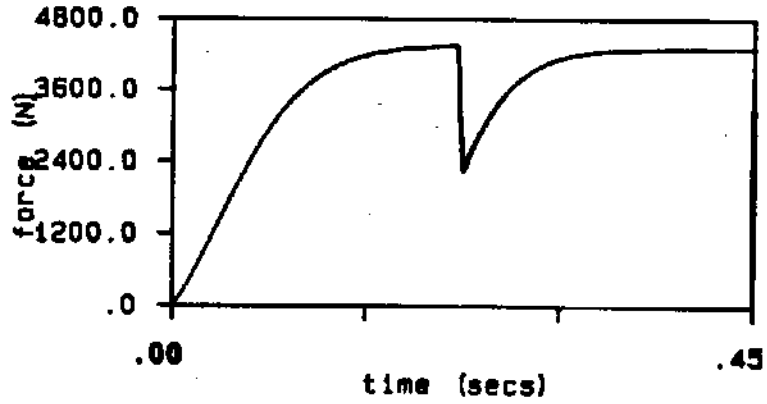
d. Parameter Identifiability, Reliability and Variability

Most of the parameters used in this study are based on those given by Hatze [21]. This was to allow for a more realistic comparison since most of the parameters given in [21] are subject specific. These parameters were determined by carrying out a series of experiments

(a)



(b)



(c)

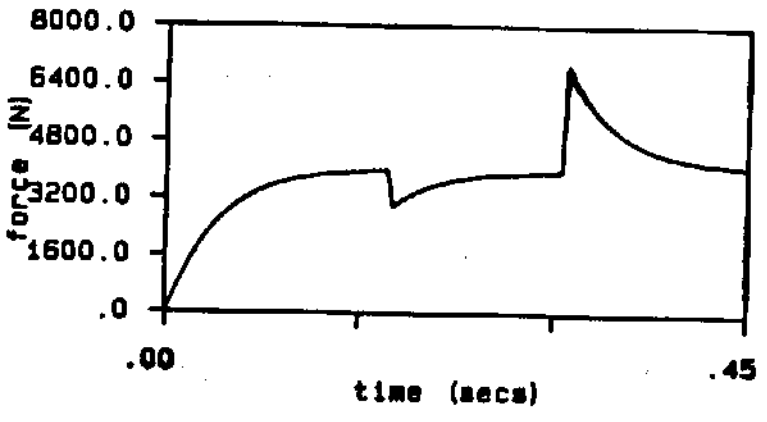


Fig. 2.17 Quick stretch and quick release simulations. (a) and (b) Quick release simulations of muscle models 3 and 4 respectively. (c) Quick release followed by quick stretch simulation of muscle model 3.

with the subject and using a parameter estimation scheme that would select the parameters such that the experimental and model outputs match. An alternative approach would be to estimate the model parameters on the basis of fundamental muscle properties and external physical data from the subject. We examined this approach at some length and concluded that it is not feasible given the current state of knowledge of muscle mechanics. The subject specific experimental determination of parameters appears to be the only realistic choice. However, in such an approach the issue of parameter identification must be addressed.

There are many parameters of the models that may defy exact definition in the actual biosystem -- for instance the length of a muscle which has a broad origin and/or insertion. To examine the significance of such variabilities the following test was carried out. In the original simulation of model 4, Figure 2.13, the length of the iliopsoas group as a function of hip angle θ is given by the relation [21]:

$$l_1 = 0.287 - 0.0497\,\theta \qquad (2.36)$$

where l_1 is in meters. There is the possibility of a large variability associated with this equation since the origin of the iliopsoas group is not a fixed point. This

equation was substituted for another one given by

$$l_1 = 0.280 - 0.0497\ \theta \qquad (2.37)$$

The simulation of model 4 was repeated using this perturbed equation. The trajectories obtained from both simulations are given in Figure 2.18. These results, as well as others we obtained illustrate the strong influence of the model parameters on solutions using these more complex muscle models; and suggest that a formal sensitivity analysis would be fruitful.

It is concluded that, within the context of the problem examined, the optimal motion history could not be realistically predicted using simple actuator models. In this problem model 3, which is somewhat less complex than model 4 provided appreciable gains in efficiency and stability while giving very similar results. Even more complex models could be used [23]; but the computational task even for this modest sized problem is already very large. Successful implementation of the more complex models in problems of appreciably larger scale using currently available optimal control algorithms can be expected to require enormous computational efforts, which will only be accomplished on large scale computing systems.

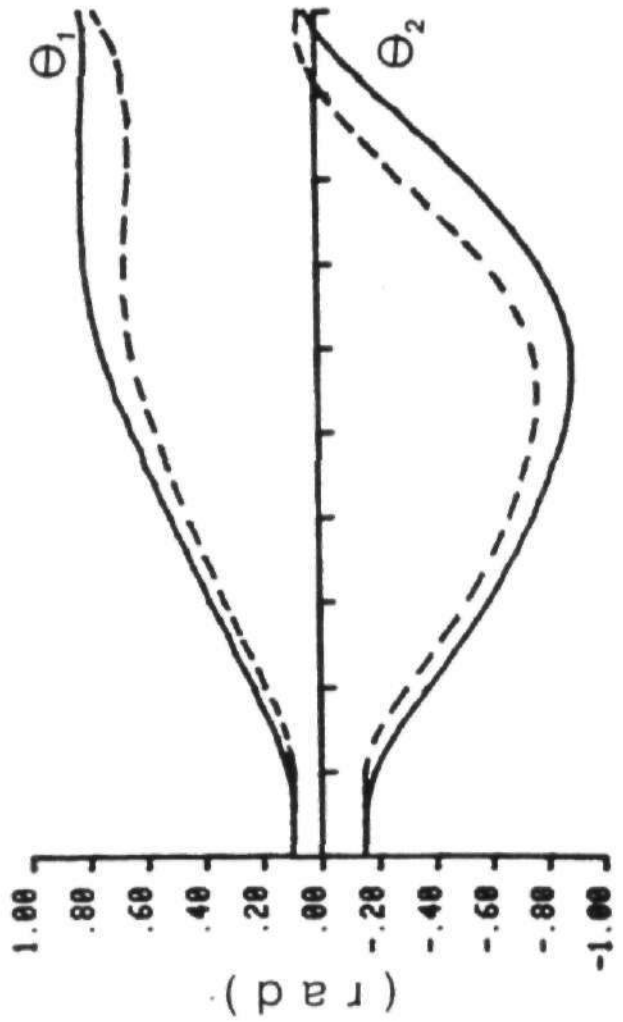


Fig. 2.18 Trajectories for muscle model 4 with muscle length defined by equation (2.32) solid line and by equation (2.33) dotted line.

CHAPTER III

A COMPARISON OF OPTIMAL CONTROL ALGORITHMS FOR MUSCULOSKELETAL MOTION STUDIES

3.1 INTRODUCTION

Several techniques have been proposed and used to solve a variety of optimal control problems. A more complete review of these techniques may be found in the literature [43]. Most of these techniques were tested by solving a variety of simpler problems. These are problems that are characterized by relatively few state variables (rarely exceeding 4) and a relatively few control variables (rarely exceeding 2). The use of these techniques to solve problems characterized by a larger number of state and control variables (over 10 and 5 respectively) is not commonly reported.

Recently, the use of optimal control has naturally emerged in the field of bioengineering where the use of redundant structures in biological organisms is hypothesized as being based on an optimality principle [58]. A typical example of this situation is related to the problem of muscle force sharing during human locomotion. It is common knowledge that the muscles crossing the joints of the body constitute a set of redundant structures [54]. The manner in which the

muscles are utilized during a given musculoskeletal activity is therefore not solvable using laws of mechanics alone. In order to solve the problem, resort must be made to some optimality criterion. The optimality problem related to muscle force sharing can be cast as an optimal control problem since in general the constraint equations for the problem are made up of dynamic equations (for the limbs and muscles). The combination of these dynamic equations lead to an optimal control problem that is characterized by a substantial number of state and control variables.

A recent attempt to solve a typical problem of this nature has shown that there are a number of issues concerning the solution procedure that are not ordinarily encountered with the smaller problems often found in the control literature. As a consequence, a study was undertaken to examine the relative merits of several optimal control algorithms for the solution of musculoskeletal dynamics problems. Our goal was to determine whether these various algorithms might allow solutions of these complex problems using modest sized computational facilities typically available to biomechanics researchers.

The purpose of this chapter is to report the experience of the author in using several optimization algorithms to solve problems of varying complexity. The

first two problems are characterized by a relatively few state and control variables. The other two problems have larger number of state and control variables and the state equations are highly nonlinear.

3.2 THE GENERAL OPTIMAL CONTROL PROBLEM

The general form of the optimal control problem considers the minimization of the functional

$$I = [g(x,p)]_1 + \int_0^1 L(x,p,t)dt \qquad (3.1)$$

with respect to the state vector $x(t)$, the control vector $u(t)$, and the parameter vector p which satisfy the vector differential constraint

$$\dot{x} = f(x,u,p,t) \qquad (3.2)$$

the nondifferential constraint

$$S(x,u,p,t) = 0 \qquad (3.3)$$

and the boundary conditions

$$x(t_0) = x_0 \quad \text{given} \qquad (3.4)$$

$$[\phi(x,p)]_1 = 0 \qquad (3.5)$$

In the above equations, the functions L and g are scalar, the function f is an n-vector, the function S is an r-vector, and the function ϕ is a q-vector. The independent variable is the time t (a scalar), and the dependent variables are the state x (an n-vector), the control u (an m- vector) and the parameter p (a d-vector).

At the initial time $t = t_0$, the n scalar relations (3.4) are specified. At the final time $t = t_f$, the q scalar relations (3.5) are specified.

To facilitate numerical solution on digital computers, the actual time τ is replaced by the normalized time t, defined in such a way that the extremal arc has a normalized time length $\Delta t = 1$. In this way, variable-time end conditions are transformed into fixed-time end conditions. The actual time τ_f in which the terminal boundary is reached is regarded to be a component of the parameter vector p being optimized.

The problem above can be recast as one of minimizing the augmented functional

$$J = \int_0^1 [\, L + \lambda^T(\dot{x}-f) + \rho^T S]\, dt + (g + \mu^T \phi)_1 \qquad (3.6)$$

subject to the conditions (3.2) to (3.5). In (3.6),

λ (t) is a variable Lagrange multiplier (an n-vector), ρ (t) is a variable Lagrange-multiplier (an r-vector), and μ is a constant Lagrange multiplier (a q-vector). The superscript T indicates transposition. If this expression is integrated by parts, there results the expression

$$J = (\lambda^T x + g + \mu^T \phi)_1 + \int_0^1 (- \lambda^T x + H) dt \quad (3.7)$$

where

$$H = L - \lambda^T f + \rho^T S \quad (3.8)$$

is called the Hamiltonian.

It can be shown [6] that the necessary conditions for extremizing (3.7) are the Euler equations (subscripts indicate partial differentiation with respect to the respective variables):

$$H_u = 0 = L_u - f_u \lambda + S_u \rho \quad (3.9)$$

$$[g_p + \phi_p \mu]_1 + \int_0^1 H_p dt = 0 \quad (3.10)$$

where the multipliers λ (t), ρ(t), and μ satisfy the differential equation.

$$- \dot{\lambda} (t) = H_x = L_x - f_x \lambda + S_x \rho \quad (3.11)$$

and the final condition

$$[\lambda + g_x + \phi_x \mu]_1 = 0 \qquad (3.12)$$

It should be noticed that solving this problem involves integrating the differential equations (3.11) backward in time using the boundary condition (3.12).

3.3 STATEMENTS OF THE PROBLEMS

Problems 1 and 2 are typically found in Optimal Control texts [6]. Problem 1 is the minimum time double integrator in which the optimal control history is bang-bang. Problem 2 is a minimum energy problem with a second order state variable inequality constraint. Problem 1 is selected because of the nature of the control history while problem 2 is selected because of the state variable inequality constraint.

Problem 4 is a minimum time kicking problem originally posed by Hatze [21]. In this problem the dynamic musculoskeletal subsystem consists of a single lower limb which can move in the saggital plane by motion about the hip and knee joints. The resulting two-degree-of-freedom system is activated by five muscle groups (Figure 2.1).

The minimum time kicking problem consists of

starting from an initial free-hanging limb position and moving the limb forward to a final fixed position as quickly as possible. At the final point, both hip angle θ_1 (state x_1), and knee angle θ_2 (state x_2) (Figure 2.1) are specified and knee angular velocity $\dot{\theta}_2$ (state x_4) is also specified. The dynamic equations for the limbs and the muscles are given in Appendix 1. The dynamic equations for the muscles are the same as those defined as model 3 in Chapter 2. Each muscle is assumed to have a single control variable. The overall problem is characterized by 14 state equations and 5 controls.

Problem 3 is similar to problem 4 except that the limbs are assumed to be actuated by the resultant hip and knee torques. The normalized joint torques are used as the control variables. This problem is characterized by 4 state equations and 2 controls.

The mathematical statements of the four problems are as follows.

Problem 1

$$\text{Minimize} \quad I = t_f \tag{3.13}$$

subject to the differential constraints

$$\dot{x}_1 = x_2, \quad \dot{x}_2 = u \tag{3.14}$$

the non differential inequality constraint

$$-1 \leq u \leq 1 \tag{3.15}$$

and the end conditions

$$x_1(0) = 0, \quad x_2(0) = 0$$

$$x_1(t_f) = 1, \; x_2(t_f) = 0$$

In the terminology of section (3.2), it can be seen that for this problem n = 2, m = 1, d = 1, q = 2, r = 1.

Problem 2

$$\text{Minimize } I = \int_0^1 u^2 \, dt \tag{3.16}$$

subject to the differential constraints

$$\dot{x}_1 = x_2, \; \dot{x}_2 = u \tag{3.17}$$

the state inequality constraint

$$0.15 - x_1 \leq 0 \tag{3.18}$$

and the end conditions

$$x_1(0) = 0, \; x_2(0) = 1$$

$$x_1(1) = 0, \; x_2(1) = -1$$

For this problem n = 2, m = 1, d = 0, q = 2, r = 1.

Problem 3

$$\text{Minimize} \quad I = t_f \tag{3.19}$$

subject to the differential constraints

$$\begin{aligned}
\dot{x}_1 &= f_1 = x_3 \\
\dot{x}_2 &= f_2 = x_4 \\
\dot{x}_3 &= f_3(x,u) \\
\dot{x}_4 &= f_4(x,u)
\end{aligned} \tag{3.20}$$

the control and state variable inequality constraints

$$\begin{aligned}
0 \le u_1 \le 1 \\
0 \le u_2 \le 1 \\
x_2 \le .05
\end{aligned} \tag{3.21}$$

and the end conditions

$$\begin{aligned}
x_1(0) &= .1, & x_1(t_f) &= .8 \\
x_2(0) &= -.15, & x_2(t_f) &= .05 \\
x_3(0) &= 0 & x_3(t_f) &- \text{free} \\
x_4(0) &= 0 & x_4(t_f) &= 0.
\end{aligned}$$

The functions $f_3(x,u)$ and $f_4(x,u)$ are given in Appendix 1.

For this problem, $n = 4$, $m = 2$, $d = 1$, $q = 3$, $r = 3$.

Problem 4

$$\text{Minimize} \quad I = t_f \tag{3.22}$$

subject to the differential constraints

$$\begin{aligned}
\dot{x}_1 &= f_1 = x_3 \\
\dot{x}_2 &= f_2 = x_4 \\
\dot{x}_3 &= f_3(x) \\
\dot{x}_4 &= f_4(x) \\
\dot{x}_{4+k} &= f_{4+k}(x,u) \quad , k = 1,\ldots,5 \\
\dot{x}_{9+k} &= f_{9+k}(x,u) \quad , k = 1,\ldots,5
\end{aligned} \tag{3.23}$$

The last two sets of equations are given by equations (2.6) and (2.18) respectively of Chapter 2.

the control and state variable constraints

$$0 \leq u_k \leq 1 , \quad k = 1,....,5$$
$$x_2 \leq .05 \tag{3.24}$$

and the end conditions

$$\begin{aligned}
x_1(0) &= .1; \quad x_1(t_f) = .8 \\
x_2(0) &= -.15; \quad x_2(t_f) = .05 \\
x_3(0) &= 0 \quad ; \quad x_3(t_f) - \text{free} \\
x_4(0) &= 0 \quad ; \quad x_4(t_f) = 0. \\
x_{4+k}(0) &= 0 , \quad k = 1,..., 5 \\
x_{10}(0) &= 1.0871 \\
x_{11}(0) &= .8637 \\
x_{12}(0) &= 1.1127 \\
x_{13}(0) &= 1.0732 \\
x_{14}(0) &= 1.4263
\end{aligned} \tag{3.25}$$

For this problem, n = 14, m = 5, d = 1, q = 3, r = 6.

3.4 SOLUTION ALGORITHMS

The following algorithms were examined in this study:

(a) Optimal Steepest Descent (S D)

(b) Fletcher Reeves Method (F R)

(c) Method of Parallel Tangents (P T)

(d) Variance Algorithm (V A)

(e) Gradient-Restoration Algorithm (G R)

In the subsequent discussion the following notation will be used:

d_i = direction of search at ith iteration

α_i = step size for the ith iteration.

v_i = set of decision variables - controls u(t) and parameters p. i.e $v_i = (u_i, p_i)$

g_i = set of gradient of objective function with respect to the decision variables. In this study the gradient of the objective function has two components, one component being the derivative with respect to the control vector u(t) and is given by equation (3.9), and the other with respect to the parameter vector p and is given by equation (3.10)

(a) Optimal Steepest Descent

In this method the search direction is the gradient direction

$$d_i = - g_i \qquad (3.26)$$

$$\alpha_i = \arg\min_{\alpha} J(v_i + \alpha d_i) \qquad (3.27)$$

Where the notation arg min (.) represents the value of the argument that minimizes the quantity in the brackets.

(b) Fletcher-Reeves Algorithm [34]

In this method the search direction is given by

$$d_i = -g_i + \beta_{i-1} d_{i-1} \tag{3.28}$$

where

$$\beta_{i-1} = \langle g_i , g_j \rangle / \langle g_{i-1} , g_{i-1} \rangle \tag{3.29}$$

$\langle \cdot , \cdot \rangle$ is the inner product in $\mathcal{R}^m$ defined as

$$\langle g_i, g_i \rangle = \int_0^1 g_i^T (t)\, g_i(t)\, dt \tag{3.30}$$

$$\alpha_i = \arg\min \quad J(v_i + \alpha\, g_i) \quad . \tag{3.31}$$

(c) Method of Parallel Tangents [60]

In this method the search direction is given by

$$d_i = -(v_{i-1} - y_i) \tag{3.32}$$

where

$$\begin{aligned} y_i &= v_i - \omega_i g_i \\ v_{i+1} &= v_{i-1} + \alpha_i d_i \\ \alpha_i &= \arg\min \quad J(v_{i-1} + \alpha\, d_i) \\ \omega_i &= \arg\min \quad J(v_i - \omega g_i) \end{aligned} \tag{3.33}$$

(d) Variance Algorithm [16]

In this algorithm the direction of search is given by

$$-d_i = H_i g_i = g_i + \sum_{j=0}^{i-1} [\, ((\lambda_j - 1)/\rho_j) \langle r_j , g_i \rangle r_j \,] \tag{3.34}$$

where

$$r_i = g_{i+1} + \sum_{j=0}^{i-1} [((\lambda_j - 1) / \rho_j) \langle r_j , g_{i+1} \rangle r_j] \quad (3.35)$$

$$\rho_j = \langle r_i , g_{i+1} \rangle \quad (3.36)$$

The step size λ_i is determined as follows

$$\lambda_i = \alpha \qquad \text{if} \quad -1 < n_i < \alpha/(1-\alpha)$$

$$\lambda_i = \beta \qquad \text{if} \quad -\beta/(\beta-1) < n_i \leq -1 \quad (3.37)$$

$$\lambda_i = n_i/(n_i+1) \qquad \text{otherwise}$$

Where

$n_i = - \langle g_i , r_i \rangle / \rho_i$, α and β are specified constants.

(e) Gradient-Restoration Algorithm [44]

This algorithm belongs to the class of quasilinearization algorithms. It consists of two main phases - a gradient phase and a restoration phase. Both phases select the directions of search d_i as in the SD algorithm.

By linearizing the equations (3.2) to (3.6), the following linear two-point-boundary-value problem is obtained :

$$\dot{A} = f_x^T A + f_u^T B + f_p^T C - k_r(\dot{x}-f) \qquad (3.38)$$

$$\dot{\lambda} = S_x \rho - f_x \lambda + k_g L_x \qquad (3.39)$$

subject to the conditions

$$(A)_0 = 0 \qquad (3.40)$$

$$S_x^T A + S_u^T B + S_p^T C + k_r S = 0 \qquad (3.41)$$

$$(\phi_x^T A + \phi_p^T C \; k_r \phi)_1 = 0 \qquad (3.42)$$

$$(\lambda + k_g g_x + \phi_x \mu \;)_1 = 0 \qquad (3.43)$$

where

$$B = f_u \lambda - S_u \rho - k_g L_u \qquad (3.44)$$

$$C = \int_0^1 (f_p \lambda - k_g L_p - S_p \rho)\,dt + H \qquad (3.45)$$

$$H = (k_g g_p + \phi_p \mu)_1 \qquad (3.46)$$

$$\rho = (S_u^T S_u)^{-1}[\, S_x^T A + S_u^T D + F] \qquad (3.47)$$

$$D = f_u \lambda - k_g L_u \qquad (3.48)$$

$$F = S_p^T C + k_r S \qquad (3.49)$$

$$A = \Delta x / \alpha \tag{3.50}$$

$k_r = 1,\ k_g = 0$ for the restoration phase

$k_r = 0,\ k_g = 1$ for the gradient phase

The aim of the restoration phase is to ensure that the constraint error P is as small as possible, where P is given by the equation

$$P = \int_0^1 N(\dot{x}-f)dt + \int_0^1 N(S)dt + N(\phi)_1 \tag{3.51}$$

The notation $N(a) = a^T a$ is used to define the norm of the vector a.

The aim of the gradient phase is to minimize the error in the optimality conditions Q:

$$Q = \int_0^1 N(B^T B)dt + C^T C \tag{3.52}$$

The restoration step-size α is selected such that $P(\alpha) < P(0)$, while the gradient step-size α is chosen such that the condition $J(\alpha) < J(0)$; where J is defined by equation (3.6).

As we shall indicate, one alternative to this formulation is the case where the non-differential constraints are handled using the Penalty function

technique. For this case equations (3.38) to (3.50)are reduced by setting $S_x = S_u = S_p = 0$. For this case the gradient step-size α_i is chosen as

$$\alpha_i = \arg\min \; J(v_i - \alpha \; g_i) \tag{3.53}$$

whereas restoration stepsize α_i is selected according to the relation

$$\alpha_i = .75 \; \alpha_{i-1} \; ; \; \alpha_0 \text{ given} \tag{3.54}$$

where $\alpha_0 = 1$ for Problems 1,2,3. However due to numerical stability problems , α_0 is set at .1 for Problem 4.

3.5 HANDLING THE CONSTRAINTS

There are three main techniques for handling constraints in optimal control :

(i) Transformation - substitution [30].

(ii) Lagrange multipliers [44].

(iii) Penalty functions [33].

(i) Transformation - substitution technique

This technique is used mainly to handle state variable inequality constraints, i.e. constraints which do not contain any of the control variables explicitly. Consider for example, a scalar state variable inequality

constraint of the form

$$C(x) \leq 0 \tag{3.55}$$

Typical of such a constraint is the requirement that the knee cannot be hyperextended (equation (3.21c)). To apply the technique, the inequality constraint is first converted to an equality constraint using a slack variable r

$$C(x) - r^2 = 0 \tag{3.56}$$

Since C(x) is not explicitly dependent on any of the control variables, an attempt is made to find some other function of C(x) that does. To do this the following reasoning is used. For equation (3.55) to apply everywhere on the interval [0,1], its first time derivative must vanish everywhere on that interval, i.e.

$$dC/dt = \partial C/\partial t \; x - 2r\dot{r} = 0 \tag{3.57}$$

Substituting for x from equation (3.2) gives

$$\partial C/\partial t \; f(x,u,p,t) - 2r\dot{r} = 0 \tag{3.58}$$

If equation (3.58) contains a control variable explicitly

then it is used to solve for that control, thus eliminating that control variable from the problem. In this process, however, one additional control variable is added to the problem. If equation (3.58) does not contain any of the controls explicitly, the differentiation process is continued until an expression is found which contains at least one control variable explicitly. If k time derivatives are required , then equation (3.55) is called a k th order state variable inequality constraint. The use of transformation - substitution results in an unconstrained optimal control problem which is characterized by k extra state equations and (k-1) extra control variables for each k th order state variable inequality constraint.

The state variable inequality constraint defined by equation (3.21c) is a second order state variable inequality constraint, while the same constraint defined by equation (3.25b) is a fourth order constraint. A quick glance at the exact forms of f_4 in Appendix 1 will show that the process of differentiating the knee acceleration is not a trivial task. It follows that the use of this technique could result in formidable problems -- the differentiation of complex expressions followed by the solution of highly non-linear equations.

(ii) Lagrange - Multipliers Technique

This technique follows a similar procedure as the transformation-substitution technique. In this case, however it is not necessary to eliminate the old controls from the system state equations. Typically, all inequality constraints are first reduced to equality constraints as explained above. For instance, the constraint $u_{min} \leq u \leq u_{max}$ (equation 3.15) is reduced to a single equality constraint of the form

$$(u_{max} - u)(u - u_{min}) - r^2 = 0 \qquad (3.59)$$

where r is a slack variable. All the resulting equality constraints are handled using Lagrange multipliers. Owing to the indeterminate nature of the multipliers, only the gradient-restoration (or other equivalent quasilinearization algorithms) can be used with this technique. Several difficulties arise in the use of this technique on large scale problems. Consider for instance the single state variable inequality constraint in problem 4 (equation (3.24b)). First, use of this technique results in four extra state equations thus aggravating further the large number of pre-existing state equations in that problem. Also, the linearized state equations (3.38) and the adjoint equations (3.39) become coupled due to the presence of the S_x term.

Because of this coupling, the whole set of 36 differential equations will have to be integrated 20 times for each adjustment of the decision variables. Thirdly, on each of these occasions, a 23x23 matrix has to be inverted to solve the consequent two-point-boundary-value problem [44]. Because of these steps the storage requirements of the algorithm become prohibitively too large.

(iii) The Penalty function technique

There are two main types of penalty functions -- interior and exterior. The interior penalty functions handle constraints of the form $S(x,u,p,t) \leq 0$ by augmenting the original objective function with terms of the form

$$K / S(x,u,p,t) \tag{3.60}$$

where K is a decreasing constant. This technique has been used successfully to solve some small scale optimal control problems [35]. Our experience with this technique in the large scale problems was, however very discouraging. First, the method requires that all the decision variables be initially chosen to lie within the feasible region; a condition that we found difficult to satisfy in cases where the number of the decision

variables is large. Secondly, near the boundary of the feasible region, the method becomes highly unstable and very often leads to a complete abortion of the algorithm (note the presence of several exponential functions in the state equations for problem 4). Because of these problems attention was concentrated on the exterior penalty function technique. In this case all inequality constraints of the form described above, each of which contains the controls explicitly, are handled by augmenting the original objective function (equation (3.1)) with terms of the form

$$\int_0^1 \sum_{i=1}^{r} \left| S_i(x,u,p,t) \right|^{m} H(S_i)\,dt \tag{3.61}$$

where $m = 2$; and $H(S_i)$ is the Heaviside step function defined as

$$H(S_i) = \begin{cases} 0 & \text{if } S_i \leq 0 \\ K & \text{if } S_i > 0 \end{cases} \tag{3.62}$$

where K is a large positive constant. For inequality constraints of the form $S_i(x,p,t) \leq 0$ each of which does not contain the control variables explicitly a similar procedure could be applied. However, a more efficient technique is to handle the constraints by introducing an additional state equation defined as

$$\dot{x}_{n+1} = f_{n+1} = \sum_{i=1}^{s} \left| S_i(x,p,t) \right|^m H(S_i) \qquad (3.63)$$

where

$$x_{n+1}(0) = 0;\ x_{n+1}(1) = 0 \qquad (3.64)$$

The end condition $x_{n+1}(1)$ is added to ϕ (equation(3.5)) and all are handled via a penalty function of the form

$$\phi^T(1)\ G\ \phi\ (1) \qquad (3.65)$$

where G is a diagonal (qxq) matrix whose elements are chosen to be large positive constants. However, for the GR algorithm the end condition constraint vector ϕ was handled via Lagrange multipliers μ (equation (3.6)).

3.6 SEARCH FOR THE ONE-DIMENSIONAL STEPSIZE

The SD, FR and PT algorithms all require a search for the step size α . For the latter two, this step is in fact critical to their success in solving the problems. One of the most popular techniques for locating the one-dimensional stepsize in optimization is the use of polynomial interpolation. In this case, the objective function is approximated by a polynomial function of the stepsize. Usually either a quadratic or a cubic function is used. The parameters of the polynomial are evaluated by calculating the function and its derivatives at some selected points. The minimum point of the polynomial is

then found and used as an approximation to the minimum of the actual objective function. We have tried using a quadratic polynomial, but found it to be very inefficient for the larger problems (Problems 3 and 4 of this Chapter). Several dozen function evaluations were needed to find the minimum, a procedure which consumes a substantial amount of computing time. The inefficiency of the method was found to be related to the fact that the objective functions are characterized by narrow valleys making it difficult to fit a quadratic across. In this study, it was found expedient to use a modified form of the method of 'regula-falsi' [18] to find the step size. An interpolation-extrapolation scheme was therefore developed and added. The detailed procedure is explained by the flow chart shown in Figure (3.1). The basic idea behind the search scheme is to find α in the i th iteration such that

$$dJ_{i+1} / d\alpha = 0 \tag{3.66}$$

where

$$J_{i+1} = J(u_{i+1}, p_{i+1})$$

$$= J(u_i + \alpha_i d_i,\ p_i + \alpha_i t_i) \tag{3.67}$$

d_i and t_i are the gradients of the objective function J with respect to the controls and the parameters

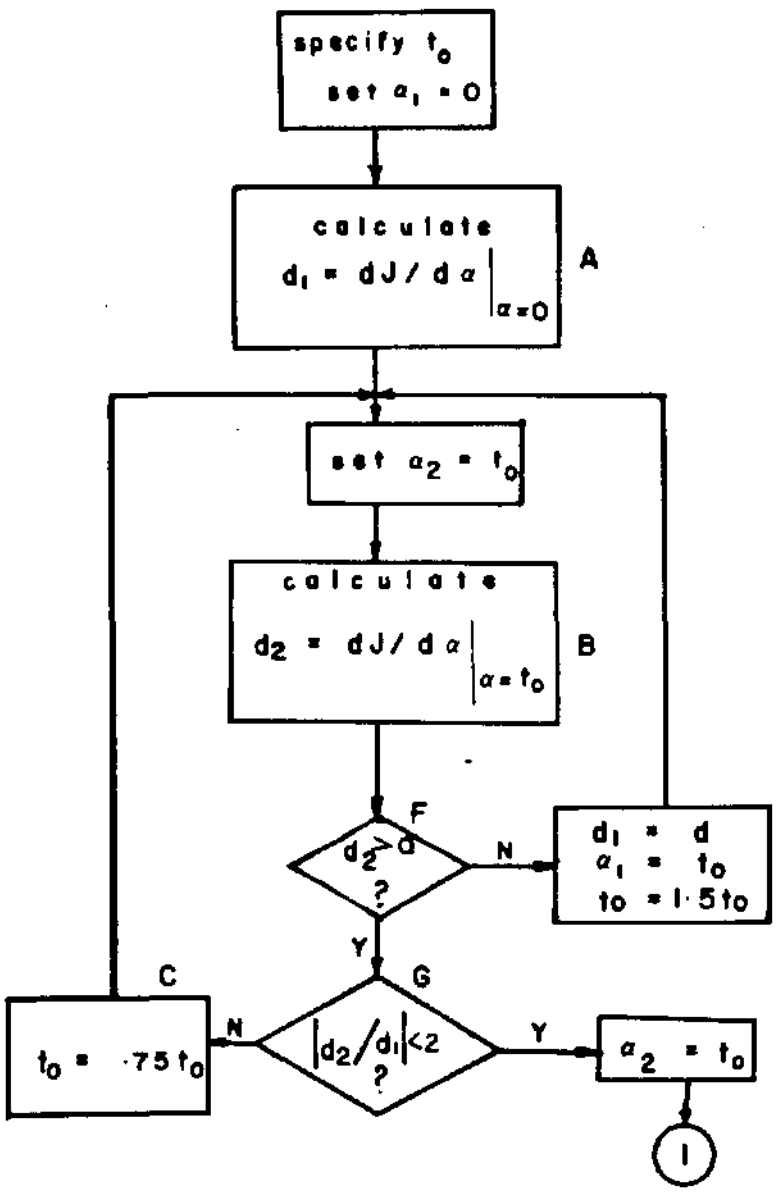


Fig. 3.1 Flowchart for the 'regula-falsi' technique .

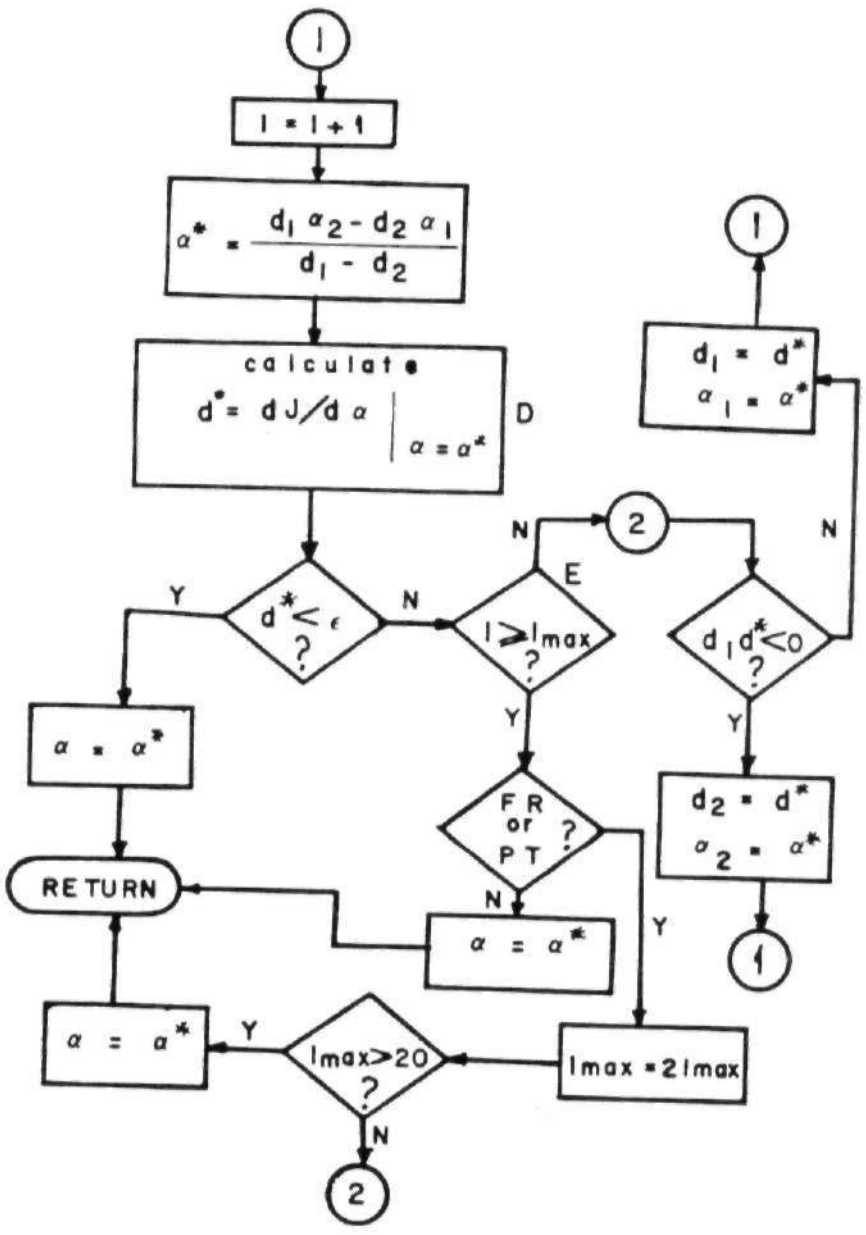


Fig. 3.1 (Continued)

respectively. It follows that

$$dJ_{i+1}/d\,\alpha = \left\langle d_{i+1},\, d_i \right\rangle + \left\langle t_{i+1},\, t_i \right\rangle \qquad (3.68)$$

It should be noted that the operations in boxes A, B and D of Figure (3.1) all require the integration of the state and adjoint equations each time they are encountered. It was found that if d_2 in the box F is positive but much larger than d_1 in box A, then an excessively large number of interpolations is performed before the root is located to the desired accuracy. This problem is alleviated by reducing the value of t_0 by some small fraction (box C) and the process repeated from box A. For moderate values of ϵ (.01 - .1) the condition in box E rarely arises for I_{max} sufficiently large (10 or over). If the condition arose, for the FR and PT algorithms, then the value of I_{max} was increased and the process continued. A ceiling of 20 was set for I_{max} after which the search was aborted and the most recent interpolate accepted as the stepsize for that iteration. The step of increasing I_{max} was not necessary for the SD and SG algorithms since their success does not depend crucially on the accuracy of the one-dimensional search.

3.7 COMPUTER IMPLEMENTATION

Computer programs were written for the implementation of each algorithm. In the implementation, all the non-differential and the end condition constraints were handled via an exterior penalty function technique.

The stopping condition for all problems was of the form

$$\langle g_i , g_i \rangle \leq \gamma \tag{3.69}$$

where $\gamma = 0.005$ for problems 1 and 2; but due to convergence difficulties the less stringent stopping condition of $\gamma = .1$ was used for Problems 3 and 4.

The one dimensional searches were carried out in the manner described in section (3.6) .

The choice of the step size λ in the VA algorithm was found to depend on the choices of α and β . The dependence is however stronger on the choice of α than on β . This is especially true for the larger problems. Owing to the presence of several exponential terms in problem 4, it was found that the use of too large a value of α numerical instability of the state equations results. It should be recalled that the first step in the algorithm is a steepest descent step. It was found that a suitable choice for α is the same as the

one-dimensional step size of that phase of the solution process.

In the GR algorithm, the stepsize for the restoration phase was selected according to equation (3.54). A suitable choice for the initial step size is 1 for problems 1,2 and 3. However, using this value for problem 4 leads to numerical instability problems of the type described above. Thus a more conservative value of .1 was used.

For the minimum time problems in this study, the actual running time t was normalized with respect to the actual (unknown) final time t_f; this was done by introducing the new independent variable $\tau = t/t_f$, where now $0 \leq \tau \leq 1$. The actual final time t_f was then made a component of the parameter vector p.

All the integrations were performed using the Hamming predictor - corrector with the Runge-Kutta as a starter. All quadratures were performed using the Simpson rule; with the integration interval divided into 100 subintervals.

3.8 RESULTS AND DISCUSSION

Figures 3.2, 3.3, 3.4 and 3.5 show the histories of the original objective function I as functions of the iteration numbers for problems 1, 2, 3 and 4

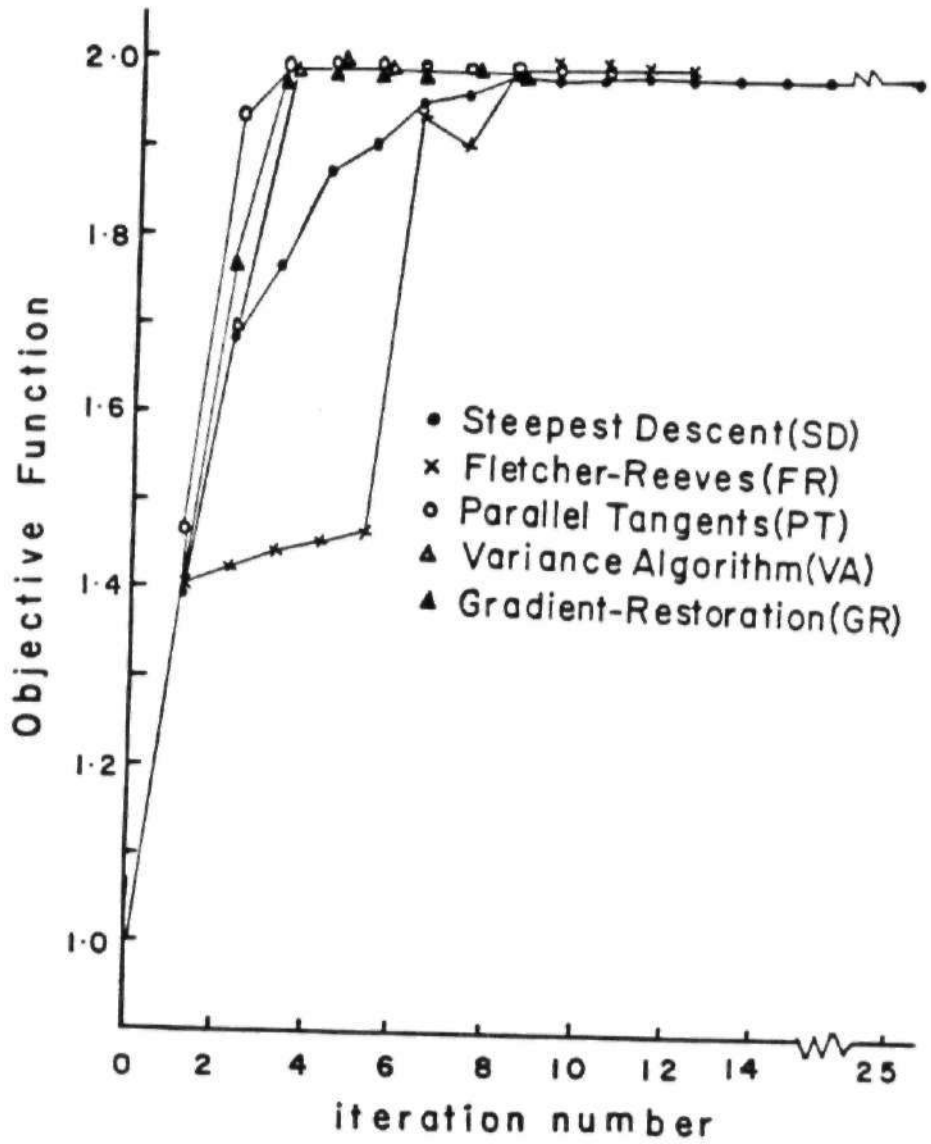


Fig. 3.2 Behavior of the objective function I for problem 1 as a function of the iteration number.

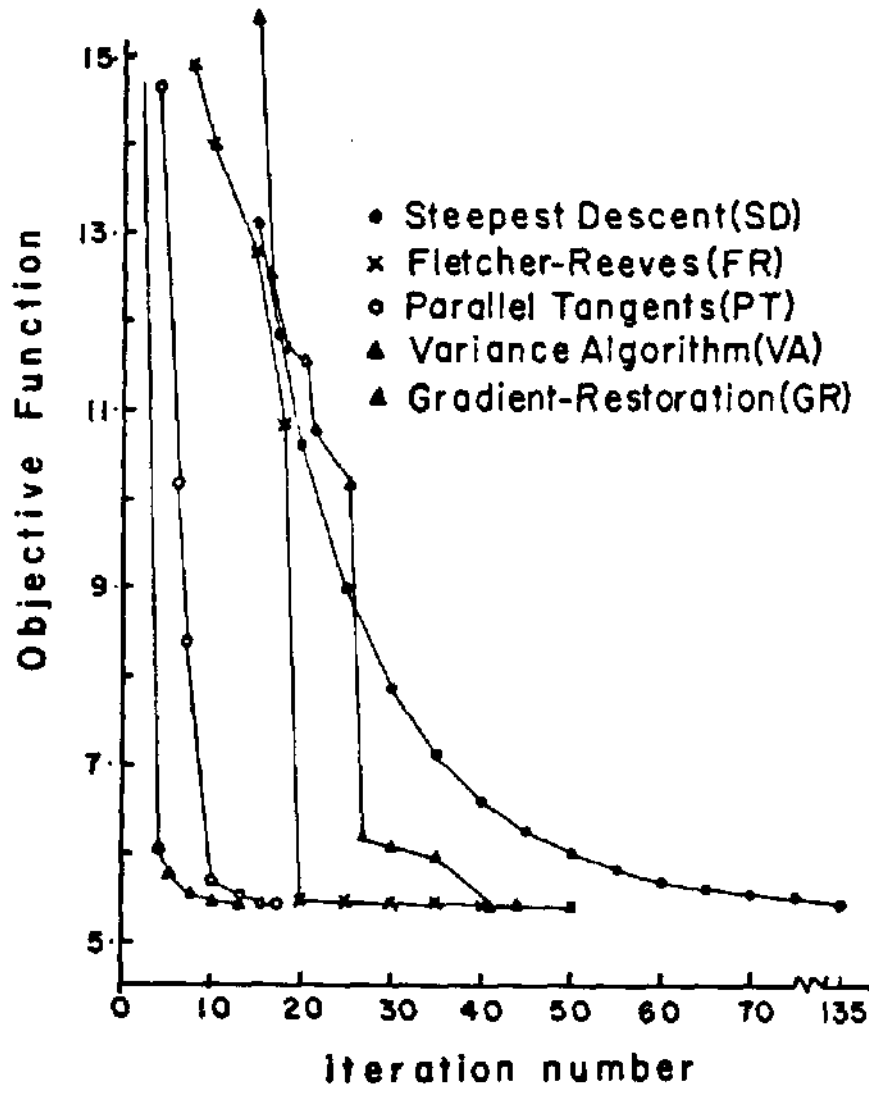


Fig. 3.3 Behavior of the objective function I for problem 2 as a function of the iteration number.

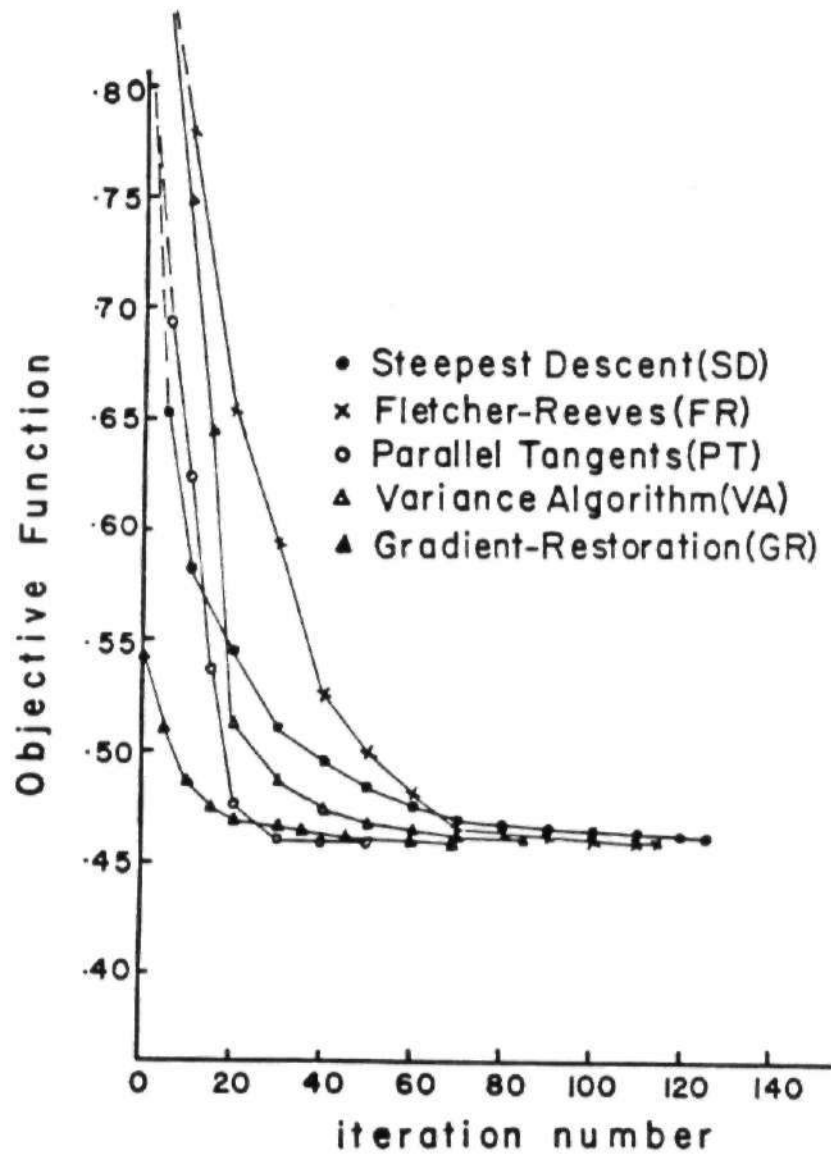


Fig. 3.4 Behavior of the objective function I for problem 3 as a function of the iteration number.

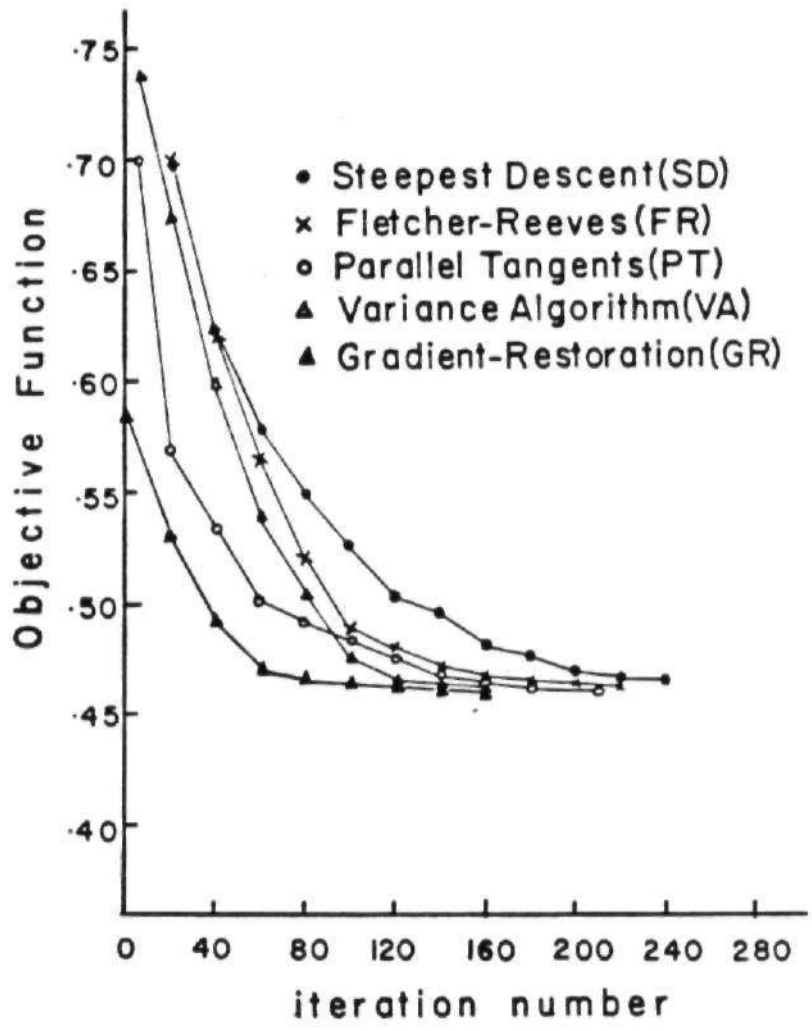


Fig. 3.5 Behavior of the objective function I for problem 4 as a function of the iteration number.

respectively. For problem 1, the initially specified value of I = 1 was below the actual minimum of 2. For problem 1 the penalty constant K (equation 3.62) was fixed at 500, while for problem 2 it was fixed at 800. However, for problems 3 and 4 it was found necessary to use much smaller values for K and to increase this value only in small steps. This is necessary to avoid numerical stability problems which could ensue if the values of the Lagrange multiplier λ in equation 3.11 become large. An appropriate starting value for K for these problems was 20. This value was increased in steps of 10. The results for problem 3 are for K = 50, and for problem 4 they are for K = 60. However much of the computing time was spent in the first run. Subsequent runs took much less time since the constraints were near satisfied after the first.

Table 3.1 gives the values of the computer running times required to solve the various problems on an Eclipse S-250 Computer. The running times of the SD Method for problems 3 and 4 in Table 3.1 are enclosed in parenthesis to indicate that the algorithm was prematurely stopped owing to repeated oscillations about the minimum point without any improvement in the objective function.

Based on the results for these four problems the five algorithms were compared using as criteria (1) rate

Table 3.1

Computer Running Times (min)

Problem	1	2	3	4
Steepest Descent	16	63	(780)	(1680)
Fletcher - Reeves	8	25	720	2100
Parallel Tangents	12	23	840	1920
Variance	9	17	480	1620
Gradient - Restoration	13	16	1020	2580

of convergence (number of iterations) ,(2) computer running time and (3) storage requirements.

(1) Rate of Convergence

From Figures 3.2 and 3.3, it can be appreciated that the VA algorithm, the PT algorithm and the GR algorithm are faster than the other two for solving the smaller problems. For problem 1 (Figure 3.2), the VA algorithm converges first. Interestingly, however, the three algorithms have converged to the same value after three iterations. It is thus clear that under a milder stopping condition, the relative positions of the three algorithms would change with respect to rate of convergence. For this problem the FR method shows a tendency to stall (between iterations 1 and 5). The sudden change after this stall period is due to the restart using the SD method. Thus the convergence characteristic of this algorithm often depends on this restart requirement which is also useful in flushing out any accumulated errors that would destroy the conjugacy property on which this algorithm depends. The SD algorithm like all the others shows a rapid convergence for the first few iterations but then slows down as the optimum is approached.

For problem 2 (Figure 3.3) the FR algorithm shows great improvement, however, as it approached the final

solution it was outperformed by the VA algorithm. The superiority of the GR algorithm for this problem is evident. The PT method performed very well also.

For the more complex problems 3 and 4 (Figures 3.4 and 3.5) the initial rapid convergence of the various algorithms was not exhibited. There is a more gradual descent to the optimum. For problem 3 (Figure 3.4) the PT method appears superior to the other four. For this problem and also for problem 4 (Figure 3.5) the FR method performed rather poorly, especially in terms of the initial rate of convergence. For these more complex problems with their highly nonlinear terms the chances of accumulation of numerical errors increases, which leads to a greater tendency for the conjugate conditions to be destroyed. It should be mentioned here that even though both the FR method and the PT method belong to the class of conjugate gradient methods, it is our experience with these two that the FR method is far more sensitive to the accuracy of the one dimensional search than the PT method. In fact for problem 4 severe difficulties were encountered in making the FR method to start off smoothly. To offset this problem the first few iterations were performed using the SD method; and then the results were used as initial results for the FR method. Owing to the difficulties in locating the minimum for the one dimensional search for problem 4, the

PT method lost its superiority for solving this problem.

(2) Computer Running Time

For problem 1 it is evident (Table 3.1) that the FR method took the least time to solve the problem. This is notwithstanding the fact that the VA algorithm solves the problem in the least number of iterations. In general the variance algorithm does not possess a descent property as the other methods [16]. Hence for this algorithm improvement is not guaranteed at every iteration. In fact there were occasions when several iterations were done before any improvement in the objective function was realized. However, it is observed that when a decrease occurs it is usually large. The larger running times for the GR algorithm stems from the fact that the linearized state and adjoint differential equations must be integrated a certain number of times (equal to the total number of end condition constraints plus one) before one iteration is made. Moreover, a large fraction of the time in one iteration could be spent in the restoration phase. The poor performance of the SD method is obvious in both problems 1 and 2.

The large computing times taken by the FR method and the PT method is owing to the excessively long times spent in the one dimensional search for a minimum. On the other hand the larger times for the GR algorithm

stems from a problem of a different nature. This algorithm in general requires the storage of a number of large size matrices. Owing to memory limitations on the computer used, some of the matrices for the larger problems had to be stored on disk. Thus the running time given involves the time required to retrieve and store these values onto the disk.

(3) Storage Requirements

Let n, m, q and s denote the number of state variables, control variables, end conditions and time stations for integration respectively. Both the SD and FR algorithms require storage for at most four (mxs) and two (nxs) matrices. In addition to these, the PT method requires storage for one (mxs) matrix. The VA algorithm requires storage for an (mxsxr) matrix; where r is the number of iterations before the algorithm is restarted. This restart has been used to minimize the storage requirement. Because of the use of an interpolation technique to solve the linear boundary-value problem of the GR algorithm, there is a need to store two (q+1) x (nxs) and one (q+1) x (mxs) matrices.

From this it is appreciated that the SD, FR and PT algorithms require minimal storage. For the VA algorithm, the storage may be large depending on the selected value for r. It is our experience that the

larger the value of r, the faster the method converges. Hence one must strike a compromise between storage and convergence. The storage requirement of the GR algorithm is very large. This led to the use of peripheral storage facilities for the larger problems in this study, a process that further increases the long computation time taken by the method.

3.9 SUMMARY AND CONCLUSION

From the results of this study it is found that the best algorithms for solving small sized optimal control problems are the GR algorithm, the VA algorithm and the PT method in that order. Even though some of these algorithms retain their superiority for the larger problems it is at the expense of either excessively long computation time (PT method) or very large computer storage requirement and further increase in computation time (GR algorithm). The VA seems to be an excellent compromise between the two, at least in the context of computer systems of the size available for this study. Since problem size and computer size are relative terms, it is expected that the choice would swing toward the GR algorithm if a very much larger machine was available for the problems considered here. However these problems are still relatively small compared to those which might be

formulated for such biological control systems. Based on our experience, successfully approaching these larger problems may well require more efficient algorithms as well as very large computational facilities.

CHAPTER IV

A DYNAMIC OPTIMIZATION TECHNIQUE FOR PREDICTING MUSCLE FORCES IN THE SWING PHASE OF GAIT

4.1 INTRODUCTION

As was mentioned in Chapter 1 a number of techniques have been used to solve the muscle force sharing problem in human gait. Most of these techniques are based on an optimization approach, but they vary in the manner in which the overall problem is formulated and in the choice of the objective function. On the one hand are techniques that completely ignore the dynamics of both the skeletal and muscular subsystems and solved the problem statically. On the other hand there are those techniques that take into account the complete dynamics of the skeletal subsystem but ignore the dynamics of the muscular subsystem. With regard to the choice of the objective function most of these techniques select one based purely on computational convenience. In one or two cases investigators have proposed and used objective functions that have some physiological background.

The purpose of this chapter is to describe a technique for predicting the muscle forces in the lower limb during the swing phase of normal gait. The dynamics of both the skeletal and muscular subsystems is fully

taken into account. The objective function selected is the metabolic energy consumption. To complete the picture, the same problem was solved using a static optimization technique and the results are compared and contrasted.

4.2 THE DYNAMIC OPTIMIZATION PROBLEM

4.2.1 Statement of the problem

The system under consideration is the lower limb consisting of four rigid bodies -- the pelvis, the thigh, the shank and the foot. This system is depicted diagrammatically in Figures (1.2) and (4.1). All movement of the system is restricted to the saggital plane and the swing phase of the limb alone is considered. The resulting system has five degrees-of-freedom -- x and y movement of the pelvis (assumed known), and the rotations about the hip, knee and ankle joints, all modeled as hinge joints. The system is actuated by nine muscle groups -- iliopsoas, hamstrings, rectus femoris, gastrocnemius, short head of biceps femoris, vasti, tibialis anterior, soleus and gluteus maximus. The resulting dynamic optimization problem can be stated as follows : given the hip, knee and ankle trajectories

$\theta_1(t)$, $\theta_2(t)$, $\theta_3(t)$ and the pelvic trajectory $(x(t),y(t))$, for the swing phase of gait ; find the

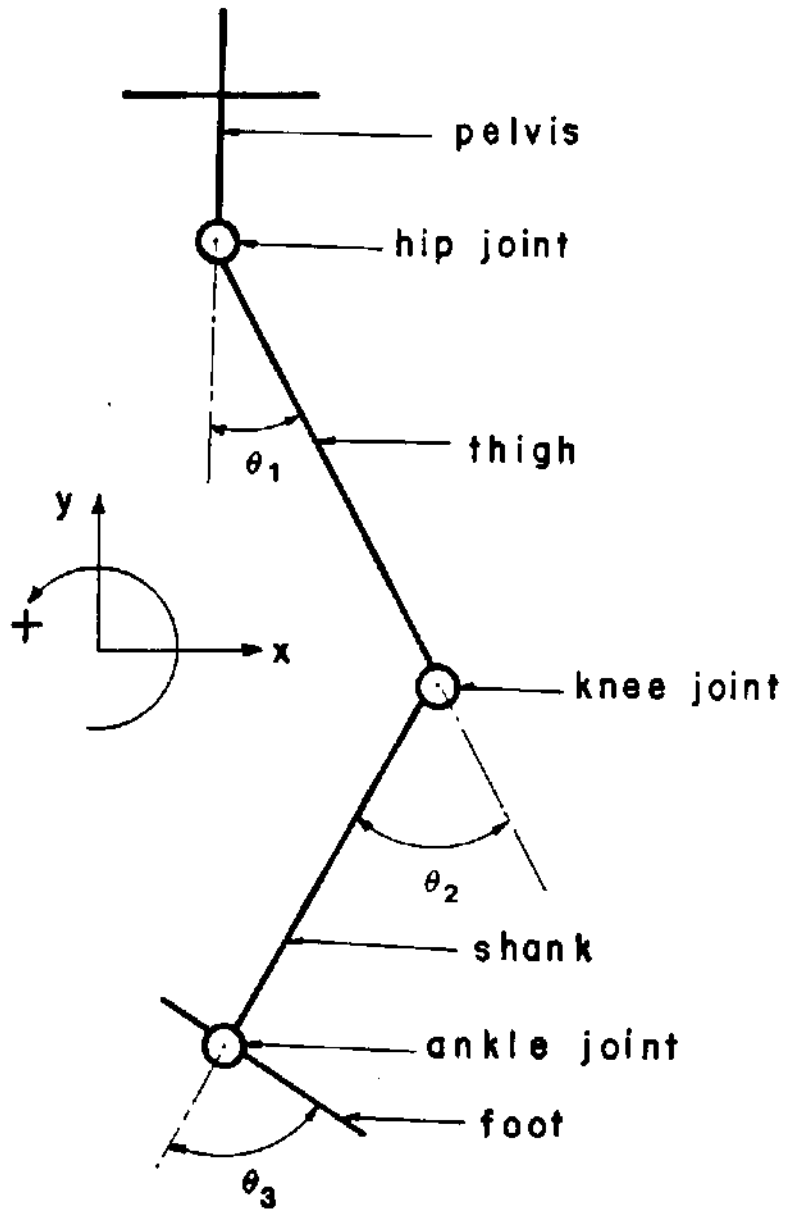


Fig. 4.1 Three-degree-of-freedom Lower limb model showing major segments.

muscle controls u(t) (and hence the muscle forces $F^M(t)$) that will generate the given trajectories while minimizing the total muscular effort expended in the process. By total muscular effort is meant the metabolic energy consumed as evidenced by the enthalpy change and the mechanical work done by the muscles. Viewed from an optimal control point of view, this problem is analogous to a nonlinear tracking problem with a limitation on the amount of energy consumed in the process. An appropriate objective function for the problem will take the form

$$J = z(t_f)^T Bz(t_f) + \int_{t_0}^{t_f} [\, z(t)^T Hz(t) + G\dot{E}(t)]dt \qquad (4.1)$$

where

$z(t) = x(t)^d - x\ (t)$

$x(t)$ = the generated trajectory

$x^d(t)$ = the desired trajectory

B, G, and H are positive definite (or semidefinite) weighting matrices.

$\dot{E}\ (t)$ = a measure of the total energy involved in process.

4.2.2 The Rate of energy consumption

The rate of metabolic energy consumption in a given activity can be shown to consist of five terms [22], [46]

$$\dot{E} = \dot{A} + \dot{M} + \dot{S} + \dot{W} + \dot{D} \qquad (4.2)$$

where

$\dot{A}$ = muscle activation heat rate

$\dot{M}$ = muscle maintenance heat rate

$\dot{S}$ = muscle shortening heat rate

$\dot{W}$ = muscle mechanical work rate

$\dot{D}$ = rate of energy dissipation in the passive structures.

The empirical relationships describing each of these quantities will now be derived.

(a) The Activation heat rate

When a resting muscle is brought into activity by stimulating it with a single stimulus, some amount of heat was found to be given off by the muscle before any mechanical activity is manifested. This heat is called the activation heat. It is believed that the activation heat is the result of the turnover of calcium immediately after the action potential that stimulates the muscle. Thus the activation heat is often associated with the excitation-contraction coupling--the energetic consequence of switching the machinery on and off.

Based on the experimental works of Gibbs and Gibson [19] ,Hatze [22] modeled this phenomenon as an

exponential function of the stimulation frequency f :

$$\dot{A} = k\ f\ H\ /\ H_m f_{max} \tag{4.3}$$

where

$H = 1 - \exp(-(e_1 + e_2/f))$

$H_m = 1 - \exp(-(e_1 + e_2/f_{max}))$

$k,\ e_1,\ e_2$ are constants

f_{max} = the maximum stimulation frequency

Defining $f\ /\ f_{max} = s$, equation 4.3 can be written as

$$\dot{A} = k\ s\ H\ /\ H_m \tag{4.4}$$

where

$H = 1 - \exp(-(e_1 + e_2/f_{max}s))$

$H_m = 1 - \exp(-(e_1 + e_2/f_{max}))$

The constants e_1 and e_2 have numerical values of 18.2 and 0.25 respectively [22]. A plot of $\dot{A}$ versus s is shown in Figure 4.2. From this figure it is seen that for most practical purposes $\dot{A}$ can be modeled as a linear function of normalized frequency s except at very low frequencies. Since at such frequencies the value of $\dot{A}$ is relatively small, only a small error is introduced by using the linear approximation.

Let H_A be the activation heat rate per unit mass. Then an appropriate model for the activation heat is

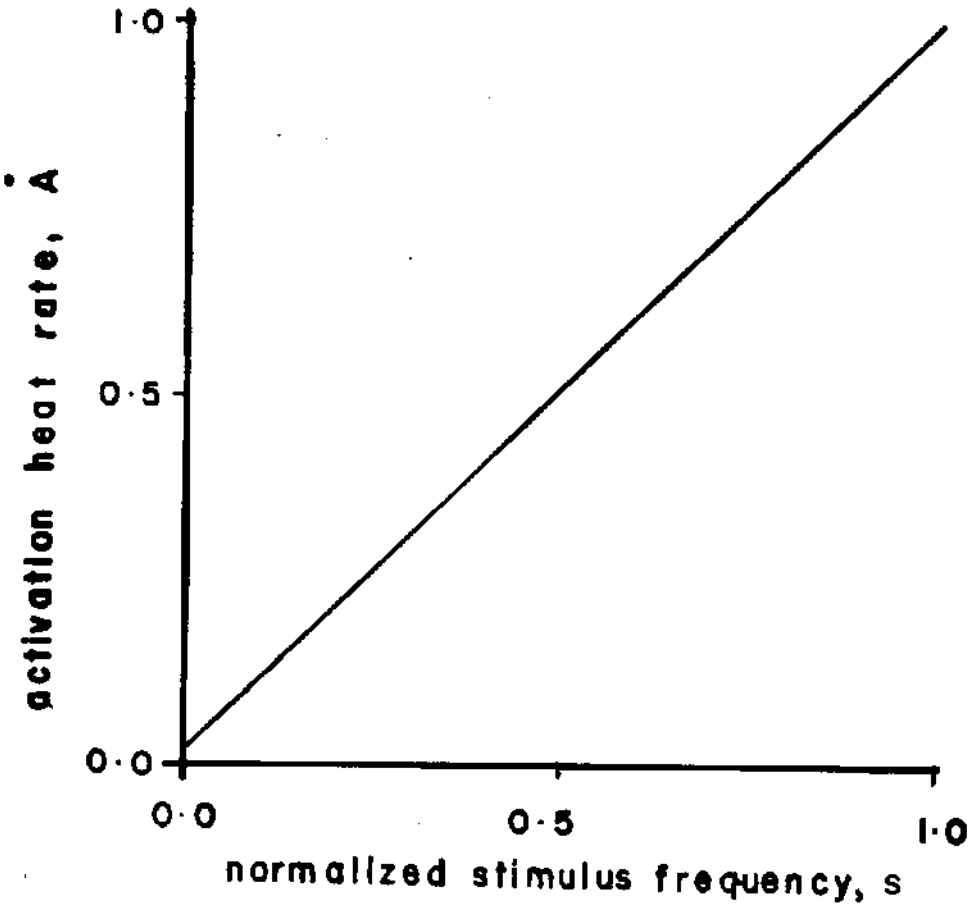


Fig. 4.2 Activation heat rate A as a function of normalized stimulus rate s.

$$H_A = a_1 f + b_1$$

where

a_1 , b_1 are constants

When $f = f_{max}$, $H_A = f_a$ and when $f = 0$, $H_A \approx 0$

$$\therefore \quad \dot{A} = W_m f_a s \qquad (4.5)$$

where

f_a = the muscle specific activation heat rate in W/kg

W_m = the muscle mass in kg.

(b) The Maintenance heat rate

Aubert [1] in his numerous experiments on muscle thermodynamics found that the heat produced in an isometric tetanus begins at a high rate and then quickly falls by about half, during a few seconds, to a steady rate. The initial rapid rate has been associated with the excitation--contraction coupling and hence identified with the activation heat rate. In their own experiments Gibbs and Gibson [19] classified the maintenance heat rate into a tension-dependent heat rate and a tension independent heat rate. The tension-independent heat rate is essentially the activation heat rate. Gibbs and Gibson [19] have also shown that the tension-dependent heat rate is also a linear function of the isometic force. It should be recalled that the isometric force is a function

of the muscle length and the active state of the muscle (equation (2.13)).

An appropriate form for this linear relationship is

$$H_2 = a_2\bar{F} = a_2\bar{F}k(Q_c)q(s)$$

where

H_2 = the muscle maintenance heat rate per unit mass

a_2 = a constant

$\bar{F}$ = the isometric force of the muscle at the optimum length of the contractile element $\bar{L}_c$ and at maximum stimulation frequency.

$k(Q_c)$ = the muscle length-tension relationship defined in equations (2.5) and (2.14).

$q(s)$ = the active state of the muscle defined in equation (2.4).

Q_c = the normalized length of the contractile element.

Identifying the constant $a_2\bar{F}$ with the muscle specific maintenance heat rate f_m, we get

$$\dot{M} = W_m f_m k(Q_c)q(s) \qquad (4.6)$$

The constants f_a, f_m and a_1 in equations (4.5) and (4.6) vary for fibers of differing speed of contraction. The decision as to which category (fast, intermediate or slow) a muscle belongs, is made using the data in Table 4

of Johnson et al [31]. From this data, all muscles with 70 per cent or more of Type II fibers are categorized as fast, all those with 40 to 70 per cent of Type II fibers are categorized as intermediate, and those with less than 40 per cent of Type II fibers as slow.

The muscle masses W_m were calculated using the relationship

$$W_m = \rho_m A_m L_0 \tag{4.7}$$

where

ρ_m = the density of muscle tissue taken as 1000 kg/m^3 [23].

A_m = the muscle cross-sectional area

L_0 = the rest length of the muscle

The cross-sectional areas A_m used in the present study are obtained from the data in [4] and [59].

(c) The shortening heat rate

Hill [25] found that when an isometrically contracting muscle is allowed to shorten, extra heat appears while shortening is taking place, after which the maintenance heat resumes approximately its original course. Moreover, he found that at a given speed (or load) the shortening heat is proportional to the distance shortened. The extra heat produced as a consequence of the shortening is called the shortening heat rate.

Following similar reasoning as in Hill [25], this quantity can be modeled by the relation

$$\dot{S} = a\ V$$

The constant of proportionality a is the same as that defined in the Hill force-velocity relationship by equation (2.21) and is given by

$$a = b_1 \hat{F}$$

where

V = muscle contraction velocity defined by the relation $V = - L_c \dot{Q}_c$

L_c = the isometric length of the contractile element

$\hat{F}$ = the maximum isometric force of the muscle

b_1 = a constant

Thus $\dot{S}$ takes the final form

$$\dot{S} = - b_1 \dot{L}_c \bar{F} k(Q_c) q(s) \qquad (4.8)$$

(d) The mechanical work rate

The mechanical work rate is the product of the muscle force and the muscle contraction velocity

$$\dot{W} = - \bar{L}_c \dot{Q}_c F^{SE} \qquad (4.9)$$

where

F^{SE} = the force in the series elastic element

(e) Rate of dissipation in the passive structures

This quantity is given by the relation [22]

$$\dot{D} = c \dot{L}^2 \tag{4.10}$$

where

$\dot{L}$ = the total muscle velocity

c = the dissipation constant

4.2.3 Calculating the muscle lengths and moment arms

Perhaps the best way to obtain the muscle lengths and the moment arms is to measure them directly on the specific subject under study. Indeed, the results of the dynamic optimization problem in this study were so strongly influenced by the choices of these two sets of parameters that the importance of accurately determining them in any actual gait analysis cannot be overemphasized. There are a number of problems, however with this direct measurement approach that make it difficult to use. One problem is that a large number of the muscles do not have well defined origins and insertions and as such, the choice of an average origin and/or insertion is bound to affect the final result. Such an effect has been discussed in connection with the kicking problem in Chapter 3. Another problem is that some of the muscles lie well below the others, making it difficult to locate their actual origins and insertions.

A number of techniques have been proposed and used in the literature for analytically estimating the muscle lengths and moment arms [51]. A unified approach to these techniques is developed by using the following assumptions :

1. For the one - joint muscles, the point of insertion is not far away from the joint it crosses.

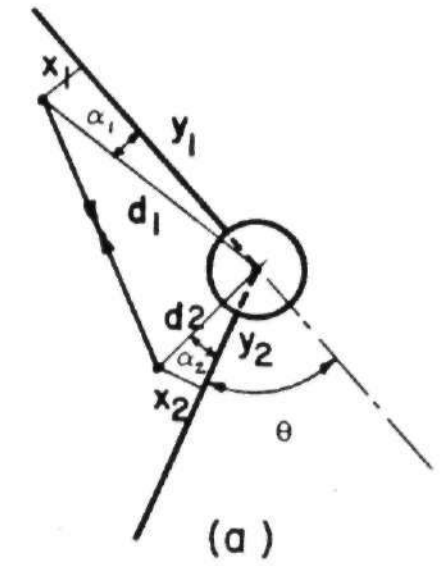
2. For most practical purposes, the muscle remains parallel to the link from which it originates.

3. For the two - joint muscles, the points of origin and insertion are close to the proximal and distal joints respectively.

4. For most practical purposes, the muscle remains parallel to the intermediate link.

5. There are pulleys of specified radii on which the muscle glides if the links rotate in a direction away from the side on which the muscle is embedded (anterior or posterior).

The possible modes of limb position and muscle length based on the above assumptions are depicted in Figure (4.3). For the model considered here (Figure 4.1), there are two possible cases to consider for the one-joint muscles depending on whether the angle θ is positive (Figure 4.3b) or negative (Figure 4.3a). For the two-joint muscles the number of possible modes is four -- depending on whether θ_1 and θ_2 are both negative (Figure



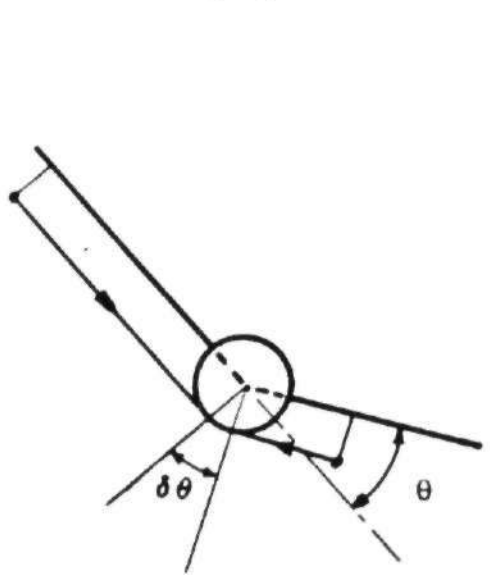


Fig. 4.3 Possible limb positions for calculating muscle length. (a-b) are for one-joint muscles and (c-f) are for two-joint muscles.

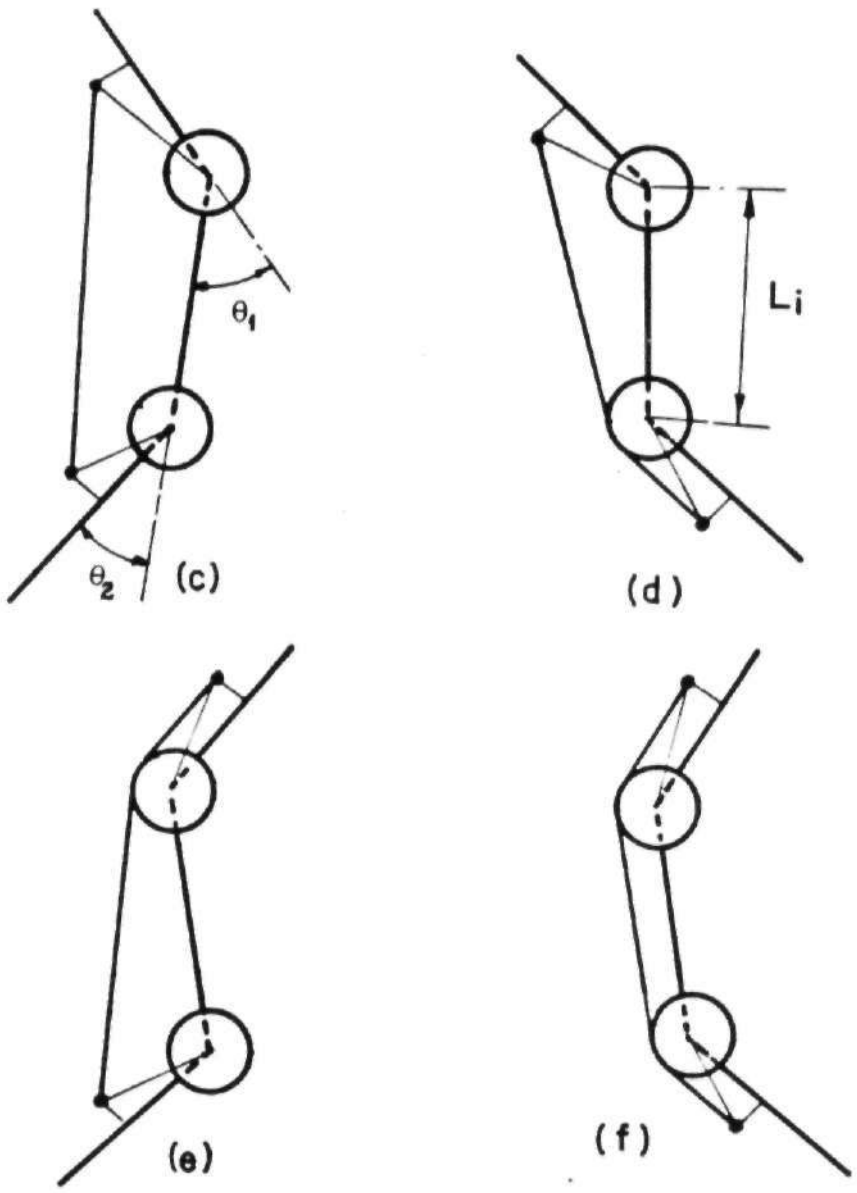


Fig. 4.3 (Continued)

4.3f) , both positive (Figure 4.3d) or one positive and the other negative (Figures 4.3c and e). From the geometry of these cases the following equations are obtained :

For the one-joint muscles

$\theta_1 > 0$

$$L = [\, d_1^{\,2} + d_2^{\,2} + 2d_1d_2\cos(\, \theta_1 + \alpha_1 + \alpha_2 \,)\,]^{1/2} \tag{4.11}$$

$$r_1 = d_2 \sin(\, \theta_1 + \alpha_2 \,)$$

$\theta_1 < 0$

$$L = Y_1 + Y_2 + x_2\theta_1 \tag{4.12}$$

$$r_1 = x_2$$

For the two-joint muscles the equations are

$\theta_1 < 0, \quad \theta_2 < 0$

$$L = L_i + d_1\cos(\, \theta_1 + \alpha_1) + d_2\cos(\, \theta_2 + \alpha_2)$$
$$r_1 = d_1\sin(\, \theta_1 + \alpha_1) \tag{4.13}$$
$$r_2 = d_2\sin(\, \theta_2 + \alpha_2)$$

$\theta_1 > 0, \quad \theta_2 > 0$

$$L = L_i + (y_1 + x_1\theta_1) + (y_2 + x_2\theta_2)$$
$$r_1 = x_1 \tag{4.14}$$
$$r_2 = x_2$$

$\underline{\theta_1 > 0, \quad \theta_2 < 0}$

$$L = L_i + d_2\cos(\theta_2 + \alpha_2) + (y_1 + x_1\theta_1)$$
$$r_1 = x_1 \qquad (4.15)$$
$$r_2 = d_2\sin(\theta_2 + \alpha_2)$$

$\underline{\theta_1 < 0, \quad \theta_2 > 0}$

$$L = L_i + d_i\cos(\theta_1 + \alpha_1) + (y_2 + x_2\theta_2)$$
$$r_1 = d_1\sin(\theta_1 + \alpha_1) \qquad (4.16)$$
$$r_2 = x_2$$

where

x_1 , y_1 = the coordinates of the muscle origin in a coordinate frame whose origin is at the joint crossed by the muscle.

x_2 , y_2 = the corresponding coordinates of the muscle insertion

d_1 , d_2 = the distances of the origin and the insertion respectively from the joint

α_1 , α_2 = the angles made by d_1, d_2 with the y - axis

r_1 , r_2 = the radii of the pulleys assumed equal to x_1 , x_2

L_i = length of the intermediate link crossed by a two-joint muscle

It should be mentioned at this point that even though this technique is quite easily implemented in a static optimization problem, our experience with it shows that it is not easily implemented in a dynamic optimization setup. This is because at the point of switching from one mode to another, discontinuities occur at the moment arm and muscle length calculations. Even though these discontinuities are relatively small at these levels of computation, they become highly amplified in the gradient matrices. Such discontinuities not only violate the smoothness assumptions on the gradient matrices but also lead to persistent divergence in the numerical solution process.

Another simpler technique that could be used to approximate the muscle lengths and moment arms is to assume that these quantities vary in a given fashion with joint position. The equations for the muscle lengths and moment arms can for most practical purposes be written as

$$L = L_0 + \Delta L(\theta) \qquad (4.17)$$

where

L_0 = the muscle length at some position of the system.

ΔL = a variation about that position

The quantity ΔL can be assumed to be a linear function of the joint angle(s) with the additional conditions

$$L(0) = 0$$

$$\Delta L(\theta) = p$$

Thus the lengths for one-joint and two-joint muscles can be written as

$$L = L_0 + k_1 \theta_1$$

$$L = L_0 + k_1 \theta_1 + k_2 \theta_2 \qquad (4.18)$$

If p percent change occurs for a given measured change in the joint angle, then

$$k_1 = p\, L_0 / 100 \times \Delta\theta \qquad (4.19)$$

Similar equations can be used for the moment arm calculations.

For purposes of the calculations in this study both these techniques were used. However, only the results using the first technique are given. Simplification is obtained for the equations describing the length and moment arms if it is noticed that for the swing phase the hip and ankle angles are always positive and the knee angle is always negative. Hence only one of the modes is applicable for all the muscles. The same set of equations are used even if the sign of the angle changes by nature of the choice of the initial controls. As the required solution is approached the specified mode

becomes applicable. The difficulty of discontinuities in the gradient calculation was avoided by this simplification.

4.2.4 Modeling the penniform muscles

Two of the muscle groups in this study - the vasti group and rectus femoris are penniform muscles. For these muscle groups, a slight modification of the force equation is required to take into account the inclination of their fibers [23]. To model the force output of the penniform muscles it is assumed that all the fibers are arranged in parallel as depicted in Figure 4.4a. Figure 4.4b shows a lumped model of the muscle. To calculate the length of the series elastic element (SE), for a given length of the contractile element, consider Figure 4.4c. From the geometry of this figure it can be deduced that

$$L_s = L-[(Q_c\bar{L}_c)^2-d^2]^{1/2}$$

and (4.20)

$$\sin\theta = [1.-(d/Q_c\bar{L}_c)^2]^{1/2}$$

where L, L_s and L_c are the average muscle length from origin of topmost fibers to insertion at the tendon end, the length of the series elastic element and the isometric length of the contractile element respectively. The resultant force in the series elastic element is then

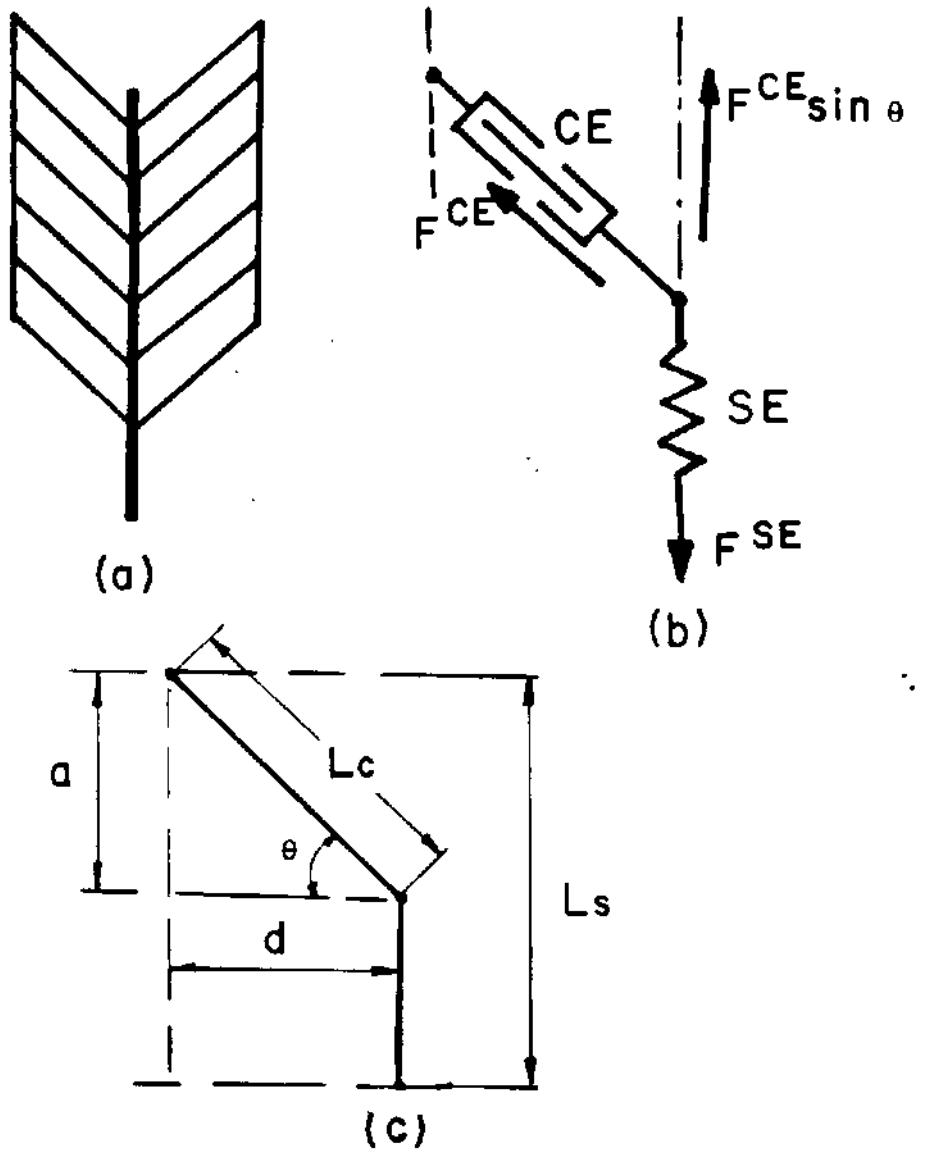


Fig. 4.4 Penniform muscle. (a) shows inclination of fibers and (b-c) show model for calculating force in muscle.

given as

$$F^{SE} = F^{CE} \sin \theta \tag{4.21}$$

4.2.5 The weighting matrices

The weighting matrices G and H in equation (4.1) are vital to the solution of the dynamic optimization problem. This is because the desired optimal solution for the objective function J relative to the error function L is zero ; whereas relative to the energy function E it may be much different from zero. For instance the quantity E may be as much as a thousand times the quantity L. To ensure that these quantities are equally weighted, it was found necessary to to use large values for the elements of H. However it was found that too large values lead to numerical stability problems. Thus it was found necessary to use as large values as possible for the elements of H and to use small values for the elements of G. Typical values for these matrices are 1000. and .1 respectively. As the calculated trajectories approach the desired trajectories the E term again tends to overwhelm the L term; making it necessary to increase the elements of the G matrix.

4.2.6 Handling the constraints on the controls

A number of techniques for handling constraints have been mentioned in Chapter 3. In solving the optimal control problem in this Chapter the Penalty Function technique was initially used to handle the inequality constraints on the control variables. However owing to larger values of the gradient matrices f_x and f_u, increments in the control variables over nominal values are often found to lead to negative updated controls in the step

$$u_{i+1} = u_i - \alpha_i J_u \qquad (4.22)$$

For u_{i+1} negative, g defined by equation (2.6) may become negative. This will lead to the exponential relationship given by equation (2.4) to become unbounded.

To alleviate this problem, a technique which has found widespread application in static optimization was used [3]. This is a technique which makes it possible to simulate inequality constraints by transformations in which the original decision variables are the range variables of a mapping from the set of real numbers to a subset which corresponds to the permitted ranges. For instance, if u is an adjustable variable then use of the following transformations with the unconstrained adjustment of v will correspond to the variation of u

only over the permitted ranges shown.

(i) $u = \sin^2 v$ $\quad 1 \geq u \geq 0$

(ii) $u = v^2$ $\quad u \geq 0$

(iii) $u = \exp(v)$ $\quad u \geq 0$

(iv) $u = a + (b - a) \sin^2 v$ $\quad a \leq u \leq b$

(v) $u = v^2 / (1 + v^2)$ $\quad 0 \leq u \leq 1$

These transformations do not introduce any local optima since every neighborhood of v is mapped into a neighborhood of u.

Originally the transformation (i) was used to handle the constraints on the controls. This choice was made because this transformation was used successfully to solve certain static optimization problems [18]. Our experience with it in dynamic optimization, however, was not encouraging. This is because the controls and the force histories obtained were characterized by sharp spikes. Since the expected solutions are assumed to be smooth functions the use of this transformation was abandoned in favor of (v) which gave smoother outputs.

4.2.7 Complete set of state equations

The complete set of state equations for the dynamic optimization problem are given below. The muscle dynamic equations are the same as those describing model 3 of Chapter 2.

$$\dot{x}_1(t) = f_1 = x_4 \tag{4.23}$$

$$\dot{x}_2(t) = f_2 = x_5 \tag{4.24}$$

$$\dot{x}_3(t) = f_3 = x_6 \tag{4.25}$$

$$\dot{x}_4(t) = f_4 \tag{4.26}$$

$$\dot{x}_5(t) = f_5 \tag{4.27}$$

$$\dot{x}_6(t) = f_6 \tag{4.28}$$

$$\dot{x}_{k+6}(t) = f_{k+6} = b_{9k}(b_{10k}s_k - x_{k+6}) \tag{4.29}$$

$$\dot{x}_{k+15}(t) = f_{k+15} = \begin{cases} -b_{11k}\, W_1 / W_2 & \text{for } F^{SE} \leq F_1 \\ -b_{12k}\, W_3 / W_4 & \text{for } F^{SE} > F_1 \end{cases} \tag{4.30}$$

$$\dot{x}_{25}(t) = f_{25} = 1 \tag{4.31}$$

The states x_1, x_2 ,x_3 represent the hip, knee, and ankle trajectories respectively; x_4, x_5 and x_6 are the corresponding angular velocities. $x_{k+6}(t)$ is the normalized calcium ion concentration defined in equation (2.6) and $x_{k+15}(t)$ is the normalized length of the contractile element defined in equation (2.18). s_k is the normalized frequency of stimulation. The exact forms of the functions f_4, f_5 and f_6 defined in equations 4.26 to 4.28 and representing the limb angular accelerations are given in Appendix 4. The index k varies from 1 to 9. In these equations

$$W_1 = (F_1 - F_k^{SE}) \tag{4.32}$$

$$W_2 = (F_k^{SE} + b_{13k}F_1) \tag{4.33}$$

$$W_3 = F_1 - F_k^{SE} \tag{4.34}$$

$$W_4 = 1.33F_1 - F_k^{SE} \tag{4.35}$$

$$F_1 = b_{4k}q(x_{k+6})k(x_{k+15}) \tag{4.36}$$

$$q(x_{k+6}) = 1 - .995\exp(-b_{1k}x_{k+6}) \tag{4.37}$$

$$k(x_{k+15}) = \exp[-(x_{k+15} - 1)^2/b_{2k}]\ K_2 \tag{4.38}$$

$$K_2 = [1. - (b_{3k}/b_{5k}x_{k+15})^2]^{1/2} \tag{4.39}$$

$$F_k^{SE} = b_{8k}\,[\exp(b_{7k}\,\delta_k - 1)] \tag{4.40}$$

$$\delta_k = L(k) - [(b_{5k}x_{k+15})^2 - b_{3k}^2]^{1/2} - b_{6k} \tag{4.41}$$

where

$L(k)$ = the length of the k th muscle. The quantity $\dot{E}$ in equation (4.2) takes the form

$$\dot{E} = Q_1 + Q_2 + Q_3 + Q_4 \tag{4.42}$$

where

$$Q_1 = a_{1k}[a_{2k}s_k + H] \tag{4.43}$$

$$H = a_{3k}k(x_{k+15})q(x_{k+6}) \tag{4.44}$$

$$Q_2 = -b_{13k}\dot{x}_{k+15}F_1 b_{5k} \tag{4.45}$$

$$Q_3 = -b_{5k}\dot{x}_{k+15}F_k^{SE} \tag{4.46}$$

$$Q_4 = a_{4k}\dot{L}^2(k) \tag{4.47}$$

In this problem formulation, the dimension of the state vector is 25 (6 link equations, 18 muscle equations and one equation due to the explicit appearance of the

time t in the equations of motion). The dimension of the control vector is 9.

The initial conditions $x_1(0)$ to $x_3(0)$ are the same as the initial values of the specified hip, knee and ankle trajectories. The initial angular velocities are set equal to the corresponding values obtained by solving the inverse dynamics problem. No information was found about possible initial values for the normalized calcium ion concentration in the muscles for the swing phase of gait. The initial values $x_7(0)$ to $x_{15}(0)$ are therefore set equal to the values of the corresponding controls at time $t = 0$. This is assumed to be a reasonable approximation since the magnitude of the impulse response of the first order system defined by equations 4.29 is approximately equal to the magnitude of the input (control). This latter quantity is assumed to be held constant over the short time interval Δt equal to the total integration interval divided by the total number of sub-intervals used in the integration of the equations. The initial values $x_{16}(0)$ to $x_{24}(0)$ are obtained by solving equations (4.40) using the values of F_k^{SE} from the previous iteration. The first set were obtained using $F_k^{SE} = 0$. Thus the initial values $x_7(0)$ to $x_{24}(0)$ all vary from iteration to iteration. The initial value $x_{25}(0) = 0$.

(a) Estimating the muscle model parameters

Some of the parameters in the model were estimated by simulating isometric experiments. To this effect, the length of the muscle was held fixed and several parameter values were tried until the muscle produces an isometric force that is as close as possible to the specified value. The values of b_1, b_2, b_7 ,b_9 and b_{10} were estimated in this way. b_3 is the amount of inclination of the penniform muscles. The values of these parameters are the same as those used by Hatze [21]. The isometric force of the muscle b_4 was obtained from the data of Pedotti et al [50]. b_5 and b_6 are the isometric length of the contractile tissue and the rest length of the tendinuous tissue respectively. The second parameter was obtained from Table 1 of Pedotti et al [50]. It is assumed that the optimal length of the contractile tissue is 1.2 times the rest length. Although there are no direct data to provide a basis for this assumption , it is known from experimental work [10] that the optimum length of the whole muscle is approximately 1.2 times the rest length. Once b_6 is known, b_5 is obtained by subtracting b_6 from the total rest length of the whole muscle and multiplying the result by 1.2. The rate constants b_{11} and b_{12} and the parameter b_{13} are obtained using the same techniques as described in Chapter 2.

The muscle masses a_1 are obtained by the technique

described in section 4.2.2. The parameters a_2 and a_3 are the muscle specific activation heat rate and the muscle specific maintenance heat rate respectively. Values for these parameters are given by Hatze [22]. a_4 is the damping constant for the damping element of the muscle model. Due to lack of information for the values of this parameter, some of the values used by Hatze [21] were used. Others were estimated to lie within the range of these values. The complete set of model parameters is given in Table 4.1.

(b) Estimating the anthropometric parameters

To estimate the anthropometric parameters it is assumed that the hypothetical subject under study weighs 80 kg and is 1.6 m tall. The lengths, masses and moment of inertias of the limbs are then calculated using the ratios of Table A.2 of Winter [59]. Estimates for the origins and insertions of the muscles are obtained from the data of Brand et al [4]. The values obtained are listed in Appendix 4.

(c) Modeling the passive structures

The passive joint structures were modeled using equation (2.30). The ranges of the joint angles x_1, x_2 and x_3 are obtained from table 2 of Mena et al [42]. The parameters k_1 to k_4 are for the hip and knee joints are

TABLE 4.1

Parameters in State Equations for Dynamic Optimization (SI Units)

MUSCLE GROUP	1	2	3	4	5	6	7	8	9
b_1	9.6	9.6	11.6	9.6	6.9	11.6	6.9	6.9	9.6
b_2	.11	.12	.11	.13	.13	.14	.12	.11	.13
b_3	0.	0.	.07	0.	0.	.14	0.	0.	0.
b_4	3800	5800	1900	3600	1450	4400	850	4100	6900
b_5	.23	.252	.35	.38	.247	.088	.198	.3]2	.24
b_6	.099	.09	.108	.15	.034	.147	.085	.03	.05
b_7	77.3	85.1	70.9	51.1	87.9	52.1	90.1	85.7	95.4
b_8	1049	1601	525	994	400	1214	235	1312	1905
b_9	11.5	11.5	15.5	11.5	9.5	15.5	9.5	9.5	11.5
b_{10}	1.	1.	1.	1.	1.	1.	1.	1.	1.
b_{11}	.575	.575	.7	.625	.425	.7	.425	.425	.575
b_{12}	.152	.152	.185	.165	.112	.185	.112	.112	.152
b_{13}	.25	.25	.23	.21	.22	.25	.24	.23	.24
a_1	.78	.55	.72	.85	.21	.90	.17	.81	.89
a_2	.83	.83	.87	.83	.75	.87	.75	.75	.83
a_3	55.5	55.5	70.	55.5	13.5	70.	13.5	13.5	55.5
a_4	275.	275.	300.	275.	200.	300.	200.	200.	275.
k_5	5.85	4.1	5.4	8.25	1.6	6.8	1.3	6.5	9.1
k_6	15.	15.	15.	15.	15.	15.	15.	15.	15.

the same as those used in Chapter 2. Values of these parameters for the ankle joint are chosen arbitrarily since no information was available for those. The passive joint damping torques are described using linear models of the form

$$M_D = - c_1 \dot{\theta} \tag{4.48}$$

where $\dot{\theta}$ is the angular velocity of the limb. At first the exponential models described by Hatze [21] were used. However persistent numerical problems made it necessary to abandon those models.

The passive parallel elastic elements are modelled using similar equations as for the passive joint structures. Since in general these elements exert force in only one direction however only a single exponential was used. The equation for the force takes the general form

$$F^{PE} = k_5(\exp(k_6(L - L_0)) - 1) + c \dot{L} \tag{4.49}$$

where L is the total length of the muscle, L_0 is the rest length and $\dot{L}$ is the muscle velocity. The muscle rest length was obtained by calculating the muscle length at hip and knee angle equal to zero and ankle angle equal to 90 degrees.

The parameters k_1 to k_4 and c_1 and the ranges of the joint angles defined in equations (2.30) and (4.48) are listed in Table 4.2. The Parameters c, k_5 and k_6 in equation (4.49) are given in Table 4.1.

(d) Modeling the pelvic trajectory

Using the results from the works of Chow and Jacobson [10] and of Mena et al [42], the pelvis is assumed to progress forward (in the x-direction) with a constant velocity during the swing phase. The up and down movement (in the y-direction) is modeled as a sinusoidal movement of the general form

$$y(t) = h \sin (4 \pi t + b) \qquad (4.50)$$

where h is the amplitude of the motion and b is the phase. The amplitude h is of the order of one inch (2.54 cm) [7]. A nominal value for b has been shown to be 0.1 rad [42] for the swing phase of normal gait.

Owing to the constant velocity assumption, the kinematics in the x-direction disappears from the equations of motion. By differentiating equation (4.50) twice ,there follows

$$y\ (t) = - (4 \pi)^2 h \sin (4 \pi t + b) \qquad (4.51)$$

Table 4.2

Parameters in Equations (2.30) and (4.43)

	Hip Joint	Knee Joint	Ankle Joint
k_1	2.6	3.1	2.0
k_2	5.8	5.9	5.0
k_3	8.7	10.5	9.0
k_4	1.3	11.8	5.0
θ_1	-.52	-1.92	.52
θ_2	1.92	.1	1.92
c_1	1.09	3.17	.943

This acceleration must be incorporated into the equations of motion for the links.

The explicit appearance of t in the state equations (through equation (4.51)) violates an implicit assumption of autonomy for the optimal control algorithms in Chapter 3 and the present Chapter. It can be shown ,however, that by defining one extra state variable

$$x_{n+1} = t \tag{4.52}$$

the system of equations (4.23) to (4.31) is transformed into one which is autonomous in the time t [37]. The same optimality conditions can then be applied.

4.3 THE STATIC OPTIMIZATION PROBLEM

4.3.1 Statement of the problem

The static optimization problem is the same as that depicted in Figure (4.1) and described in the first paragraph of Section 4.2.1. In addition to the hip, knee and ankle trajectories, it is assumed the the corresponding angular velocities and angular accelerations are also known or calculated. With these quantities known it is possible to solve the inverse dynamics problem. This involves calculating the joint moments required to generate the given kinematics. Given

the joint moments , the static optimization problem then becomes that of finding the muscle forces that will generate the moments. Since there are more unknowns in the problem than there are independent equations of motion, the problem is indeterminate. To render the problem solvable, the unknown muscle forces will be found using static optimization techniques. This implies that the forces will be found at discrete points in time . The next subsection will be used to describe the techniques for solving the inverse dynamics problem. This will be followed by a mathematical statement of the problem.

4.3.2 Calculating the joint resultant moments

There are two major methods for calculating the joint resultant moments given the kinematics of the problem.

Method 1 -- differentiation

In this method the angular positions are differentiated numerically to get the angular velocity and the angular accelerations. Suppose the equations of motion are written in the form

$$A(\theta)\ddot{\theta} = b(\theta, \dot{\theta}) + T \qquad (4.53)$$

where

$A(\theta)$ = the dynamic coupling matrix

$b(\theta, \dot{\theta})$ = the vector of dynamic moments

T = the vector of applied moments

Then given θ, $\dot{\theta}$, $\ddot{\theta}$ T can be calculated using the equation

$$T = A(\theta)\ddot{\theta} - b(\theta, \dot{\theta}) \qquad (4.54)$$

Method 2 -- Optimization

In this technique the moments are assumed to be unknowns (decision variables) which are to be found in such a fashion that an objective function of the form

$$J = \int_{t_0}^{t_f} H[\theta^{d}(t) - \theta(t)]^2 dt \qquad (4.55)$$

is minimized.

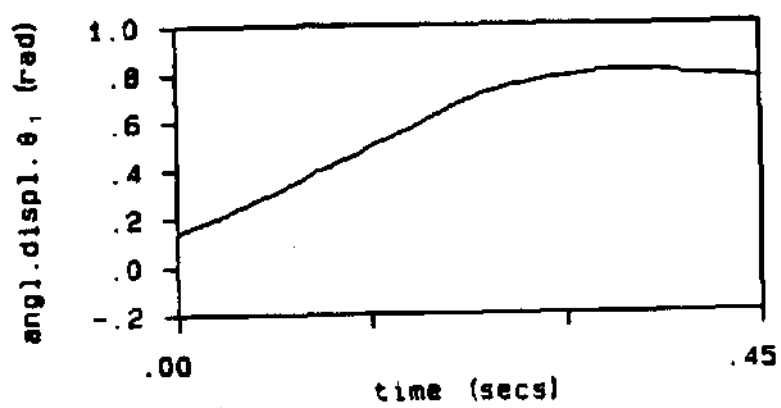
This technique was used by Chao and Rim [8] to determine the hip, knee and ankle moments during a portion of the stance phase of gait. Although the problem appears to be a relatively simple one it leads to a well known problem of optimal control called Singular optimal control. Our experience with this problem shows that it is hard to solve using the algorithms described in Chapter 3. Attempts to use other techniques such as those of Jacobson et al [29] did not alleviate the difficulties

and often lead to physiologically unfeasible solutions (saturation of the controls).

In this study, the differentiation technique was used to solve the inverse dynamics problem. The angular displacement data were first differentiated using the central difference scheme. However owing to sampling and quantization errors the derivatives were very noisy. A typical result of such a differentiation is depicted in Figure 4.5b which shows the angular velocity for the hip. The angular displacement history which was differentiated is depicted in part a of the same figure. To alleviate this problem the data were first smoothed using a finite impulse response (FIR) digital filter designed by McClellan et al [41]. Using central difference on the smoothed data still resulted in noisy derivatives. To get smoother derivatives a derivative filter was used. To this effect, the Nearly Equal Ripple Derivative filter (NERD) designed by Kaiser and Reed [32] was used and the smoothed derivatives calculated using the convolution formula

$$\theta'[n] = \sum_{k=1-N_p}^{N_p} c[k] \ \theta \ [n-k] \qquad (4.56)$$

(a)



(b)

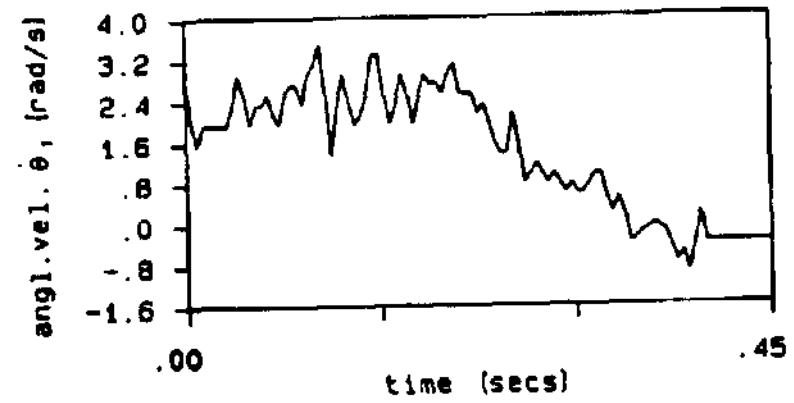


Fig. 4.5 Typical derivatives of gait data using finite-difference. (a) actual data, (b) velocity calculated by finite-difference.

where

$\theta'[n]$ = the derivative at the n th time station

$\theta[n]$ = the raw data

c[k] = the filter coefficients

N_p = half the filter width in samples.

The main characteristics of the NERD filter are depicted in Figure 4.6. This diagram shows the frequency response of the filter as a function of the normalized frequency. The parameter β represents the cutoff frequency; and δ represents allowable variations about the cutoff frequency. The importance of properly choosing these parameters in the smoothing of gait data will be demonstrated shortly.

Lesh et al [38] have proposed a more elegant technique for evaluating the convolution using Fast Fourier transforms (FFT). Since only a relatively few samples are used in this study, the direct convolution proves sufficiently efficient. Prior to carrying out the differentiation, the data was first de-trended by removing the straight line joining the first and last points. In order to determine the amount of distortion by the filtering operation, the angular acceleration obtained was integrated twice using Simpson's integration rule.

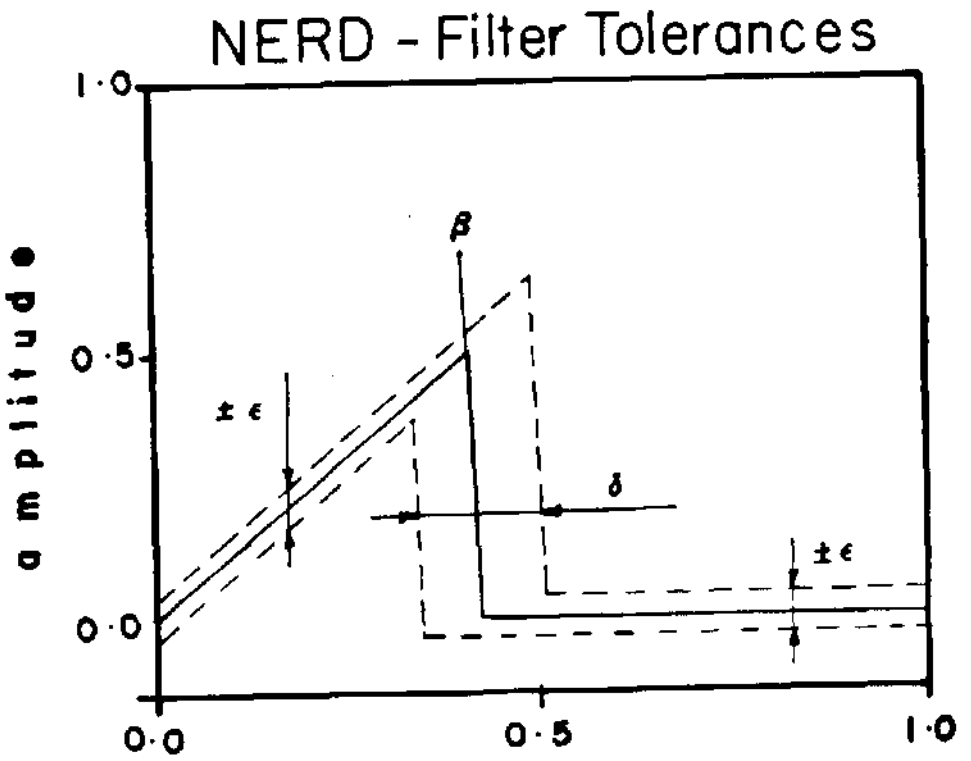


Fig. 4.6 Frequency response characteristics of the Nearly Equal Ripple Derivative Filter (NERD). β is the cutoff frequency and δ and ϵ are the design tolerances.

4.3.3 Mathematical Statement of the Problem

The static optimization problem can be stated as follows

$$\min_{f_i} \; J = \left[\sum_{i=1}^{m} (f_i / A_i)^3 \right]^{1/3} \qquad (4.57)$$

subject to the equality and inequality constraints

$$\sum_{i=1}^{m} r_i \times f_i - T_j = 0 \qquad j = 1,\ldots,3 \qquad (4.58)$$

$$f_i \geq 0 \qquad i = 1,\ldots,m$$

where

T_j = the resultant joint torque at the joint j

r_i = the moment arm of muscle i

f_i = the force generated by muscle i

A_i = the cross - sectional area of muscle i

The objective function J in equation (4.57) was proposed by Crowninshield [15] on the basis of muscle fatigue considerations. The cubic root was necessary to reduce the size of J and hence make it less ill-conditioned. Also by taking its cubic root, J is made to have the units of muscle stress.

The static optimization problem was solved at 101 discrete time points which correspond to the discrete time points used in the dynamic optimization problem. The algorithm used was the static version of the Gradient-restoration algorithm [45]. To this effect all the

inequality constraints were first converted to equality constraints using slack variables. All the equality constraints were then augmented to the objective function using Lagrange multipliers.

By the definition of the problem the decision variables f_i are the muscle forces and hence have units of Newtons. Two problems with the formulation prompted the need for normalizing the problem. First, the equality constraints given in equation (4.58) were difficult to satisfy especially during the first restoration phase. Secondly, numerical problems were encountered in the gradient phase with the exponentiation in equation (4.57). This happens when some of the equality constraints become so grossly violated that some of the controls assume negative values. To alleviate these problems, the problem was normalized by introducing dimensionless controls $\bar{f}_i$ given by

$$\bar{f}_i = f_i / \hat{f} \qquad (4.59)$$

where $\hat{f}$ is a scaling constant. An appropriate value for $\hat{f}$ was found to be 10 N.

The static optimization problem is then characterized by a total of 18 independent variables (9 corresponding to the normalized muscle forces and 9 slack variables).

4.4 RESULTS

In solving the dynamic optimization algorithm a sampling interval of .0045 secs was used. The whole swing phase was assumed to last .45 secs. The state equations defined by equations (4.23) and the adjoint equations were integrated using the Hamming predictor-corrector method with the Runge-Kutta method for starting. This integration routine was chosen in order to minimize the number of function evaluations and also because of its stability characteristics. All quadratures were performed using the Simpson's rule. The optimization algorithm selected was the Fletcher-Reeves conjugate-gradient algorithm. A better choice would be either the gradient-restoration algorithm or the variance algorithm. The use of these algorithms is however limited by storage capabilities available on the computing machine used (Chapter 2). The one-dimensional step size was found using the 'regula-falsi'-extrapolation-interpolation technique described in Chapter 3.

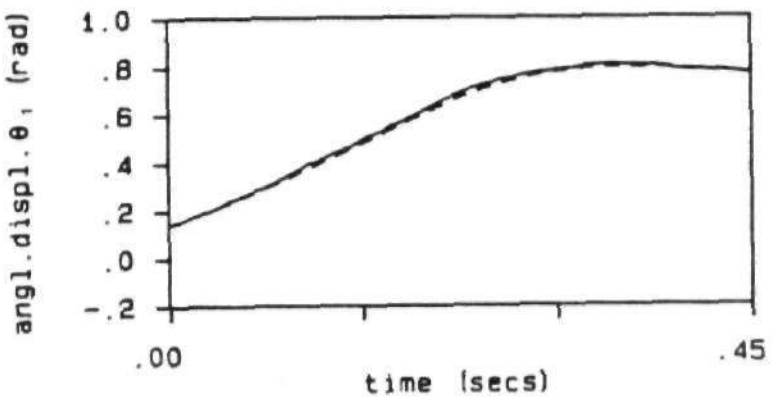
The static optimization problem was solved using the static version of the Gradient - Restoration algorithm The same technique was used to find the one-dimensional step size as for the dynamic optimization algorithm. In the restoration phase, the step size was found using the relationship $\alpha_i = 0.75\ \alpha_{i-1}$ with $\alpha_0 = 1$

(a) Results of smoothing and differentiation

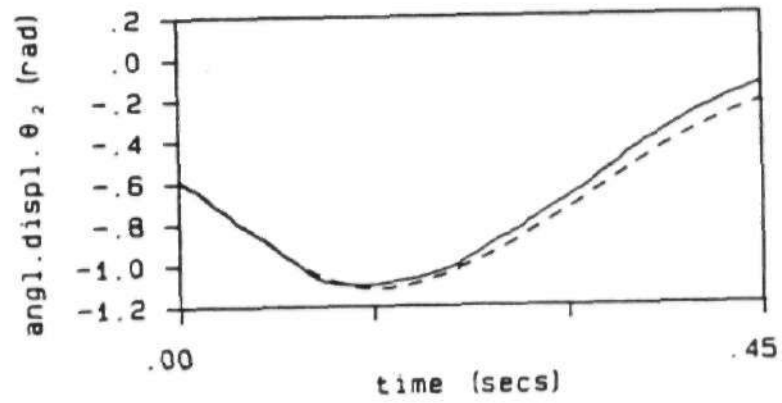
Figure 4.5 shows a typical result obtained by differentiating the hip trajectory using the central difference equation. The differences can be appreciated by comparing these with the corresponding results in Figures 4.7 or 4.8 obtained using the NERD filter. In Figure 4.7, parts a,b and c show the actual hip, knee and ankle trajectories (solid lines). The dotted lines on the same figures show the corresponding results obtained by integrating the acceleration twice. Parts d,e and f of the same figure show the corresponding angular velocities (solid lines), obtained by differentiating the trajectories using NERD (with $N_p = 30$, $\beta = .08$ and $\delta = .01$). The dotted lines on the same figures show the angular velocities obtained by integrating the accelerations which are shown in parts g, h and i.

By varying the filter characteristics a little, the results shown in Figure 4.8 are obtained. In this case the filter characteristics were set at $N_p = 30$, $\beta = .05$ and $\delta = .01$ for the hip and knee trajectories; and $N_p = 30$, $\beta = .1$ and $\delta = .01$ for the ankle trajectory. The results obtained using these two sets of filter characteristics will be discussed shortly.

(a)



(b)



(c)

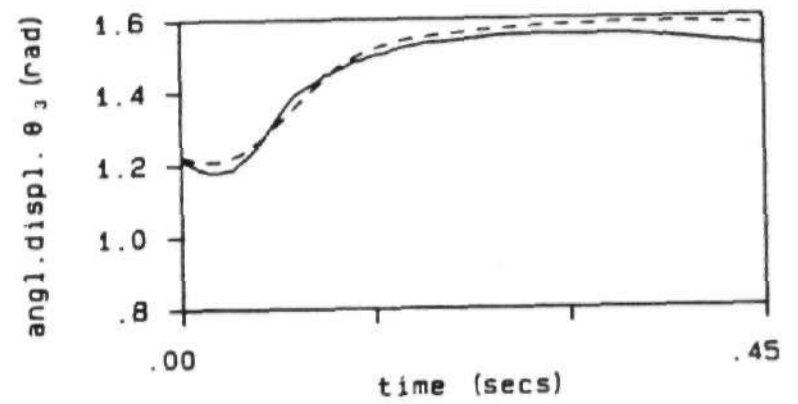
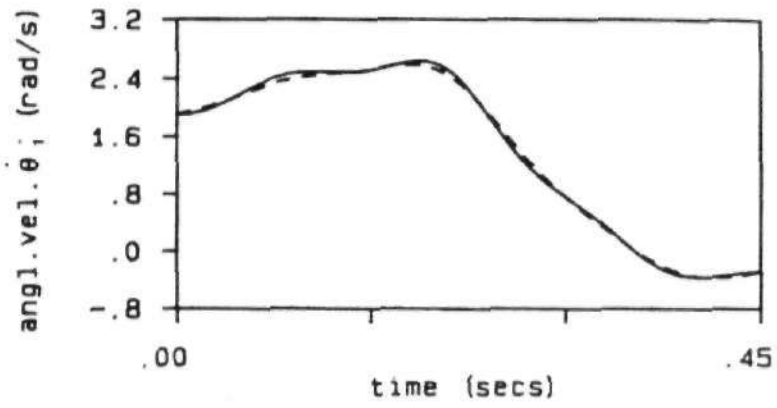
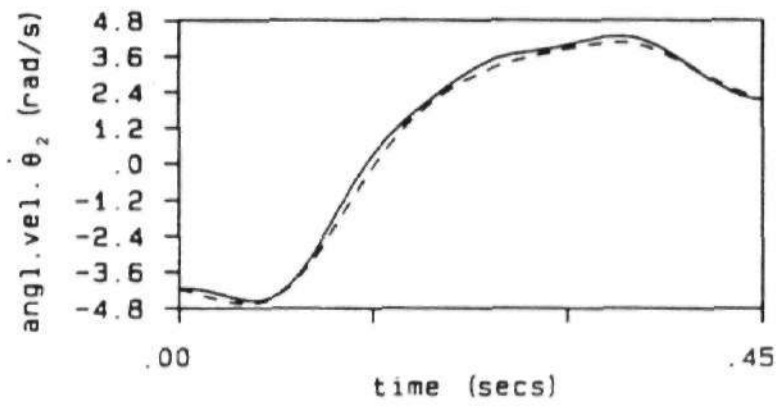


Fig. 4.7 Hip, knee and ankle kinematic data. (a-c) angular displacements, (d-f) velocities and (g-i) accelerations . Dotted lines obtained by integration and derivatives by using NERD with (β = .08, δ = .01, and N_p = 30).

(d)



(e)



(f)

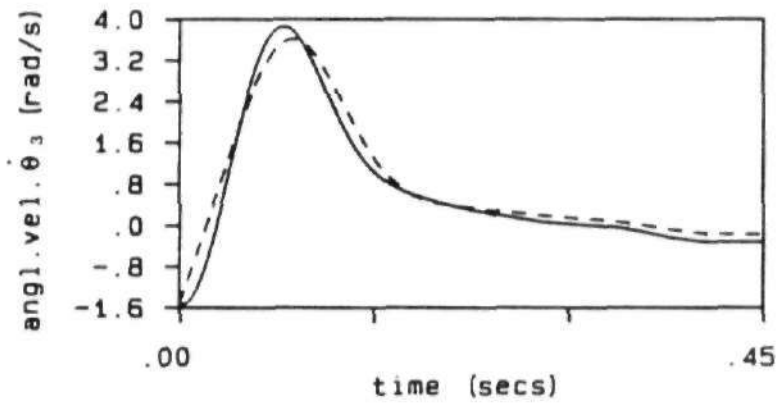
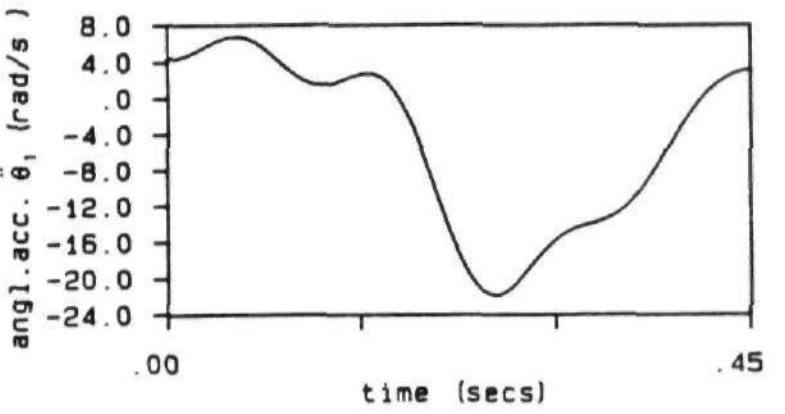
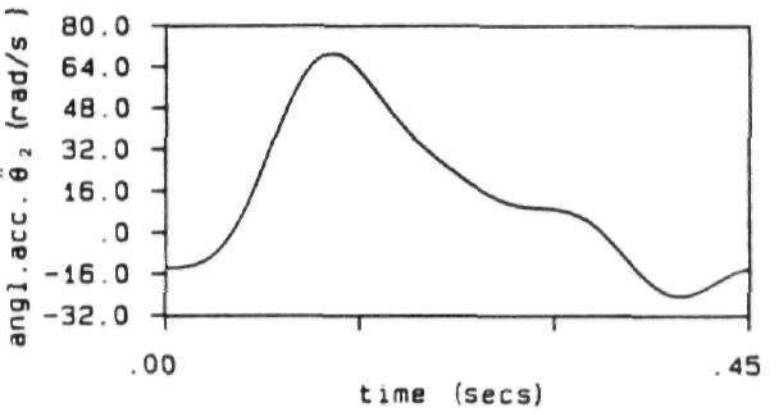


Fig. 4.7 (Continued)

(g)



(h)



(i)

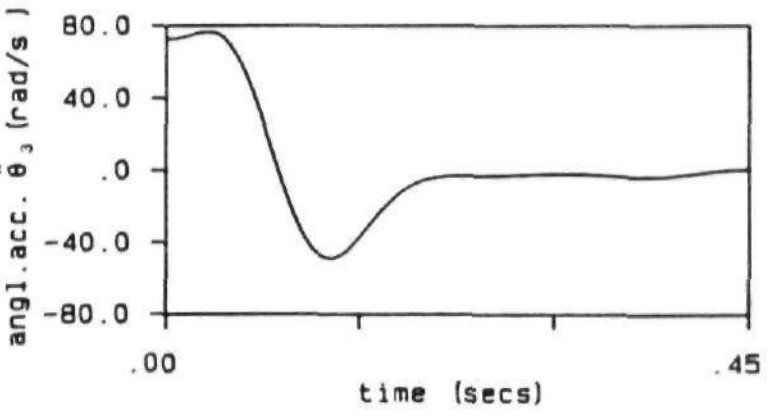


Fig. 4.7 (Continued)

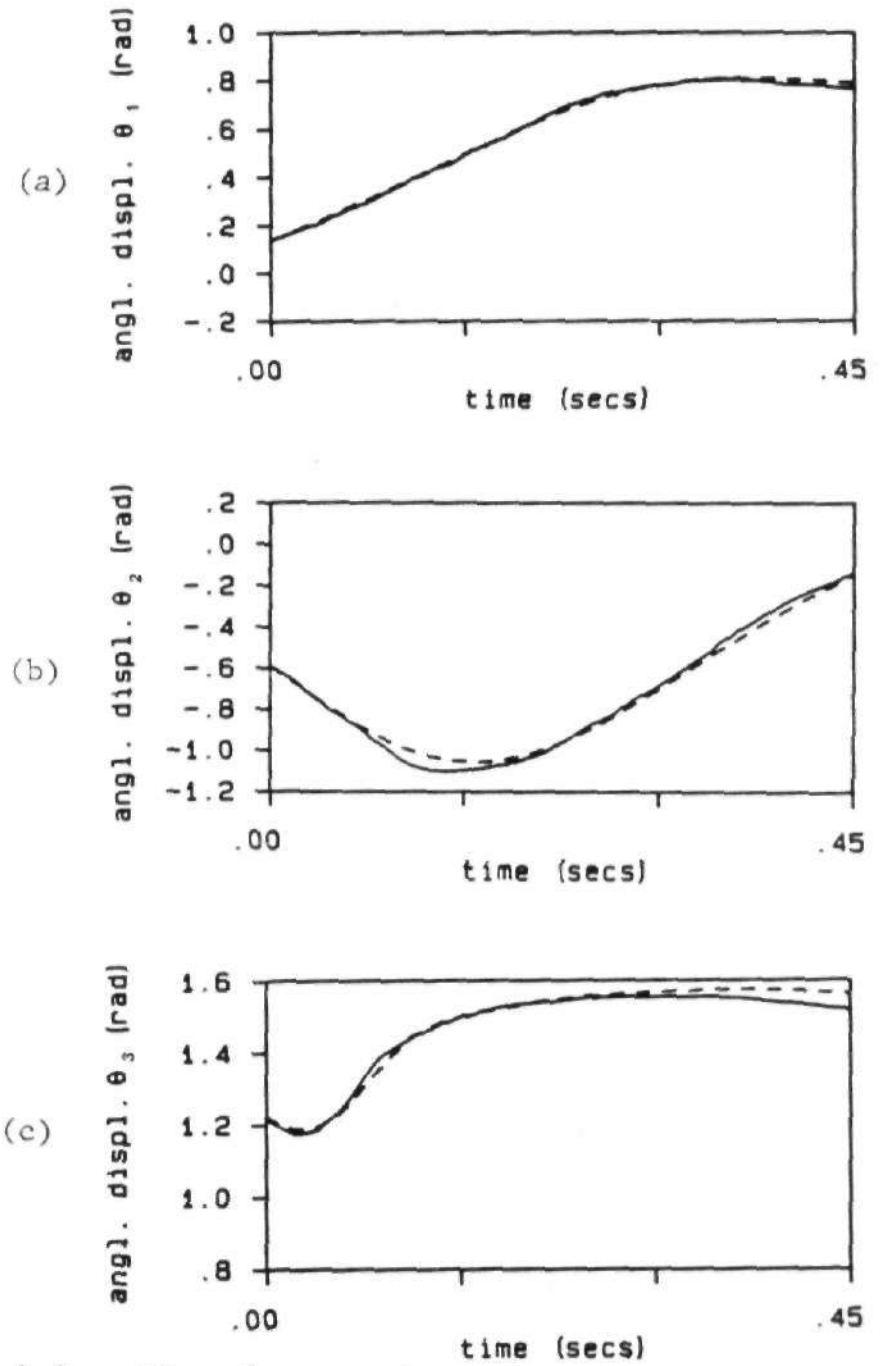
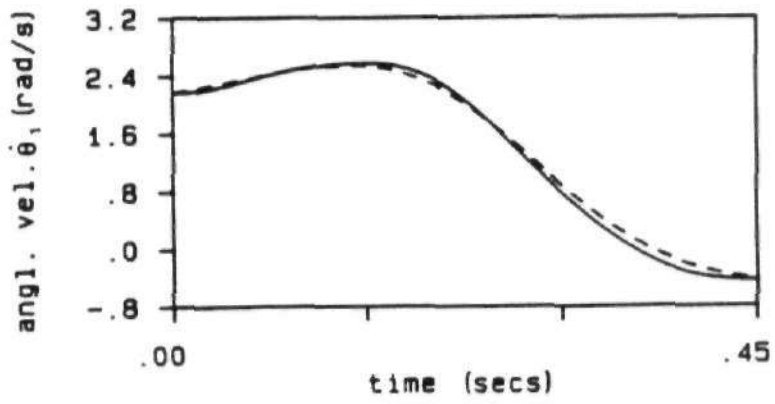
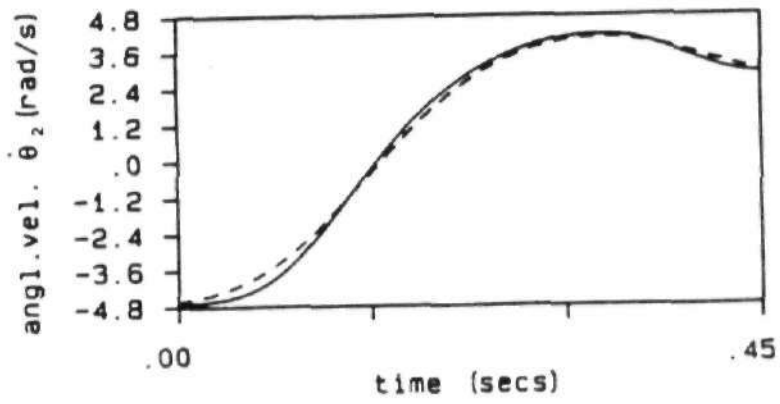


Fig. 4.8 Hip, knee and ankle kinematic data. (a-c) angular displacements, (d-f) velocities and (g-i) accelerations. Dotted lines obtained by integration and derivatives by using NERD with (β = .05, δ = .01, and N_p = 30).

(d)



(e)



(f)

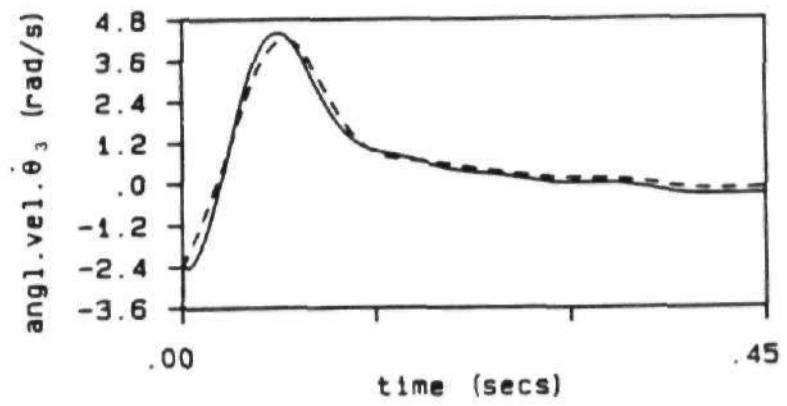
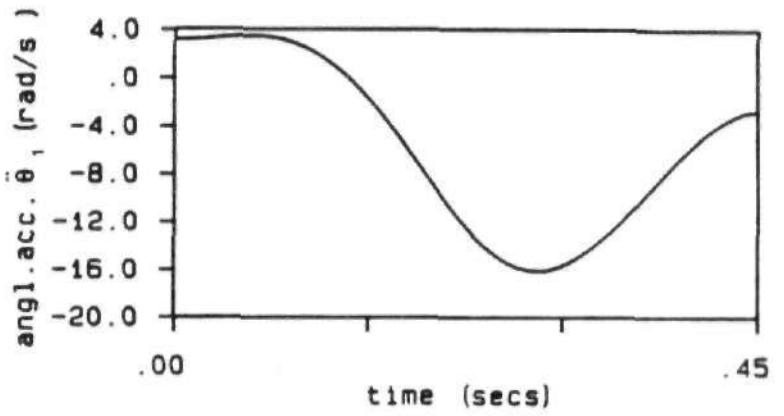
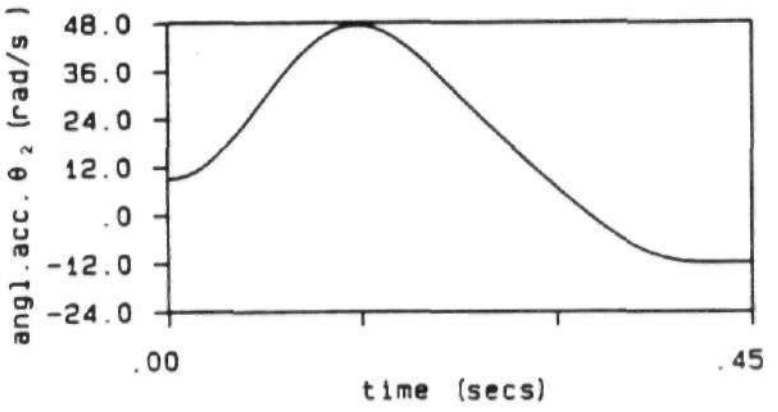


Fig. 4.8 (Continued)

(g)



(h)



(i)

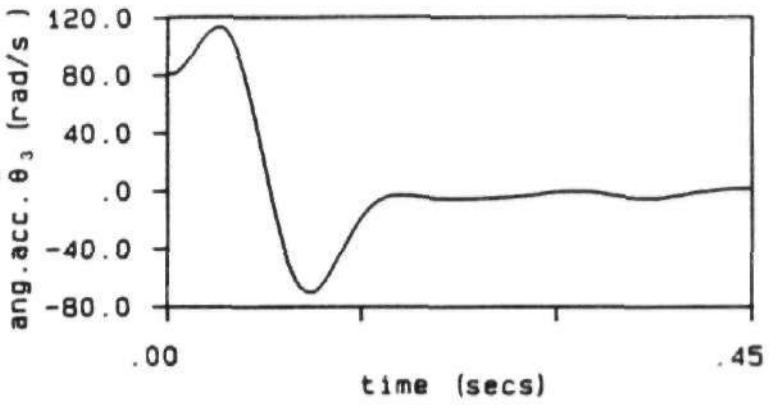


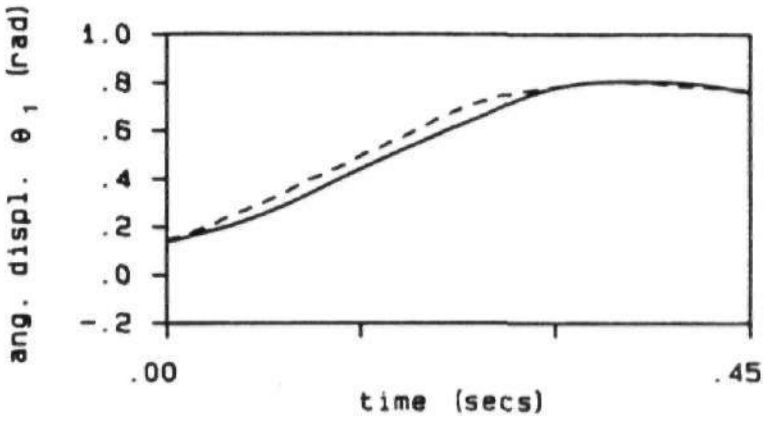
Fig. 4.8 (Continued)

(b) Results of the dynamic optimization

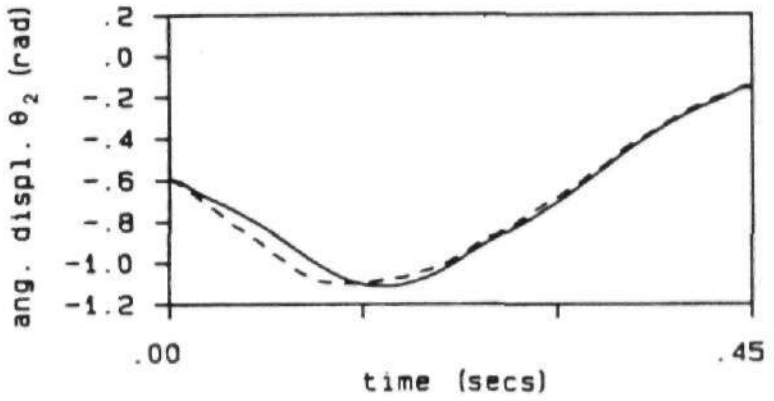
The specified hip, knee and ankle trajectories are depicted by the solid lines in Figure 4.9a-c. Also shown on the same plots are the predicted trajectories (dashed lines). From these plots it can be appreciated that good tracking was obtained for the most part of the swing phase. The major discrepancies tend to occur at the earlier parts where the generated trajectories tend to persistently lag behind the specified trajectories. The implications of these lags will be discussed shortly.

Figures 4.10a-c show the joint torques obtained by the dynamic optimization algorithm (solid lines) and those obtained by solving the inverse dynamics problem using the second set of filter characteristics (dashed lines). The time histories of these curves generally agree with each other except for the initial portions where the curves obtained by the dynamic optimization algorithm lag those obtained by solving the inverse dynamics problem. This lag also appeared toward the end of the phase. Also, a comparison of these torque curves with those given in Pedotti [51] shows that the time histories of these torques agree well with the general patterns of the joint torques in actual gait. This general pattern for normal gait is such that there is a flexor moment at the hip during the first fifty or so percent of the swing phase, and an extensor torque for

(a)



(b)



(c)

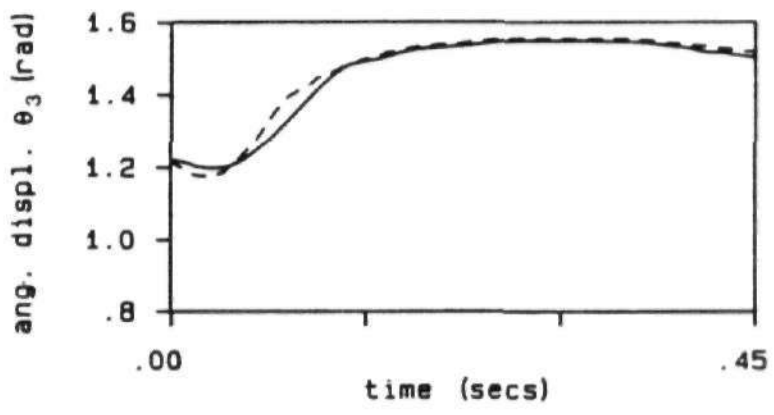
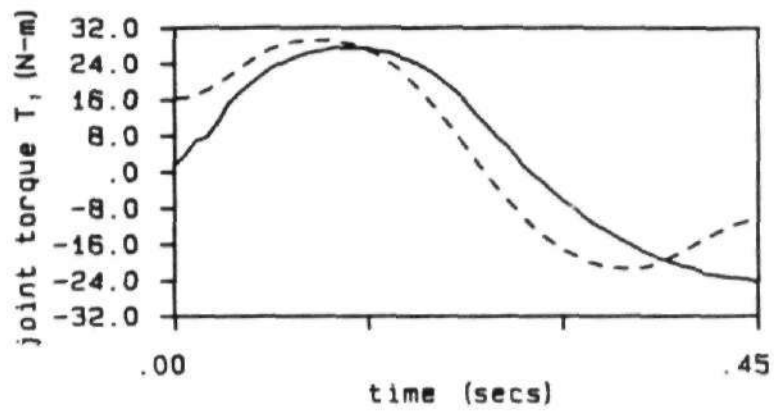
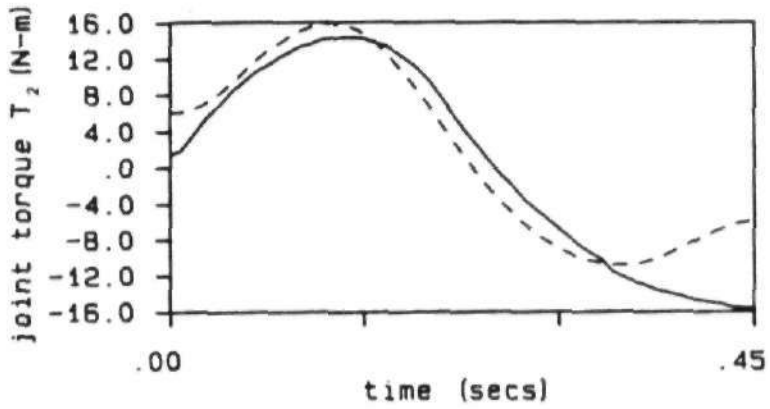


Fig. 4.9 (a) Hip, (b) knee and (c) ankle angular displacements obtained by dynamic optimization (solid lines). Dotted lines are given data.

(a)



(b)



(c)

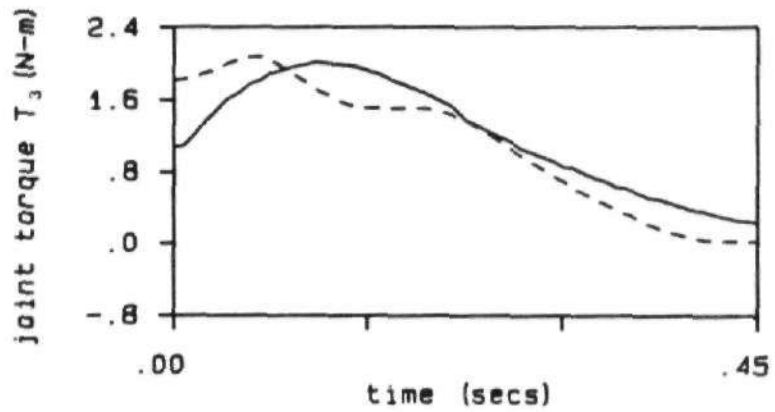
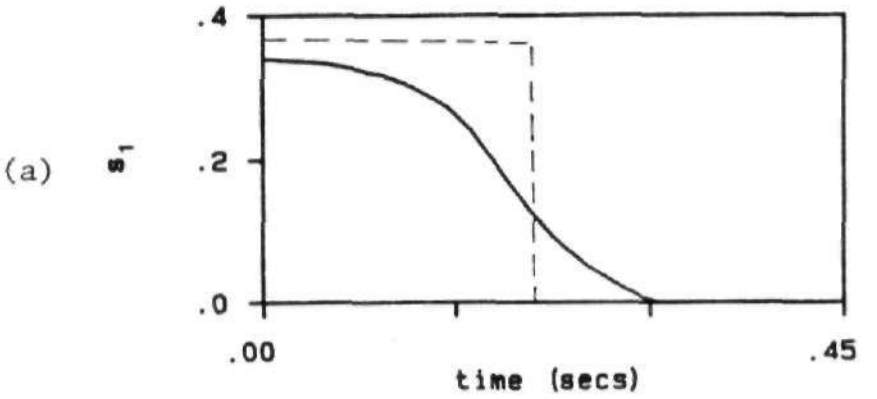
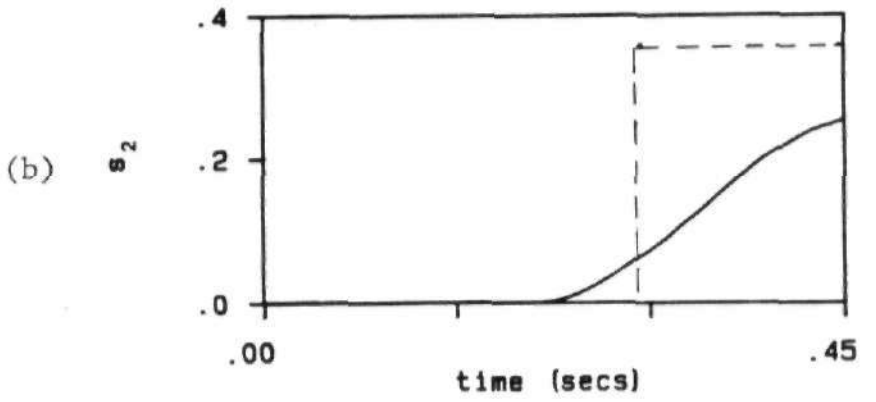


Fig. 4.10 (a) Hip, (b) knee and (c) ankle joint torques obtained by dynamic optimization (solid lines) and by solving inverse dynamics using data of Fig. 4.8 (dotted lines).

the rest. The flexor torque at the hip and the extensor torque at the knee tend to agree with each other in phase but the extensor torque at the knee is relatively smaller in magnitude than the corresponding flexor torque at the hip. Toward the end of the swing phase, the torque at the knee becomes a flexor torque. The ankle torque during the swing phase is generally smaller than that during the stance phase so its magnitude is not easily discerned from the torque curves in Pedotti [51]. However, studies by Mena et al [42], indicate that the ankle torque is mostly dorsiflexor over the whole of the swing phase. This is the case for the predicted torques in Figure 4.10c.

The control histories (stimulation rates) are shown in Figure 4.11a-c. An attempt will be made to compare these controls with the electromyographic (EMG) data given in Pedotti [51]. To this effect the estimated envelopes of the EMGs are shown in Figure 4.11 (dotted lines). Figures 4.12a-i show the corresponding muscle force histories for the nine muscle groups studied. From these figures it can be appreciated that the initial flexor torque at the hip is realized by the activities of iliopsoas and rectus femoris muscle groups (Figures 4.12a and c). These muscles remain active during the first fifty to sixty percent of the swing phase. The control histories for these muscles (Figures. 4.11a and c) show a





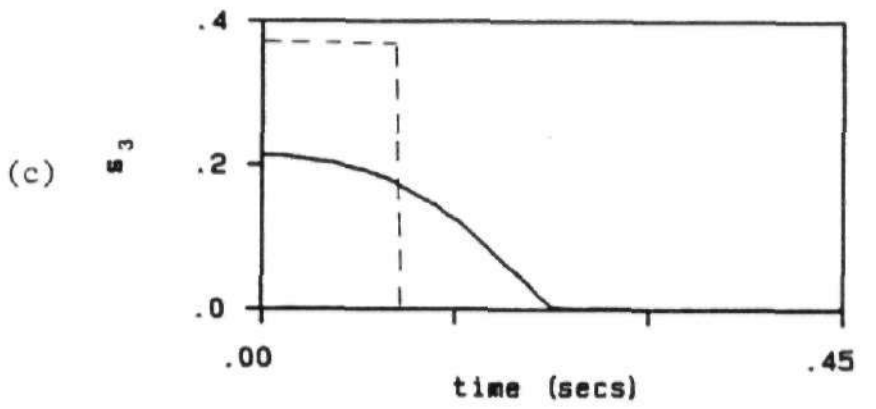
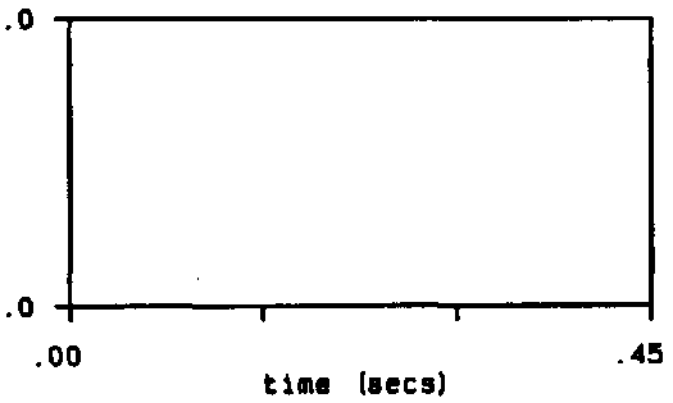
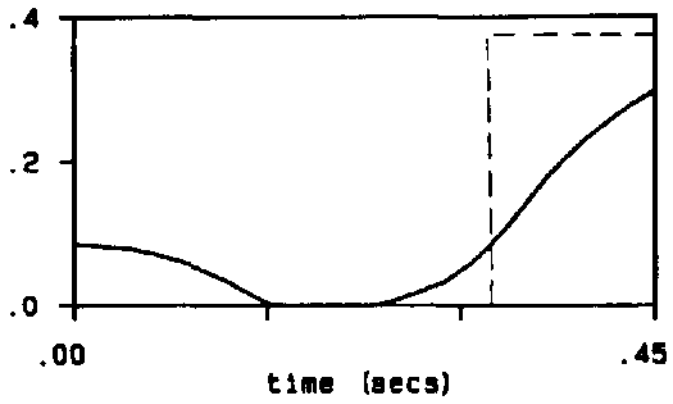


Fig. 4.11 Control histories in muscle groups 1 through 9 obtained by dynamic optimization.

(d) a_4



(e) a_5



(f) a_6

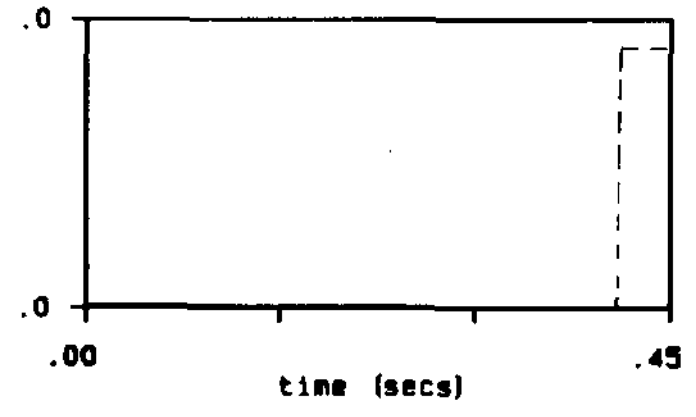
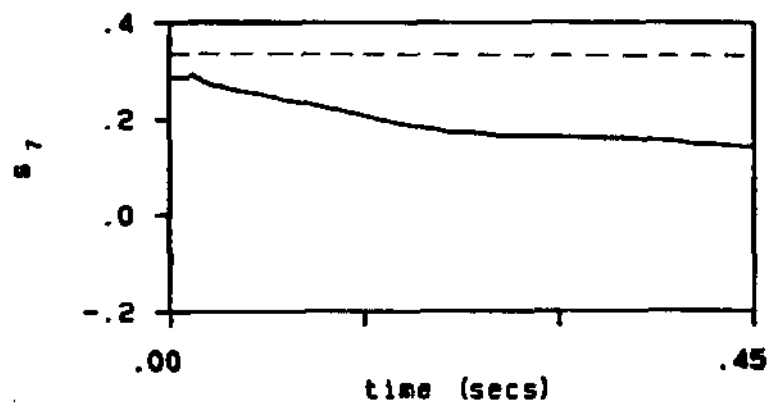
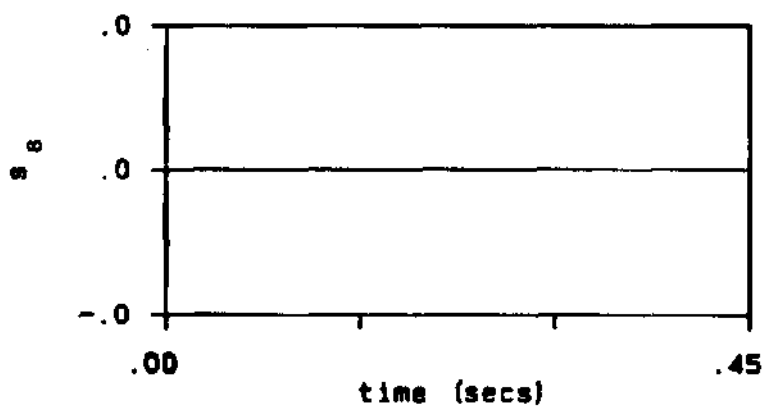


Fig. 4.11 (Continued)

(g)



(h)



(i)

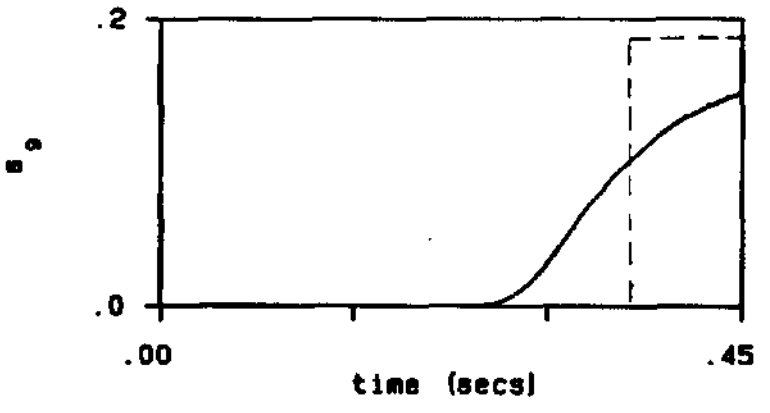
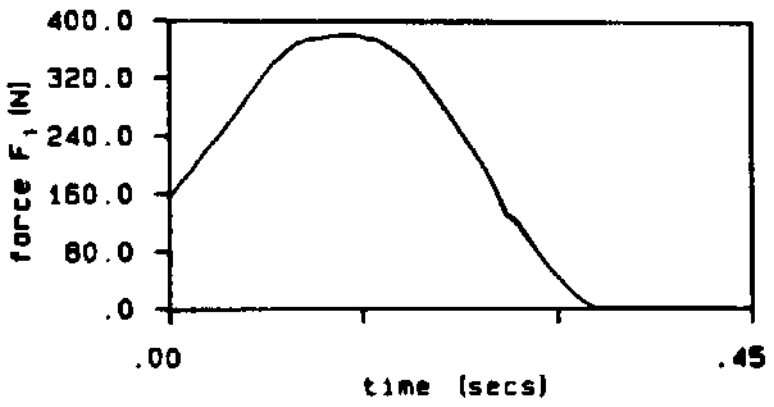
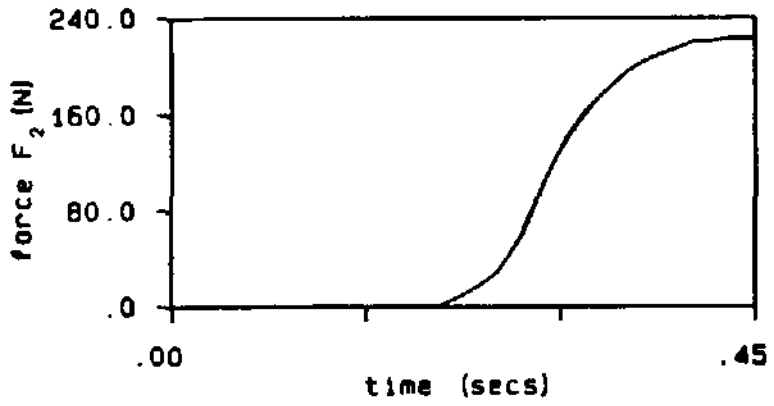


Fig. 4.11 (Continued)

(a)



(b)



(c)

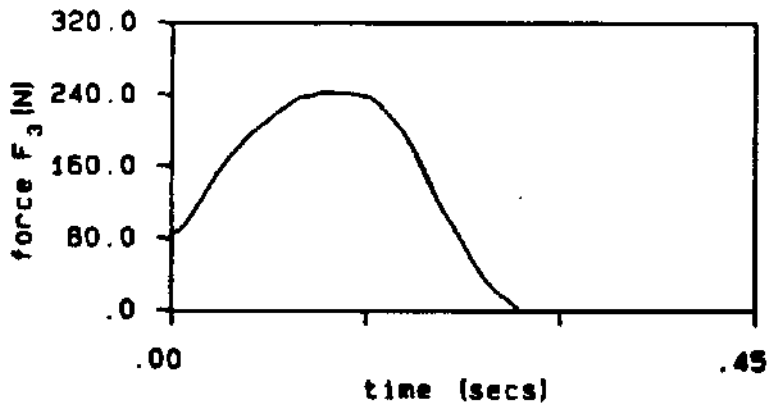
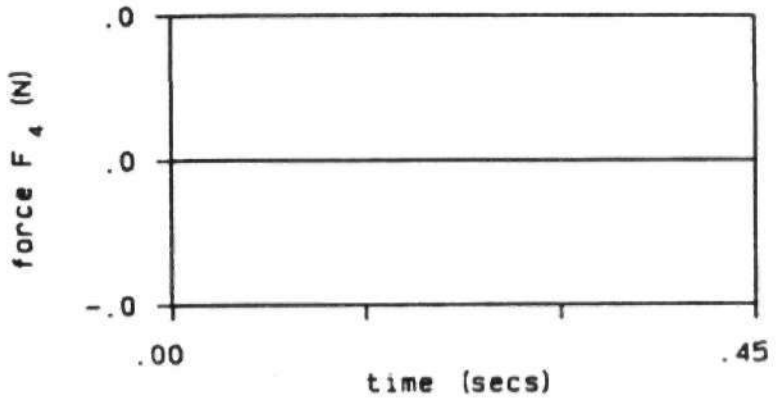
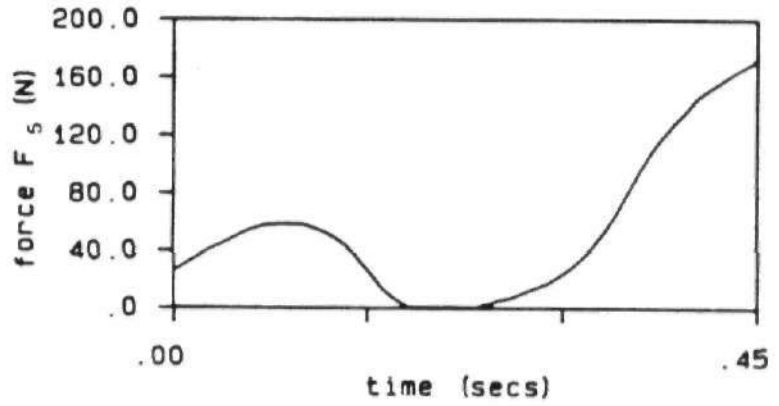


Fig. 4.12 Predicted muscle forces in muscle groups 1 through 9 obtained by dynamic optimization.

(d)



(e)



(f)

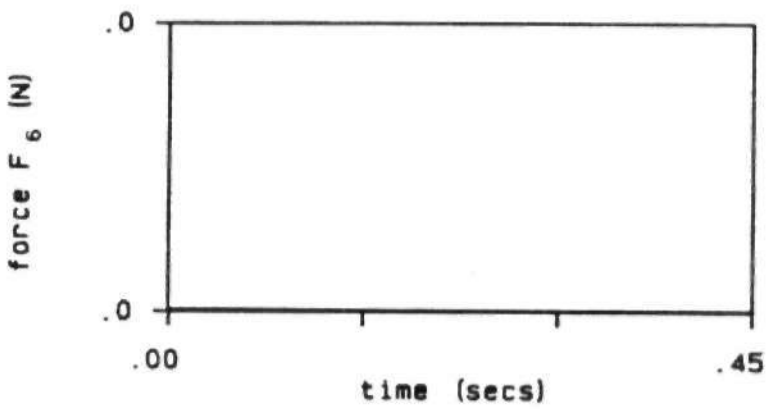
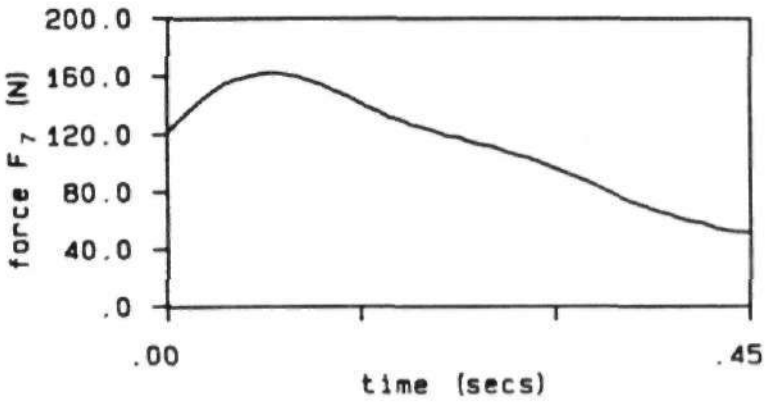
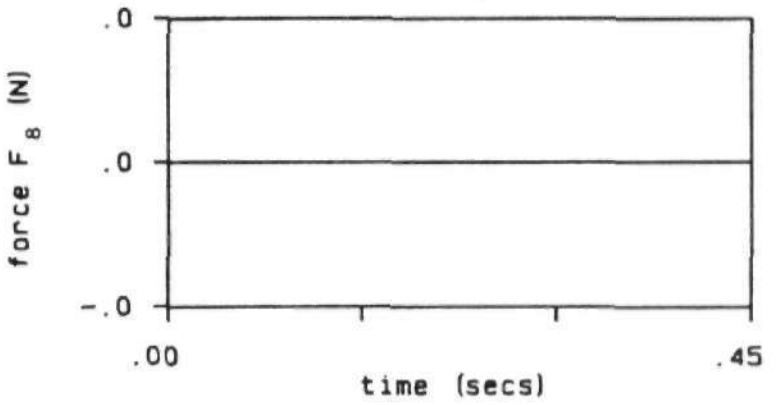


Fig. 4.12 (Continued)

(g)



(h)



(i)

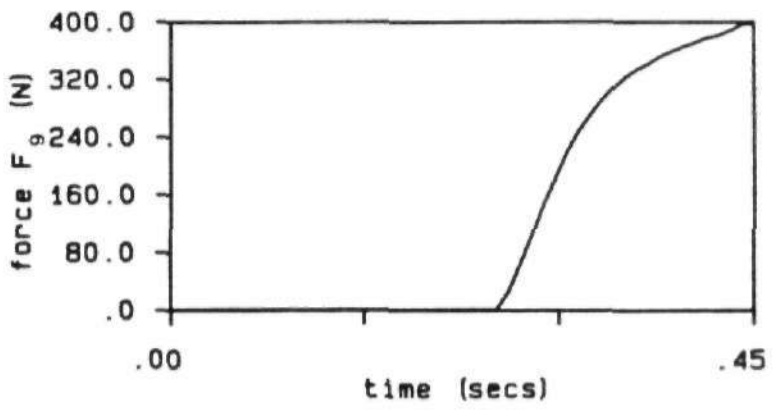


Fig. 4.12 (Continued)

good temporal agreement with their EMG envelopes. It should be mentioned that the EMG record for the iliopsoas is not available because it is not easy to measure. This is because this muscle group is a deep lying muscle group. The EMG envelope shown is only an estimated approximation. The hip extensor moment at the end of the swing phase is realized by the activities of gluteus maximus and the hamstring groups (Figures. 4.12i and b). In fact, the EMG records in Pedotti [51] showed that the hamstring muscle group is the most active muscle group during the swing phase. This activity is necessary to bring the swinging limb to rest in preparation for heel strike.

A major part of the extensor moment at the knee is provided mainly by the inertia of the swinging limb. The knee flexor torque at the end of the swing phase is realized by the activity of the hamstrings and the short head of biceps (Figures. 4.12b and e). A comparison of the EMG envelopes and the predicted controls again show good temporal agreement. One interesting observation is that the vasti group (Figure 4.11f) is predicted to have no activity at all during the swing phase. Contrary to this, the EMG records show that these muscles have some activity at the very end of the swing phase. The same is also true for the rectus femoris group (Figure 4.11c). The activities of these muscle groups generally continue

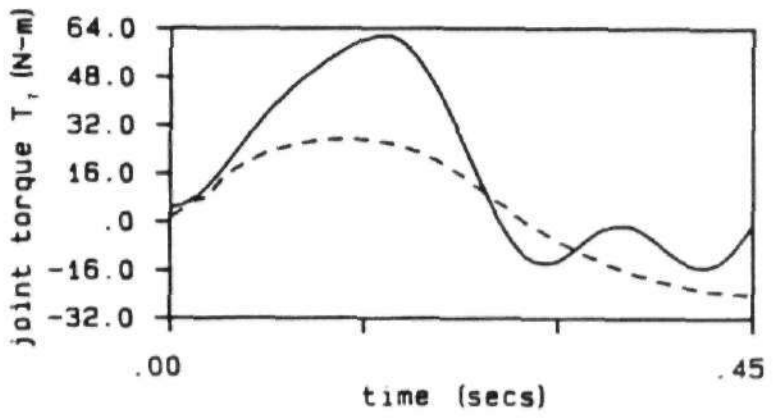
into the stance phase. The importance of this observation will be discussed shortly.

Finally, it should be mentioned that among the muscles that cross the ankle joint, only tibialis anterior (Figures. 4.11g and 4.12g) is active. The gastrocnemius (Figures 4.11d and 4.12d) and the soleus (Figures 4.11h and 4.12h) are silent throughout the swing phase. The EMG records for these muscle groups tend to confirm these predictions. The activity of tibialis anterior provides the necessary dorsiflexor torque at the ankle (Figure 4.10c).

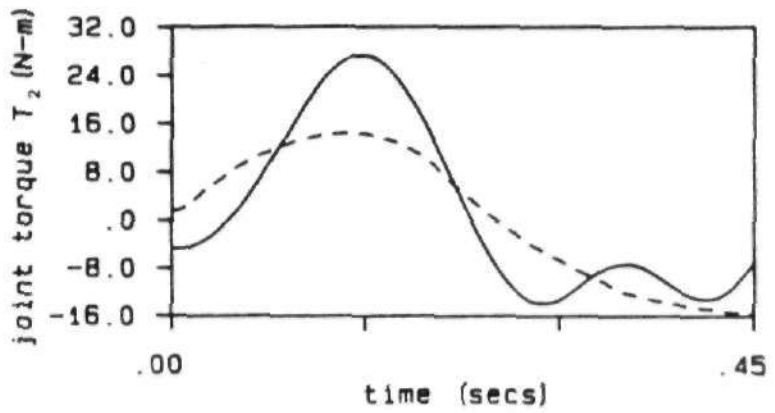
(c) Results of the static optimization

The corresponding joint torque and the muscle force histories predicted using the static optimization for the data of Figure 4.7 are depicted in Figures 4.13 (solid lines) and 4.14 respectively. For the filtering results of Figure 4.8, the corresponding results are shown in Figures 4.10(dotted lines) and 4.15 respectively. The differences between the predicted force histories shown in Figures 4.14 and 4.15 are obvious. One sharp contrast is the predicted force history of the hamstring group (Figures 4.14b and 4.15b). In the first case, that muscle group was recruited only at the very beginning of the swing phase, to provide the small knee flexor moment shown in Figure 4.13a. This completely contradicts the

(a)



(b)



(c)

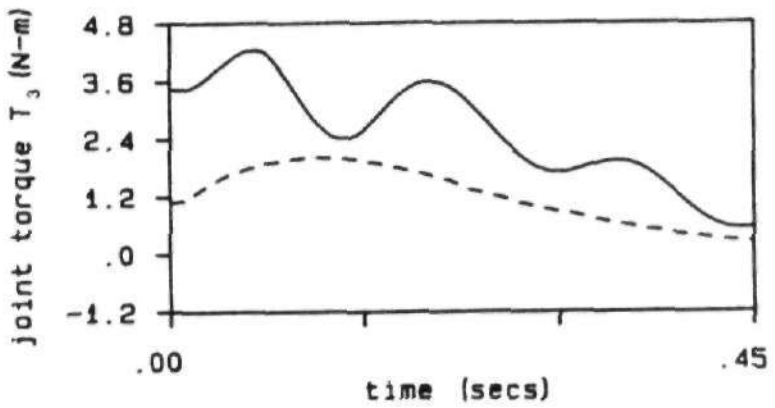
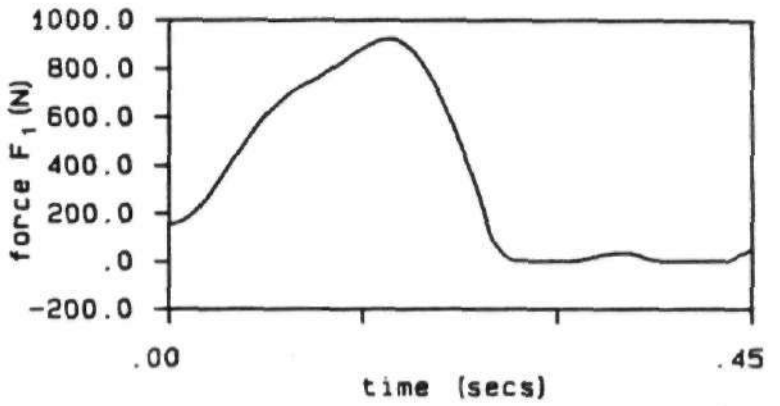
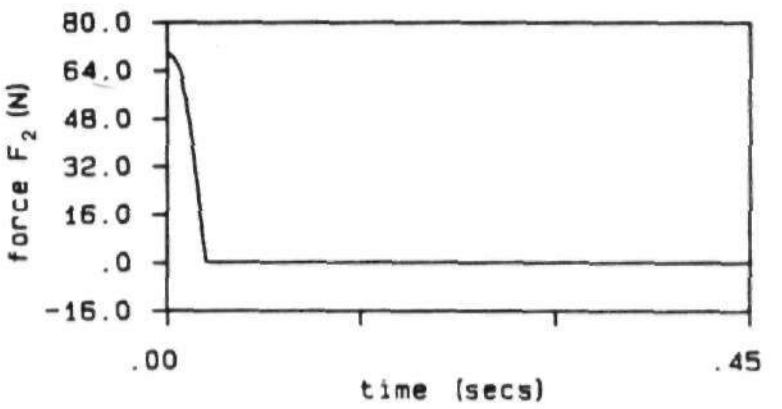


Fig. 4.13 (a) Hip, (b)knee and (c) ankle torques obtained by solving inverse dynamics problem with kinematic data of Fig. 4.7. Dotted lines show same obtained by dynamic optimization.

(a)



(b)



(c)

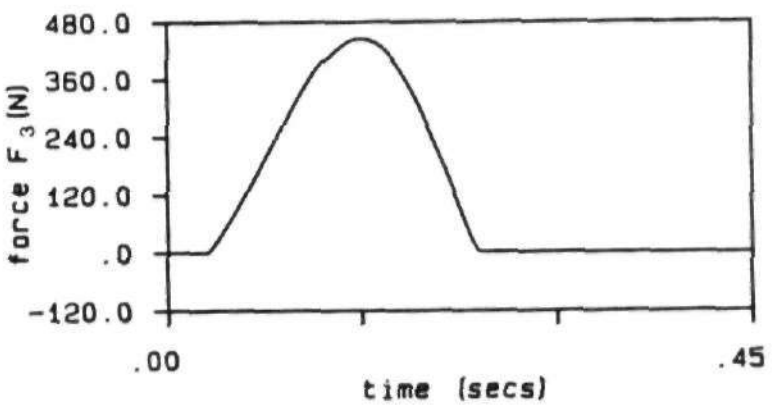
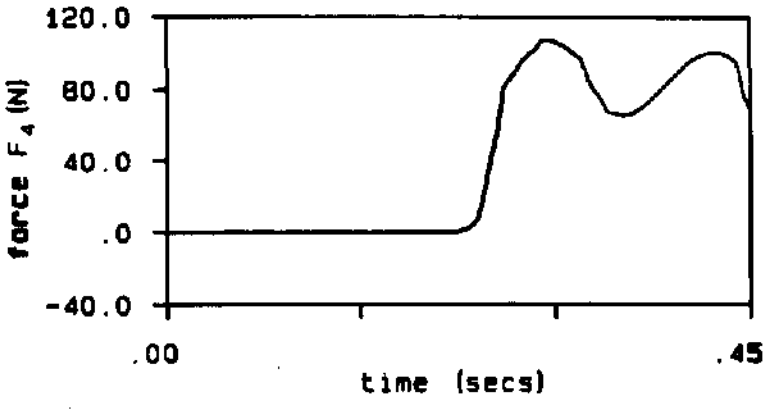
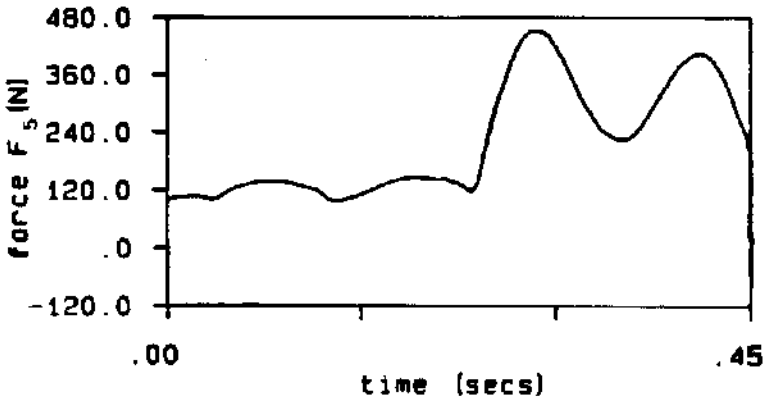


Fig. 4.14 Predicted muscle forces in muscle groups 1 through 9 obtained by static optimization using data of Figs. 4.7 and 4.13.

(d)



(e)



(f)

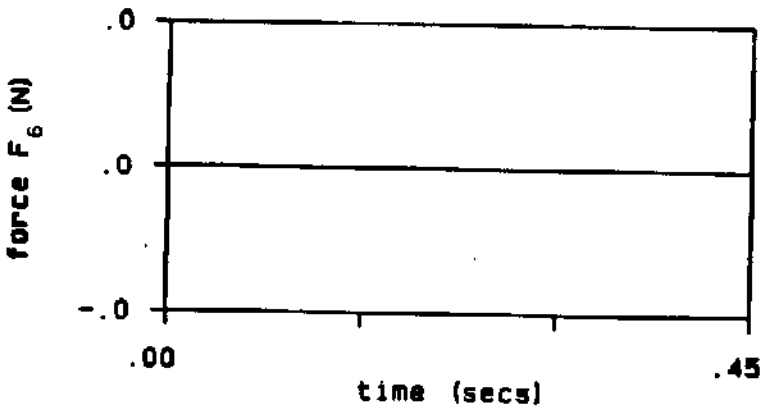
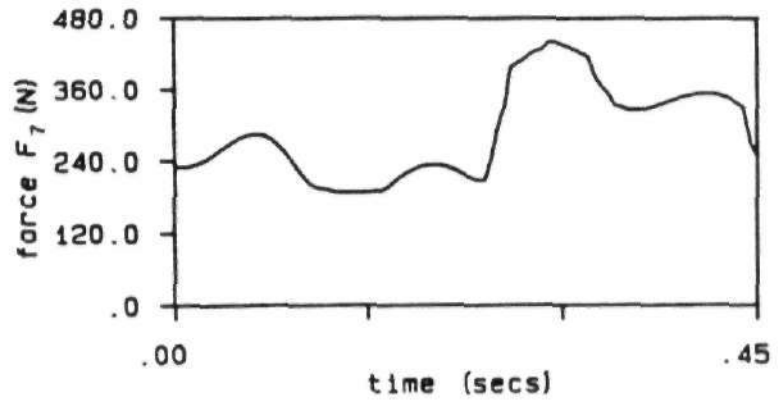
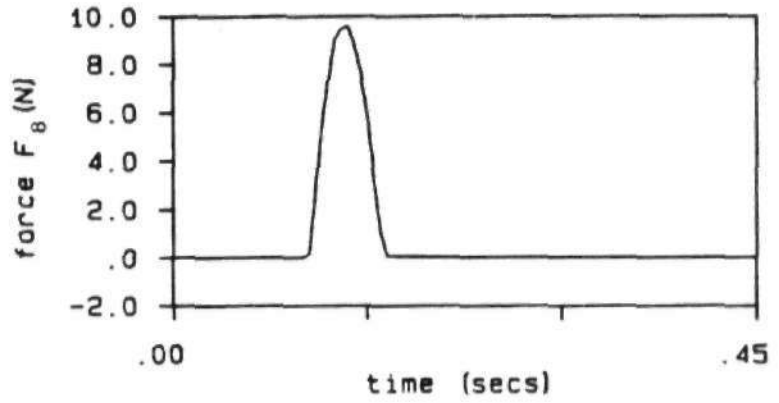


Fig. 4.14 (Continued)

(g)



(h)



(i)

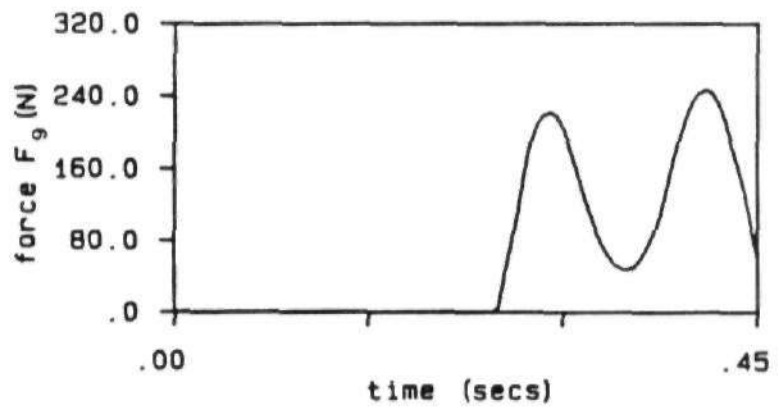


Fig. 4.14 (Continued)

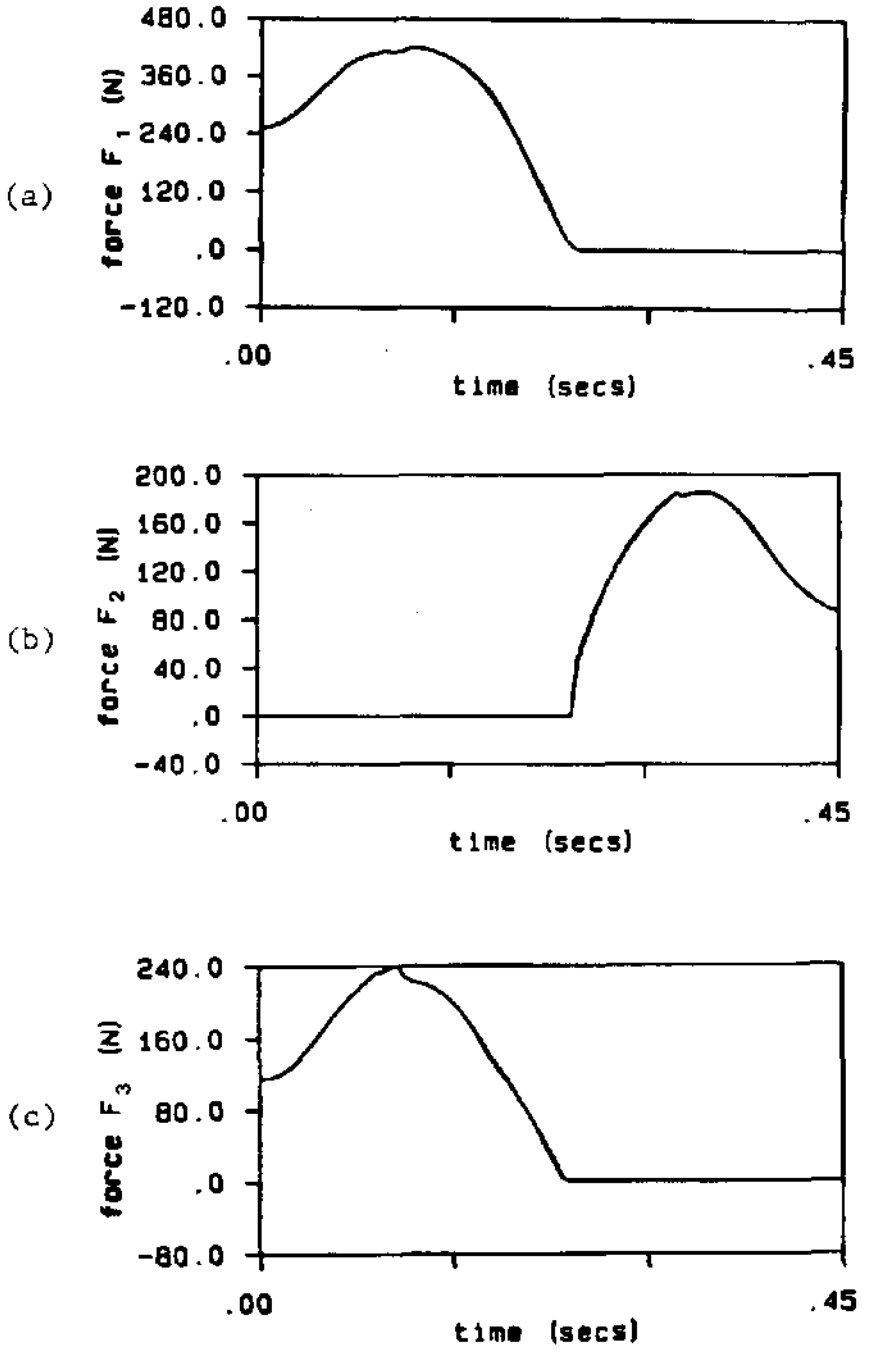
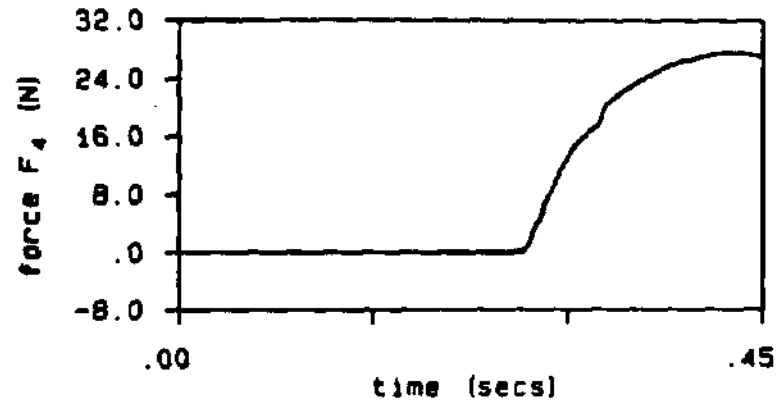
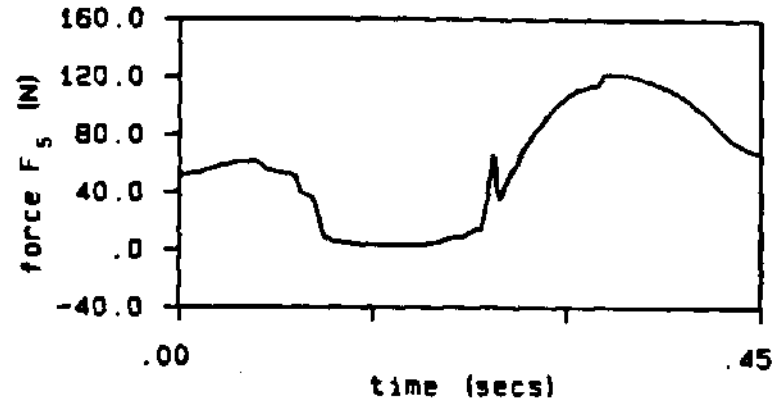


Fig. 4.15 Predicted muscle forces in muscle groups 1 through 9 obtained by static optimization using data of Fig. 4.8.

(d)



(e)



(f)

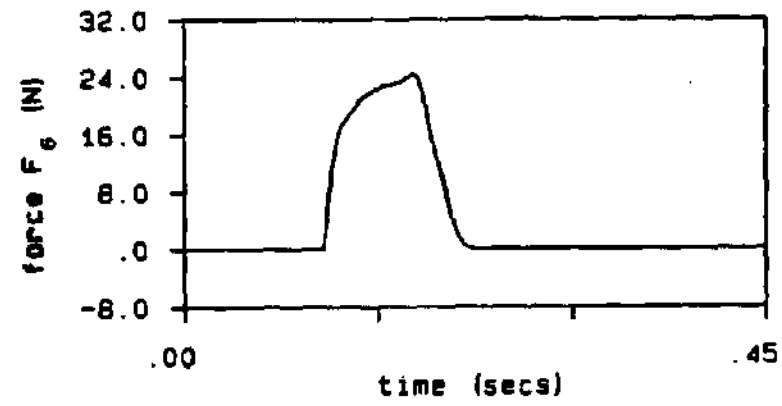
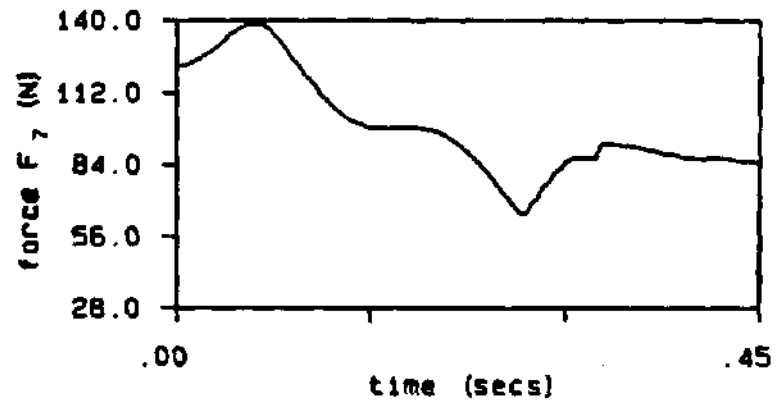
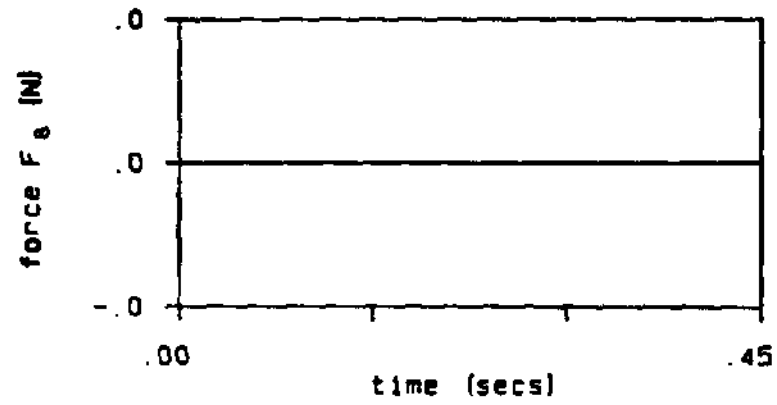


Fig. 4.15 (Continued)

(g)



(h)



(i)

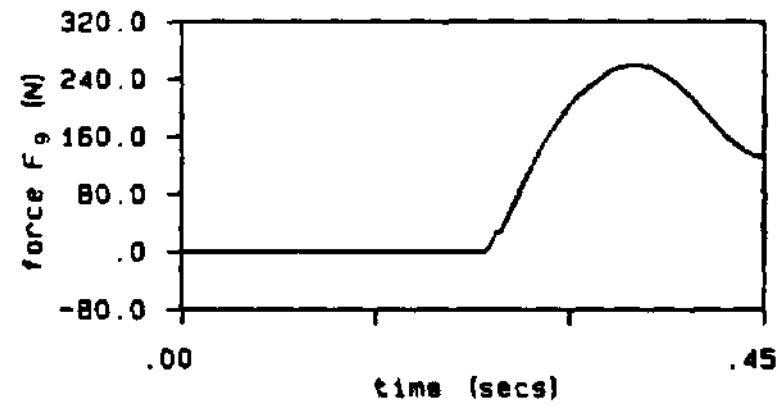


Fig. 4.15 (Continued)

strong activity of this muscle group at the end of the swing phase as evidenced by its EMG record. This latter function was entirely left to the short head of biceps (Figure 4.14e).

Figures 4.15a-i show the force histories obtained using the static optimization algorithm. From these figures it is observed that there is a good agreement between the predicted force histories obtained by this method and those obtained by the dynamic optimization algorithm.

4.5 DISCUSSION

One of the prominent features in the results obtained by dynamic optimization is a characteristic lag between the input controls (Figure 4.11) and the resultant force output (Figure 4.12). This is mainly for the iliopsoas muscle group and the biceps femoris group. One of the consequences of this lag is that the joint torques produced by the dynamic optimization algorithm lag those produced by solving the inverse dynamics problem at the beginning of the swing phase. This difference also manifests itself in the predicted trajectories. (Figure 4.9). A closely related observation is the fact that the EMG records for most of the muscles shown in Pedotti [51], start off slightly earlier than

the expected activities as required by the history of the resultant joint torques. Typical of this behavior are the EMG records of the vasti group. The EMG records of this muscle group shows that they start activity toward the end of the swing phase -- perhaps in anticipation of an increasing knee moment just after heel strike [51]. The activity of the vasti at the end of the swing phase may also be needed to stabilize the joint; but would otherwise completely contradict the increasing flexor moment at the knee required at the end of the swing phase. On the contrary, the solution of the inverse dynamics problem results in an increasing knee moment at the end of the swing phase. To achieve this change in the moment, the vasti group were recruited for a short interval of time.

Such a characteristic lag between muscle input and muscle force output is one of the major differences between simple input-output muscle models discussed in Chapter 2. This lag is an inherent characteristic of the muscular subsystem which results from the presence of elastic and damping elements - making it impossible for the muscles to produce force instantaneously in response to stimuli.

Another observation is that the forces predicted by the dynamic optimization algorithm are generally larger than the corresponding forces predicted by the static

optimization algorithm. It should be recalled from the muscle modeling procedures in Chapter 2, that one of the important elements in the more complex models is a damping element. This element generally dissipates some of the force generated by the muscle. Moreover, the dynamic optimization algorithm takes into account the presence of the passive joint structures. These elements are not ordinarily considered in the static optimization algorithm and hence resulting in a difference in the magnitudes of the force predictions by the two methods.

Another interesting difference in the two results is that some of the muscle force predictions by static optimization exhibit sharp discontinuities (Fig. 4.15d). Such discontinuities are a direct consequence of the absence of memory in the static optimization. That is, the values of the forces obtained at any instant of time are independent of the values obtained at previous points in time. Such is not the case in dynamic optimization where the state and hence the control variables depend on the previous values obtained.

Finally, it is noted that during the swing phase, muscle activity is minimal for the thigh and shank. That is, most of the muscles are active only at the very beginning and the very end, with very little activity in-between. The situation is different with the foot where a continuous dorsiflexing moment acts at the ankle

joint. The minimal muscle activity for the thigh and shank is in agreement with the ballistic concept for the swing phase [42]. The continuous activity of tibialis anterior provides the necessary dorsiflexor moment at the ankle joint. This works to keep the foot clear of the ground throughout the swing phase.

In summary, the results of this study strongly point to the importance of accurate determination of link kinematic variables for use in the static optimization algorithm. The results obtained show that dramatic differences can be obtained for very small changes in the smoothing and differentiating methods used. Considering that actual gait data is more noisy than the data used in this study, it goes without saying that extra care is needed in actual gait analysis to ensure accurate determination of the muscle forces.

Finally, it is appreciated that the use of dynamic optimization and static optimization could lead to comparable results of the muscle forces if sufficient care is taken to obtain accurate joint torques for use by the former method. One possible reason for the results of the two techniques being nearly the same could well be that the prediction of muscle force sharing is influenced strongly by the kinematics of the problem than by the kinetics as defined in the choice of the objective function. One obvious advantage of the dynamic

optimization algorithm, and one which could have far reaching consequences is its ability to predict not only the muscle forces but also the neural controls necessary to produce those forces. Considering that the interest in musculoskeletal modeling is moving toward the neural subsystem, the dynamic optimization approach will remain an important one.

CHAPTER V

SUMMARY, CONCLUSIONS AND RECOMMENDATIONS

5.1 SUMMARY

In Chapter 2 four different muscle models were considered. The ability of these models to predict a given musculoskeletal motion was studied. The musculoskeletal motion considered was the minimum time kicking problem. The effect of model complexity on the overall formulation of the musculoskeletal motion problem was also considered. It is observed that one of the major characteristics of muscle that makes a mathematical model complex is the force-velocity relationship. This is mainly because of the different curvatures exhibited by this function for the two possible modes of muscle contraction - concentric and eccentric. Proper modeling of this behavior has led to models that are often not easy to apply owing to serious numerical stability problems.

A muscle model was proposed which avoids most of these problems while not losing contact with the physiological reality of the situation. This new model is a modified form of the Hill force- velocity relationship; with an added term to take into account the phenomenon of

muscle yielding during eccentric contractions.

In Chapter 3, several optimal control algorithms were examined. The main algorithms studied were, the optimal steepest descent (SD), the Fletcher-Reeves conjugate gradient method (FR), the method of parallel tangents (PT), the variance algorithm (VA) and the gradient-restoration algorithm (GR). These algorithms were used to solve four different problems of varying complexity. Two of these were relatively simple problems typically found in the control literature. The other two were characterized by a larger number of linear and highly nonlinear state equations and are typically found in the biomechanics literature. Three criteria were used to evaluate these algorithms - rate of convergence, computer running time and storage requirements. In all cases the constraints in the problems were handled using the Exterior Penalty Function technique.

In Chapter 4, the muscle force sharing problem was solved for the swing phase of gait using a dynamic optimization algorithm. For comparison purposes a typical static optimization algorithm was solved. A simplified system consisting of 4 links and 9 muscle groups was considered. The objective function for the dynamic optimization algorithm was a combination of the tracking error and the metabolic energy consumption. The latter quantity was assumed to be the sum of the total work done

by the muscles and the enthalpy change during the contraction. The objective function for the static optimization problem was the sum of the cubes of the muscle stresses. To solve this problem, the inverse dynamics problem was first solved in order to determine the resultant joint torques required to generate the given hip, knee and ankle trajectories. To this effect the angular velocities and accelerations were obtained by numerical differentiation using low-pass digital filters. The dynamic optimization problem was solved using the Fletcher-Reeves conjugate gradient algorithm, and the static optimization problem was solved using the Gradient-restoration algorithm.

5.2 CONCLUSIONS

The following conclusions have been drawn.

1. The complex muscle models are almost indispensible for the accurate prediction of human movement. However, these models often lead to large scale problems that require large computational facilities for their implementation. Moreover, the more sophisticated models are seen to be plagued by numerical instability problems. The concept of model reduction can be used to produce minimal models required to accurately predict a given motion history.

2. The most powerful and most versatile of the dynamic optimization algorithms for the motion studies considered here is the Gradient-Restoration algorithm. This is because of its ability to solve optimization problems rapidly and to handle all forms of constraints in the most elegant manner. However, the storage requirements of this algorithm are almost prohibitive to all but the small and averagely sized problems. On the other hand , the simplest algorithm to code and implement is the optimal steepest descent algorithm. This algorithm is however characterized by very slow convergence especially after the first or second iterations. For the large problems, the Fletcher-Reeves conjugate gradient algorithm offers a suitable compromise between rapid convergence rate and storage requirement.

3. The use of dynamic optimization to predict the muscle forces during the swing phase of gait results in good temporal agreement between the EMG signals and the control histories. Moreover, some of the subtle characteristics of the muscular subsystem can be predicted using such an approach. Typical of such characteristics are the lag times that occur between the inputs to the muscle and the resultant force output. A natural selection for the objective function in the dynamic optimization problem is the metabolic energy

consumption. This quantity is shown to be easily modeled, empirically, in terms of the quantities used to define the muscle model - the state and control variables. For the muscle force sharing problem comparable results could be obtained with a well defined physiologically based objective function.

5.3 RECOMMENDATIONS

Further research in this work could be carried out based on the following recommendations

1. Extend the muscle force sharing problem to include the stance phase of gait. In this regard it may be necessary to include both limbs or to generate data on the effect of one limb on the other.

2. In the dynamic optimization problem extend the control variables for each muscle or muscle group to include recruitment of motor units. Such an extension can be used to study other factors which enter into the physical description of the muscle besides those which have been considered, for instance, the possibilities of weakening of the muscle due to partial paralysis and the influence of fatigue on the muscle performance.

3. Consider the possibility of splitting the dynamic

optimization problem into two sub-problems. The first subproblem is to be concerned with solving the inverse dynamics problem to determine the joint torques required to generate the joint trajectories. The second sub-problem is to be concerned with finding the muscle forces via dynamic optimization. This step will not only help to reduce the dimensionality of the problem, but most importantly, it will help create two dynamic problems that have compatable variables. By this is meant that the variables describing the skeletal subsystem such as limb masses and inertias will be made local to the skeletal subproblem alone, while the variables describing the muscular subsystem will in turn be local to the muscular subproblem alone.

4. One of the important findings of this study is the fact that the muscle lengths and moment arms can strongly influence the results of the muscle force sharing problem using optimization techniques. This calls for a need to develope schemes for accurately determining these quantities for any actual gait analysis.

REFERENCES CITED

1.) Aubert, X., "Le Couplage Energetique de la Contraction Musculaire", Brussels: Editions Arscia, 1956, pp 1-315.

2.) Bahler A,S., "Modeling of Mammalian Skeletal Muscle", IEEE Trans., Biomed. Engr., BME-15, pp249-257, 1968.

3.) Box, M,J., "A New Method of Constrained Optimization and a Comparison with other Methods", Computer Journal, vol. 8, No. 1, pp 42-52,1965.

4.) Brand R.A, Crowninshield R.D, Wittstock C.E, Pedersen D.R., Clark C.R., and van Krieken F.M., "A Model of Lower Extremity Muscular Anatomy", Trans. ASME Journal of Biomed. Engr., vol 104, pp 304-310, 1982.

5.) Brunnstrom, S., Clinical Kinesiology, Davis Publishing Co., Philadelphia, 1972.

6.) Bryson, A.E., and Ho, Y., Applied Optimal Control, Hemisphere Publishing Corporation, Washington, 1975.

7.) Capozzo, L.T. and Pedotti, A., "A General Computing Method for the Analysis of Locomotion", J. of Biomechanics, vol. 8, pp 307-320, 1975.

8.) Chao, E.Y., and Rim, K., "Application of Optimizationn Principles in Determining the Applied Moments in Human Leg Joints During Gait", J. of Biomechanics, vol. 6, pp 487-510, 1973.

9.) Chapman, A.E., and Harrower, P.T., "Linear Approximations of Muscle Mechanics in Isometric Contraction", Biol. Cybernetics, vol 27, pp 1-7, 1977.

10.) Chow, C.K., and Jacobson , D.H., "Studies in Human Locomotion via Optimal Programming", Math. Biosc., vol 10, pp 239-306, 1971.

11.) Close, R.I., "Dynamic Properties of Mammalian Skeletal Muscle", Physiol. Rev., vol 52, pp 129-197,1973.

12.) Crowe, A., "A Mechanical Model of Muscle and its Application ti the Intrafusal Fibers of the Mammalian Spindle", J. of Biomechanics, vol. 3, pp 583-592,1970.

13.) Crowninshield, R.D., "Use of Optimization Techniques to Predict Muscle Forces", Trans. of ASME, J. of Biomech. Engr., vol.100, pp 88-92,1978.

14.) Crowninshield,R.D.,Johnston, R.C., Andrews, J.G., and Brand R.A., "A Biomechanical Investigation of the Human Hip", J. of Biomechanics, vol 11, pp 75-85, 1978.

15.) Crowninshield, R.D., and Brand, R.A., "A Physiologically Based Criterion of Muscle Force Prediction in Locomotion", J. of Biomechanics, vol. 14, pp 793-801, 1981.

16.) Davidon, W.C., "Variance Algorithm for Minimization", Computer Journal, pp406-410, 1968.

17.) Ebashi, S., and Endo, M., "Calcium ion and Muscular Contraction", Prog. in Bioph. and Mol. Biol., vol 18, pp 125-183, 1968.

18.) Fox, R.L., Optimization Methods for Engineering Design, Addison-Wesley Publishing Co.,1971.

19.) Gibbs, C.L., and Gibson, W.R., "Energy Production of Rat Soleus Muscle", Am. J. of Physiology, vol 233, pp 864-871, 1972.

20.) Hardt, D.E., "Determining Muscle Forces in the Leg During Normal Human Walking - An Application and Evaluation of Optimization Methods", Trans. ASME, J. of Biomech. Engr.,vol 100, pp72-78, 1978.

21.) Hatze, H., "The Complete Optimization of the Human Motion", Math. Biosc., vol. 28, pp 99-135, 1976.

22.) Hatze, H., and Buys, J.D, "Energy Optimal Controls in the Mammalian Neuromuscular System", Biol. Cybern., vol.27, pp9-20, 1977.

23.) Hatze, H., Mycybernetic Control Models of Skeletal Muscle, University of South Africa Press, Pretoria, 1980.

24.) Hill, A.V., "The Heat of Shortening and the Dynamic Constants of Muscle", Proc. of the Royal Soc., vol. 126, pp 136-195, 1938.

25.) Hill, A.V., "A Reinvestigation of Two Critical Points in the Energetics of Muscular Contraction", Proc. of the Royal Soc., vol. 141, pp 503-510,1953.

26.) Hill, T.L., "Theroretical Formalism for the Sliding Filament Model of Contraction of Striated Muscle", Prog. in Bioph. and Mol. Biol., vol. 28, 267-340, 1974.

27.) Hof, A.L.,and Van den Berg, J.W., "EMG to Force Processing II: Estimation of Parameters of the Hill Muscle Model for the Human Triceps Surae by Means of a Calfergometer", J. of Biomechanics, vol.14, pp 759-770, 1981.

28.) Huxley, A.F., "Muscle Structure and the Theories of Contraction", Prog. in Bioph. and Mol. Biol., vol. 7, pp 257-318, 1957.

29.) Jacobson, D.H., Gershwin, S.B , and Lele, M.M., "Computation of Optimal Singular Controls", IEEE Trans. on Autom. Control, vol. AC-15, pp 67-73, 1970.

30.) Jacobson, D.H., and Lele M.M., "A Transformation Technique for Optimal Control Problems with a State Variable Inequality Constraint", IEEE Trans. on Autom. Control, vol AC-14, pp457-464, 1969.

31.) Johnson M.A., Polgar, J., Weightman, D., and Appleton, D., "Data on the Distribution of Data Types in Thirty Six Human Muscles - An Autopsy Study", J. of Neurol. Sci., vol. 18, pp 111-129, 1973.

32.) Kaiser, J.F., and Reed, W.A.,"Data Smoothing Using Low Pass Digital Filters", Rev. Sci. Instrum., vol.48, pp 1447-1457,1977.

33.) Kelley, H.J., "Method of Gradients", Optimization Techniques, G. Leitman, ed., Academic Press, New York,1962, Chapter 6.

34.) Lasdon, L.S., Mitter, S.K., and Warren, A.D., "The Conjugate Gradient Method for Optimal Control Problems", IEEE Trans. on Autom. Control, vol. AC-12, pp 132-138,1967.

35.) Lasdon, L.S., Warren A.D., and Rice, R.K., "An Interior Penalty Method for Inequality Constrained Optimal Control Problems", IEEE Trans. on Autom. Control, vol. AC-12, pp 388-395, 1967.

36.) Lee, E.B., and Markus, L., Foundations of Optimal Control Theory. John Wiley and Sons, New York, 1967.

37.) Leitman, G., The Calculus of Variations and Optimal Control. Plenum Press, New York, 1981.

38.) Lesh, M.D., Mansour, J.M., and Simon, S.R., "A Gait Analysis Subsystem for Smoothing and Differentiation of Human Motion Data", Trans. of ASME, J. of Biomech. Engr., vol. 101, pp205-212,1979.

39.) Levin, A., and Wyman, J., "The Viscous Elastic Properties of Muscle", Proc. of the Royal Soc., vol. 101, pp 218-243, 1927.

40.) Mansour, J.M, and Audu, M.L., "The Passive Elastic Moment in the Knee and its Influence on Human Gait", Submitted to the J. of Biomechanics.

41.) McClellan, J.H., Parks, T.W., and Rabiner, L.R., "A Computer Program for Designing Optimum FIR Linear Phase Filters", IEEE trans on Audio Electroacoustics, vol. AU-21, pp 506-526, 1973.

42.) Mena, D., Mansour, J.M., and Simon, S.R., "Analysis and Synthesis of Human Swing Leg Motion During Gait and its Clinical Applications", J. of Biomech., vol. 14, pp 823-832, 1981.

43.) Miele, A., "Gradient Algorithms for the Optimization of Dynamic Systems", Advances in Control and Dynamic Systems, Leondes C.T., ed., Academic Press, New York, 1960, Chapter 1, pp 1-52.

44.) Miele, A., Damoulakis, J.N., Cloutier, J.R., and Tietze, J.L., "Sequential Gradient-restoration Algorithm for Optimal Control Problems with Nondifferential Constraints", J. Opt. Theory and Appls., vol. 13, pp 218-255, 1974.

45.) Miele, A., Huang, H.Y., and Heideman, J.C., "Sequential Gradient-restoration Algorithm for the Minimization of Constrained Functions - Ordinary and Conjugate Gradient Versions", J. Opt. Theory and Appls., vol. 4, pp 213-243, 1969.

46.) Mommaerts, W.F.H.M., "Energetics of Muscular Contraction", Physiol. Revs., vol. 49, pp 427-508, 1969.

47.) Otis, J.C., A Mathematical Model for the Evaluation of Neuromuscular Performance, Ph.D Dissertation, Case Western Reserve University, 1974.

48.) Patriarco, A.G., Mann,R.W., Simon, S.R., and Mansour, J.M., "An evaluation of the Approaches of Optimization Models in the Prediction of Muscle Forces During Human Gait", J. of Biomech., vol. 14, pp 513-525, 1981.

49.) Paul, J.P., "Forces Transmitted by Joints in the Human Body", Proc. of the Inst. of Mech. Engrs., vol. 181, pp 307-320, 1975.

50.) Pedotti A., Krishnan V., and Stark, L., "Optimization of Muscle-Force Sequencing in Human Locomotion", Math. Biosc., vol. 38, pp 57-76, 1978.

51.) Pedotti, A., "A Study of Motor Coordination and Neuromuscular Activities in Human Locomotion", Biol. Cybern., vol. 26, pp 53-62, 1977.

52.) Penrod, D.D, Davy, D.T., and Singh, D.P., "An Optimization Approach to Tendon Force Analysis", J. of Biomech., vol. 7, pp 123-129, 1974.

53.) Ritchie J.M., and Wilkie, D.R., "The Dynamics of Muscular Contraction", J. of Physiol., vol. 143, pp 104-113, 1958.

54.) Seireg, A., and Arvikar, R.J., "A Mathematical Model for Evaluation of Forces in Lower Extremeties of the Musculoskeletal System", J. of Biomech., vol. 6, pp 313-326, 1973.

55.) Seireg, A., and Arvikar, R.J., " The Prediction of Muscular Load Sharing in the Lower Extremeties During Walking", J. of Biomech., vol. 8, pp 89-102, 1975.

56.) Sugi, H., "Tension Changes During and After Stretch in Frog MUscle Fibers", J. of Physiol., vol. 255, pp 237-253, 1972.

57.) Taylor, C.P.S., "Isometric Muscle Contraction and the Active State: An Analog Computer Study", Bioph. J., vol. 9, pp 759-789, 1969.

58.) Tomovic, R., and Bellman, R., "A Systems Approach to Muscle Control", Math. Biosc., vol.8, pp 265-277, 1970.

59.) Winter, D.A., Biomechanics of Human Movement. John Wiley and Sons, New York, 1979.

60.) Wong, P.J., Dressler, R.M., and Luenberger, D.G., "A Combined Parallel Tangents/ Penalty-Function Approach to Solving Trajectory Optimization Problems", AIAA J., vol. 9, pp 2443-2448, 1971.

61.) Yoon, Y.S., and Mansour, J.M., "The Passive Elastic Moment at the Hip", J. of Biomech., vol. 15, pp 905-910, 1982.

62.) Zahalak, G.I., "A Distribution-Moment Approximation for Kinetic Theories Of Muscular Contraction", Math. Biosc.vol. 55, pp 89-114, 1981.

APPENDIX 1

The hip and knee angular accelerations for the two-degree-of-freedom link system are calculated using the expressions

$$\dot{x}_3 = f_3 = (a_3 b_1 - a_2 b_2)/d$$
$$\dot{x}_4 = f_4 = (a_1 b_2 - a_2 b_1)/d$$

Where

$$d = a_1 a_3 - a_2^2$$
$$a_1 = I_1 + I_2 + m_2 l_1^2 + 2K_1$$
$$a_2 = I_2 + K_1$$
$$a_3 = I_2$$
$$b_1 = K_3 + K_4 + K_5 + K_2(x_4^2 + 2x_3 x_4) + T_1$$
$$b_2 = K_2 x_3^2 + K_4 + T_2$$
$$K_1 = m_2 l_1 z_2 \cos x_2$$
$$K_2 = m_2 l_1 z_2 \sin x_2$$
$$K_3 = m_1 g z_1 \sin x_1$$
$$k_4 = m_2 g z_2 \sin (x_1 + x_2)$$
$$K_5 = m_2 g l_1 \sin x_1$$

In these equations I_1, I_2 are the moments of inertia of the thigh and combined shank and weighted foot respectively about the hip and knee joints ; m_1 ,m_2 are the respective masses of the limbs ;l_1, z_1, z_2 are

the length of the thigh from the hip to the knee joint, the distance of the center of mass of the thigh from the hip joint , and the distance of the center of mass of the combined shank and weighted foot from the knee joint respectively ; g is the acceleration due to gravity. The numerical values of these parameters are : m_1 = 8.692 kg, m_2 = 15.492 kg, I_1 = .48 kg-m^2, I_2 = 4.7 kg-m^2, l_1 = .447 m, z_1 = .189 m, z_2 = .501 m, g = 9.81 m/s^2.

T_1, T_2 are the resultant torques about the hip and knee joints respectively . They are the same as the control variables for problem 3; but for problem 4 they are calculated as follows,

$$T_1 = F_1 d_1 + F_3 d_3 - F_4 d_4{}^1$$
$$T_2 = F_2 d_2 + F_3 d_2 - F_4 d_4{}^2 - F_5 d_5$$

Where the moment arms d_i of the muscles are specific to the subject studied and are given by equations (15) - (20) of [21].

APPENDIX 2

The hip, knee and ankle angular accelerations for the three-degree-of-freedom link system are given by the relations

$$\dot{x}_4 = c_1 b_1 + c_2 b_2 + c_3 b_3$$
$$\dot{x}_5 = g_1 b_1 + g_2 b_2 + g_3 b_3$$
$$\dot{x}_6 = h_1 b_1 + h_2 b_2 + h_3 b_3$$

where

$$c_1 = (a_4 a_6 - a_5^2)$$
$$c_2 = (a_3 a_5 - a_2 a_6)$$
$$c_3 = (a_2 a_5 - a_3 a_4)/d$$
$$g_1 = (a_3 a_5 - a_2 a_6)/d$$
$$g_2 = (a_1 a_6 - a_3^2)/d$$
$$g_3 = (a_2 a_3 - a_1 a_5)/d$$
$$h_1 = (a_2 a_5 - a_3 a_4)/d$$
$$h_2 = (a_2 a_3 - a_2^2)/d$$
$$d = d_1 - a_4 a_3^2 - a_1 a_5^2 - a_6 a_2^2$$
$$d_1 = a_1 a_4 a_6 + 2 a_2 a_3 a_5$$
$$b_3 = -d_3 e_5 k_1 + T_3$$
$$b_2 = b_3 + d_3 e_2 e_5 t_6 \sin(t_3 - t_2) + Z_1$$
$$b_1 = b_2 - k_3 + k_4 + k_5 + T_1 - T_2 + T_3$$
$$Z_1 = T_2 - T_3 - k_2$$
$$a_6 = f_3$$
$$a_5 = a_6 + w_1$$

$$a_4 = f_2 + f_5 + w_1 + d_3 e_2^2$$

$$a_3 = a_5 + w_2$$

$$a_2 = a_4 + w_2 + w_3 - w_1$$

$$a_1 = f_1 + d_2 e_1^2 + a_4 + 2(w_3 + w_2) + d_3 e_1^2$$

$$w_1 = d_3 e_2 e_5 \cos(t_3 - t_2)$$

$$w_2 = d_3 e_1 e_5 \cos(t_3 - t_1)$$

$$w_3 = (d_2 e_4 + d_3 e_2) e_1 \cos(t_2 - t_1)$$

$$k_1 = v_1 + v_2 + v_3$$

$$k_2 = v_4 + v_5$$

$$k_3 = g v_6 \sin t_1$$

$$k_4 = v_7 v_8$$

$$k_5 = d_3 e_1 e_5 t_6 \sin(t_3 - t_1)$$

$$v_1 = g \sin t_3$$

$$v_2 = e_1 t_4 \sin(t_3 - t_1)$$

$$v_3 = e_2 t_5 \sin(t_3 - t_2)$$

$$v_4 = (d_2 e_4 + d_3 e_2) g \sin t_2$$

$$v_5 = e_1 t_4 \sin(t_2 - t_1)$$

$$v_6 = d_1 e_3 + d_2 e_1 + d_3 e_1$$

$$v_7 = e_1 t_5 \sin(t_2 - t_1)$$

$$v_8 = d_2 e_4 + d_3 e_2$$

$$g = 9.806 + h b^2 \sin(bt + c)$$

$$t_1 = x_1$$

$$t_2 = x_1 + x_2$$

$$t_3 = x_1 + x_2 + x_3$$

$$t_4 = x_4^2$$

$$t_5 = (x_4 + x_5)^2$$

$$t_6 = (x_4 + x_5 + x_6)^2$$
$$T_1 = i_1F_1 + o_2F_2 + o_3F_3 - i_9F_9 + T_1^P$$
$$T_2 = -i_2F_2 + i_3F_3 - o_4F_4 - i_5F_5 + i_6F_6 + T_2^P$$
$$T_3 = -i_4F_4 + i_7F_7 - i_8F_8 + T_3^P$$

In these equations, d_1, d_2 and d_3 are the masses of the thigh, shank and foot respectively; f_1, f_2 and f_3 are the corresponding moments of inertia of the limbs about the hip, knee and ankle joints. e_1 is the length of the thigh and e_2 is the length of the shank. T_1, T_2 and T_3 are the torques about the same joints. o_k and i_k are the moment arms of the force developed by muscle k about its origin and insertion respectively. The muscle force F_k is given by the relation:

$$F_k = F_k^{SE} + F_k^{DE} + F_k^{PE}$$

Where F_k^{SE}, F_k^{DE} and F_k^{PE} are the forces in the series elastic element, damping element and the parallel elastic element respectively. The torques T_k^P are the passive torque acting across joint k. Let e_3, e_4 and e_5 be the distances of the centers of mass of the thigh, shank and foot from the hip, knee and ankle joints respectively. Then the following represent the numerical values of the anthropomorphic data used in the simulation of the model:

$d_1 = 8.$ kg

d_2 = 3.72 kg

d_3 = 1.16 kg

f_1 = .286 kg-m^2

f_2 = .183 kg-m^2

f_3 = .0267 kg-m^2

e_1 = .35 m

e_2 = .42 m

e_3 = .15 m

e_4 = .182 m

e_5 = .11 m

b = 12.566

c = .008

h = .0254 m

APPENDIX 3

The quantities p_1 - p_6 in equations (2.24) - (2.28) are defined as follows

$$p_1 = b_{13} \exp(-b_{14}(b_{15} + b_{16}(L_c - \bar{L}_c))^n)$$
$$p_2 = \sin (b_{17}(L_c - \bar{L}_c) + b_{18})$$
$$p_3 = b_4 \ (\exp(-b_5(L_c - \bar{L}_c + b_6)^2 - P))$$
$$p_4 = 19.3 \exp(-b_{19}(L_c - \bar{L}_c - b_{20})^2)$$
$$p_5 = b_{21} \exp(-b_{22}(L_c - \bar{L}_c)) - b_{23}$$
$$p_6 = (1 - b_2^2 / (L_c - \bar{L}_c + b_3)^2)^{1/2}$$
$$P = 1.43 \ (q-1)^2$$

The parameters b_1 - b_{23}, m, C and n are given in [21].